

Thin Film Silicide Formation by Thermal Annealing:
Study of Kinetics, Moving Species,
Impurity Effect, and Electrical Properties

Thesis by

Chuen-Der Lien

in Partial Fulfillment of the Requirements

for the Degree of

Doctor of Philosophy

California Institute of Technology

Pasadena, California 91125

1985

(Submitted August 13, 1984)

ACKNOWLEDGMENTS

I would like to express my sincere appreciation to my advisor, Professor Marc-A. Nicolet, for his guidance and support throughout my stay at Caltech. I am deeply indebted to him.

I am grateful to Professor S. S. Lau from the University of California at San Diego, for his very good suggestions and discussions. I also thank Dr. Leszek Wieluński and Ilka Suni for their very useful instructions and assistance during the beginning phase of my research. I am grateful to Professor Jim McCaldin for helping me with his very good insight into physics problems, and to Professor Thomas Caughey for his help with some mathematical problems.

I also thank Bai-Xin Liu and Dr. M. Van Rossum for making X-ray diffractions and Dr. Uri Shreter for making TEM pictures.

I would like to thank Rob Gorris, Rouel Fernandez, and Ali Ghaffari for assistance with the experimental apparatus, and Michell Parks for excellent typing and proofreading of many of my manuscripts and her very useful instructions regarding my English usages.

Helpful discussions and suggestions from Dr. David Scott, Dr. Bruce Paine, Dr. Meir Bartur, Dr. K. T. Ho, Tom Banwell, Frank C. T. So, and Manuela Finetti are also acknowledged here.

The research described in this thesis was sponsored in part by the Jet Propulsion Laboratory, California Institute of Technology, Director's Discretionary Fund through an agreement with the National Aeronautics and Space Administration (A. Morrison).

Finally, I acknowledge the support and encouragement from my wife, Sheue-ling.

PREFACE

Most of my work done at Caltech to fulfill the requirements of my thesis is published, or accepted for publication, or in preparation for publication. This thesis will review most of my work but the details are found in the published work. To make this thesis a comprehensive presentation of my work, I have my publications listed separately in the thesis as “REFERENCE II” and have them numbered by Roman numerals. These publications constitute an integral part of the thesis. The unpublished part will be included in the “APPENDIX” of the thesis. The results that are published in my papers but were obtained by my colleague are identified by footnotes in this thesis.

ABSTRACT

Growth kinetics, dominant moving species (DMS), impurity effect, and electrical properties of thermally formed silicides have been studied by using MeV $^4\text{He}^+$ Rutherford backscattering spectrometry, $^{18}\text{O}(p,\alpha)^{15}\text{N}$ nuclear reaction analysis, four-point probe measurement, and I-V measurement.

The growth kinetics (including growth rate and activation energy of growth rate) measurements are done for silicides formed on different kinds of Si substrates, viz., single crystalline (100) Si (Si^c) and amorphous evaporated Si (Si^e). Results show that the substrate can have different effects on different silicides. Some silicides grow much faster on Si^e than on Si^c (e.g., NiSi_2 , CoSi_2), some show the reverse phenomenon (e.g., Co_2Si , CoSi), and some have similar growth rates (e.g., NiSi , Ni_2Si , Pt_2Si , PtSi) (see Table 2). Some silicides are more uniform and form at lower temperature on Si^e than on Si^c (e.g., CrSi_2 , NiSi_2 , CoSi_2). These interesting phenomena are discussed and explained in terms of the different properties between the samples with either substrate (see Chapter 2).

When studying the formation of a silicide, one would like to know the DMS in silicide during the silicide formation. Not only is it an important property of the silicide but it is closely related to the silicide formation. The DMS is, in general, measured by inert marker experiments. In Chapter 3, we use such marker experiments to study the DMS in a silicide during silicide formation and two other silicide reactions (viz., solid-phase-epitaxy (SPE) of Si^e through silicide and silicide oxidation). The reason for measuring the DMS for the two additional types of silicide reactions is that all these reactions are related and additional information can be obtained from this comparison. The results, in fact, show that in all three reactions, the DMS in the silicide is the same when the silicide formation is diffusion-controlled. An explanation is given (with some assumptions) by considering the detailed atomic motion in

the silicide during these reactions (see Chapter 3).

Inert marker experiments can identify the DMS in a silicide. They cannot, however, distinguish whether the DMS diffuses by an interstitial (or grain boundary) or a vacancy mechanism. One possible way to determine the diffusion mechanism of the moving species is by using tracer experiments. The problem with the tracer studies is that the measured tracer profiles can be (and have been) misinterpreted. We review several models that were used to explain the tracer profiles, point out incorrect considerations and finally give a plausible model to explain what information can be obtained from the tracer experiments (see Chapter 4).

During marker experiments, one may find that the marker used to monitor the DMS can affect the growth rate of silicide, and sometimes even change the DMS. This points to a general problem, namely, how foreign atoms (impurities) introduced in a sample affect the properties of silicide. Since the effect of impurity is important in our thin film reactions, we have systematically studied the effect of oxygen on the growth rates of silicide, and its redistribution, by using a rare isotope of oxygen, ^{18}O , as an impurity. The results are explained in terms of a modified model which was originally proposed by Scott (see Chapter 5).

Finally, we study the electrical properties of Co silicides. Co silicides formed from Si° (silicides thus formed are more uniform than that formed from Si^{\ominus}) are used for the measurements of Schottky barrier height, resistivity, Hall mobility, and carrier concentration. From the result of this study, we suggest that CoSi_2 is a potential candidate for contacts to shallow junctions and as an interconnection material in VLSI (see Chapter 6).

Further works, arising out of the implications of these studies, are suggested and summarized in the last chapter of the thesis.

Table of Contents

	Page
ACKNOWLEDGMENTS	ii
PREFACE	iii
ABSTRACT	iv
Table of Contents	vi
Figures and Tables.	ix
Chapter 1. Introduction	1
Chapter 2. Kinetics of Silicides on Different Si Substrates	4
2.1 Introduction.	4
2.2 Experimental Procedures.	5
2.3 Results and Discussions	6
2.4 Conclusion	11
Chapter 3. Dominant Moving Species during Silicide Reactions . .	12
3.1 Introduction.	12
3.2 Experimental Procedures.	13
3.3 Results	14
3.4 Discussions	17
3.5 Conclusion	20
Chapter 4. Tracer Profiles in Silicide after Silicide Formation . .	21
4.1 Introduction.	21
4.2 Models.	23
4.3 Discussion	27
4.4 Conclusion	30

Chapter 5. Effect and Redistribution of Oxygen in Silicide Formation	31
5.1 Introduction.	31
5.2 Experimental Procedures.	32
5.3 Results and Discussion	34
5.3.1 Bulk oxygen	34
5.3.2 Interfacial oxide	36
Chapter 6. Electrical Properties of Thin Co Silicides	41
6.1 Introduction.	41
6.1.1 Schottky Barrier Height	41
6.1.2 Resistivity	42
6.2 Experimental Procedures.	42
6.2.1 Schottky Barrier Height	42
6.2.2 Resistivity	43
6.3 Results and Discussion	44
6.3.1 Schottky Barrier Height	44
6.3.2 Resistivity	46
6.4 Conclusion	49
Chapter 7. Further Work.	50
7.1 Ion Irradiation Improved Contact	50
7.2 Diffusion of Ni and Co in Si	51
7.3 Strange Behavior of CrSi ₂	53
7.4 Nucleation Controlled Silicides Formed from Si ^e	53
7.5 Different amorphous Si	54

REFERENCES I – General	55
REFERENCES II – Work published by Chuen-Der Lien	61
Appendix A – A Modified Model for a Planar Compound Formation	64
Appendix B – Kinetics of Silicides on (100) Si and Evaporated Si Substrates	82
Appendix C – Growth of Co-Silicides from Single Crystal and Evaporated Si	107
Appendix D – Effects of Ion Irradiation on Thermally Formed Silicides in the Presence of Interfacial Oxide	124

Figures and Tables

	Page
Table 1. Results on the reaction kinetics of silicides formed on Si ^c (100) and the Si ^e substrates.	7
Table 2. Differences between silicides formed on Si ^e and Si ^c and possible causes. The order of the causes represents their likelihood.	10
Figure 1. Three kinds of silicide (M _β Si _{1-β}) reactions are shown here. The positive direction of coordinate, <i>x</i> , is defined pointing from left to right. The fluxes of metal and Si are shown with arrows pointing to their respective positive directions.	15
Table 3. Comparison of the dominant moving species (DMS) for formation of silicide, oxidation of silicide, and SPE of Si ^e with that silicide.	16
Figure 2. Schematics of the sample used for an ³¹ Si experiments: (a) initial tracer position, and (b) a sample when Si tracer is just consumed to form silicide.	22
Figure 3. Schematics for the model proposed by Pretorius et al. [29] to explain the profile of ³¹ Si when the metal is completely consumed.	23
Figure 4. Schematics for a computer simulation proposed by Pretorius et al. [36] and a mathematical model by the author of this thesis [VIII] to explain the ³¹ Si profile (assuming that Si is the DMS, Si moves interstitially and convectively, and that the mobile interstitial Si can exchange position with the fixed lattice Si).	25
Figure 5. Schematics for the Model 3 proposed in ref. IX to explain the profile of Si tracer (³¹ Si).	26
Table 4. Information that can be obtained from the Si tracer profile after silicide formation.	28
Table 5. Three categories of bulk impurity redistributions in media with different impurity diffusion rates during annealing. Entries in the table identify the main mechanisms for the impurity redistribution.	33

Figure 6. A model is proposed to explain the redistribution of the immobile impurity during silicide formation. The impurity is initially located either (a) in the stationary species layer, or (b) in the moving species layer, or (c) at the Si/metal interface [10, x]. In all cases, the metal (M) is assumed to be the moving species and Si to be the stationary species. 35

Table 6. Redistribution and effect of implanted ^{18}O in samples: Si/M or Si/silicide. 37

Table 7. Redistribution and effect of interfacial impurities in samples consisting of a Si substrate and a metal overlayer. 38

Figure 7. 2 MeV RBS spectra (Pt signal only) of Si-Pt samples annealed at 400°C for 1 hr.. Solid line shows the spectrum of the unimplanted sample. Dotted-lines and dashed-lines show the spectra of 2.5 and 5×10^{15} Si/cm^2 implanted samples, respectively. The ^{18}O signals of the unimplanted sample (open circles), the low dose implanted sample (triangles), and the high dose implanted sample (full circles) are also shown here [XVI].. . . 40

Table 8. The table lists Schottky barrier heights (in eV) of Co silicides on an n-type (100) Si in samples whose configurations prior to annealing were I (Si^e/Co), II ($\text{Si}^e/\text{Co}/\text{Si}^e(\text{B})$), and III ($\text{Si}^e/\text{Co}/\text{Si}^e(\text{B})/\text{Co}$) [XVII].. . . . 44

Figure 8. Data of $(\sigma)_s/t_0$ versus $R\sigma_s^2/t_0$ for samples containing two silicide phases [XVIII].. . . . 47

Table 9. Electrical Properties of Co_2Si , CoSi , and CoSi_2 [XVIII].. . . 48

Chapter 1

Introduction

Thin metal silicides are used extensively as interconnections, as Schottky barriers, or as ohmic contacts in semiconductor devices [1–7]. One way to form a thin silicide film is to deposit a thin metal layer on top of a Si substrate (Si/M) and then thermally anneal the sample [1]. Silicide thus formed is via a solid phase reaction between the metal layer and the Si substrate (Si/silicide/M). To have a thorough understanding of silicides, we need to study basic properties of silicides thus formed. Some of these properties are:

- a. Growth kinetics: Phases of silicides formed, their growth rates, activation energy of growth, lateral uniformity, grain size, crystalline orientation, and the controlling process of silicide formation.
- b. Moving species: Dominant moving species (DMS) in a silicide during its formation, and the mechanisms (e.g., vacancy or interstitial) through which the DMS diffuses.
- c. Impurity effect: Effect of impurities on the properties of silicides; e.g., on growth rate, uniformity, moving species, electrical properties, and so on, and the evolution of an impurity profile during silicide reaction.
- d. Electrical property: Resistivity, Hall mobility, carrier concentration, contact resistivity, and Schottky barrier height of silicides.

To have a good control on silicide formation, it is important to understand the growth kinetics of silicides. This information is also essential for choosing proper silicides for a particular application. There

have been lots of researches on the growth kinetics of silicides [1]. We have studied and compared the growth kinetics of several silicides formed on a Si (100) (Si^c) substrate and on an evaporated Si (Si^e , which is amorphous) substrate. The motivation for studying silicide formation on these two kinds of substrates is the followings:

- (1) The metal and poly Si reactions are important for silicides used as interconnection materials. The two extreme cases of this reaction are metal- Si^c and metal- Si^e reactions.
- (2) Due to the scaling down of dimensions, junctions are very shallow in VLSI. By using Si^e , we can control the amount of Si consumed from the Si substrate during silicide formation and, therefore, form a good shallow junction contact [8, 9].

The results of this study are summarized and discussed in Chapter 2.

The DMS in a silicide is closely related to the silicide growth kinetics. DMS information is also important for a silicide contact. In Chapter 3, we use inert marker experiments to measure the DMS in silicides during three kinds of silicide reactions; namely, silicide formation, solid-phase-epitaxy (SPE) of Si^e through silicide, and silicide oxidation. It is interesting to know that, generally, all three reactions (for a fixed silicide) have the same DMS when the silicide formation is diffusion controlled. Although inert marker experiments can determine the DMS in a silicide, they cannot identify the diffusion mechanisms of the DMS. Tracer experiments are thus proposed to monitor the DMS diffusion mechanisms. In Chapter 4, we review models used to interpret tracer profiles measured from tracer experiments. We also propose a satisfactory model to explain what information can be obtained from the tracer studies.

Impurities can affect the growth kinetics, DMS, and other important properties of a silicide. It is very important to understand the roles of impurities in a silicide so that the properties of the silicide can be controlled and reproduced. In Chapter 5, we study the effects of im-

purities (^{18}O only) on the formation of silicides. A modified model is used to explain the effect of oxygen.

From the application point of view, the electrical properties of silicides are among the very important ones. In Chapter 6, we measure the Schottky barrier height, resistivity, Hall mobility, and carrier concentration of Co silicides formed from Si^e. The possibility of using CoSi_2 as an interconnection and contact material is proposed.

We would like to point out that the following interesting order applies to our investigations: In the growth kinetics study, there is no intentionally added impurity in the sample; i.e., we consider "clean" samples; in the moving species study, a very small amount of impurity is added in the sample but its presence is assumed to have no effect on the DMS data; in the impurity effect study, additional impurity is introduced into the samples. In this sense, the impurity effect study is important to check the assumption used in the DMS study. For the case of electrical measurement, the "clean" samples are used. There are some other correlations between these studies as observed from the experimental data:

- (1) In general, when metal is the DMS, the silicide formed is more uniform and the formation temperature is lower than in the cases where Si is the DMS.
- (2) When metal is the DMS, the first silicide formed is, in general, metal rich and when Si is the DMS, the first silicide formed is, in general, Si rich [1].
- (3) The effect of an immobile impurity on the silicide growth strongly depends on the DMS [10, x].

All the studies are performed as systematically as possible. For each property, the experimental results are discussed and interpreted with a simple model.

Chapter 2
Kinetics of Silicides
on
Different Si Substrates

2.1 Introduction

Silicide growth kinetics studies are, in general, performed on an Si substrate which is single-crystalline (Si^c), poly-crystalline (Si^p), or amorphous (Si^a). The metal- Si^c reaction is important for contacts in Si devices, while the metal- Si^p reaction is important for application in interconnections in integrated circuits. The reaction between metal and Si^a is an extreme case for the metal- Si^p reaction and is important for shallow junction contacts [8, 9]. There has been much activity in the study of the growth kinetics of silicides on Si^c [1], but only few have been reported for silicide formation on Si^p [12, 13] and Si^a [13-16].

Generally, experimental results show that the thickness of the silicide is either proportional to the annealing time (t) (e.g., CrSi_2) or to the square root of the annealing time (\sqrt{t}) (e.g., Ni_2Si). This can be explained by assuming that the silicide growth is controlled by either interfacial reactions (t dependence) or by diffusion through the silicide (\sqrt{t} dependence) [17, 1]. There are also a few silicides which will not form below some threshold temperatures (e.g., NiSi_2). The growth of these silicides is believed to be controlled by the initial nucleation of the silicide at the Si/M interface [18].

In this chapter, we study and compare the formation of silicides on Si^c and Si^a (note that the Si^c and Si^a are in fact two extreme cases of

Si^p). In all cases, Si (100) is used as Si^c and evaporated Si (Si^e) as Si^a . There are several differences between samples with Si^c substrate (Si^c/M) or Si^e substrate (Si^e/M):

- (I) There is more impurity at the Si^c/M interface than at the Si^e/M interface. This is because the Si^e evaporation is followed by the metal evaporation without breaking the vacuum.
- (II) Si^c may contain less impurity than Si^e which getters impurities during evaporation.
- (III) The Si substrates, therefore, the silicides results, have different microstructures.
- (IV) The Si^a has a positive formation energy (about 2.8 kcal/mol for noble gas implanted Si^a [19] or about 2.4 kcal/mol for sputtered Si^a [20]), and so does Si^e .

Aside from studying the growth kinetics of silicides, we would like to know how the differences mentioned above affect the formation process of the silicides.

2.2 Experimental Procedures

Procedures of sample preparation have been published in detail in ref. [III-IV]. A general picture is sketched as follows:

- (1) Wafer cleaning: commercially prepared Si^c wafers were cleaned ultrasonically with trichloroethylene, acetone and methanol (organic cleaning) and then etched in a 20% HF solution. After a 5 min etch, the wafer was rinsed in deionized water, oxidized in RCA solution ($\text{H}_2\text{O}_2:\text{NH}_4\text{OH}:\text{H}_2\text{O} = 1:1:5$) for 5 min, and then etched in a 6% HF solution for another 5 min.

- (2) Evaporation: immediately after cleaning, the wafers were loaded into an oil-free e-gun evaporator. Si films of various thicknesses (1 kÅ to 10 kÅ) were evaporated on half of each wafer, several metal films (Ni, Co, Pt, Cr) of different thicknesses (500 Å to 4000 Å) were then deposited on the top of the full wafers. This procedure assures that the metal used on Si^c and on Si^e have the same evaporation conditions and, therefore, have similar properties. During evaporation, the pressure was kept below 3×10^{-7} Torr and the evaporation rates of metal and Si are about 35–45 Å/s and 20–30 Å/s, respectively.
- (3) Annealing: samples were then annealed in a vacuum furnace. During isothermal annealing, samples of both Si^c and Si^e substrates were placed side by side in the same boat and annealed for the same length of time. The vacuum during annealing was about 5×10^{-7} Torr. Annealing temperatures ranged from 200°C to 500°C.
- (4) Measurement: the thicknesses and atomic ratio in the silicides were measured by MeV Rutherford backscattering spectrometry (RBS). Read camera X-ray diffraction films¹ were used to establish the phases of silicides present in the sample. The surface morphology of the silicides was monitored by optical microscopy.

2.3 Results and Discussions

The silicides formed, their formation temperatures, activation

¹The X-ray diffractions were made by Bai-Xin Liu and Dr. M. Van Rossum.

Silicide	Time Dependence	Silicon Substrate	Activation Energy(eV)	Temperature Range(°C)	Ref.
Ni ₂ Si ^a	\sqrt{t}	(100)	1.5±0.1	210-335	II
	\sqrt{t}	Si ^e	1.4±0.1	210-335	II
NiSi ^b	\sqrt{t}	(100)	1.55±0.1	250-400	II
	\sqrt{t}	Si ^e	1.55±0.1	250-400	II
NiSi ₂ ^{d,i}	N. C. ^f	(100)		> 750	III
	\sqrt{t}	Si ^e	1.65±0.2	350-425	III
Co ₂ Si ^g	\sqrt{t}	(100)	1.7±0.1	385-490	IV
	\sqrt{t}	Si ^e	1.85±0.1	385-490	IV
CoSi ^g	\sqrt{t}	(100)	1.8±0.1	385-490	IV
	\sqrt{t}	Si ^e	1.9±0.1	385-490	IV
CoSi ₂ ^{d,i}	\sqrt{t}	(100)		> 500	V
	\sqrt{t}	Si ^e	2.3±0.1	405-500	V
Pt ₂ Si ^a	\sqrt{t}	(100)	1.4±0.1	194-305	II
	\sqrt{t}	Si ^e	1.4±0.1	194-305	II
PtSi ^a	\sqrt{t}	(100)	1.5±0.1	250-370	II
	\sqrt{t}	Si ^e	1.5±0.1	250-370	II
CrSi ₂ ^{a,h,i}	t	(100)	2.0±0.1	455-505	II
	t	Si ^e	2.0±0.1	400-505	II

a: Silicide grows faster on Si^e than on Si^c.

b: No visible difference in growth rates of the silicide on Si^e and Si^c.

d: Silicide will not form on Si^c below some threshold temperature.

f: Growth of the silicide is controlled by the silicide nucleation [18].

g: Silicide grows faster on Si^e than on Si^c.

h: Formation temperature of the silicide is lower on Si^e than on Si^c.

i: The silicide is more uniform on Si^e than on Si^c.

Table 1

Results on the reaction kinetics of silicides formed on Si^c (100) and the Si^e substrates.

energy, and the time dependence of thickness, are listed in Table 1. The results show that:

- (1) Some silicides have lower formation temperature on Si^e than on Si^c (namely, NiSi_2 , CoSi_2 , and CrSi_2).
- (2) Some silicides are more uniform on Si^e than on Si^c (namely, NiSi_2 , CoSi_2 , and CrSi_2).
- (3) Most silicides have faster growth rate on Si^e than on Si^c (namely, Ni_2Si , NiSi_2 , CoSi_2 , Pt_2Si , PtSi , and CrSi_2), but Co_2Si and CoSi have the reverse phenomenon.
- (4) If the formation of a silicide on Si^c is diffusion controlled (i.e., \sqrt{t} dependent) or interfacial reaction controlled (i.e., t dependent), then that time dependence remains the same on Si^e .
- (5) On Si^c , the formation of NiSi_2 or CoSi_2 has a threshold temperature [18], but not on Si^e .

That silicides that form on Si^c and Si^e have different properties can be attributed to various causes. Four have been mentioned in the introduction of this chapter and are listed in Table 2. We do not know which of these applies to any particular case. We nevertheless list those that we believe apply in each case. They are listed in Table 2 in order of their likelihood.

The impurities at the Si^c/M interface can stop the silicide formation at a temperature which is sufficient for silicide formation at the clean Si^e/M interface. When the temperature increases, the silicide forms first at weak spots of a contaminated interface. The silicide thus grows laterally nonuniformly. If the annealing temperature further increases, the effect of the interfacial impurities is much reduced. Therefore the interfacial impurities can explain why the CrSi_2 (1) has lower formation temperature when formed on Si^e than on Si^c substrates and (2) is more uniform when formed on Si^e than on Si^c . The above results are also ob-

served for the cases of TiSi_2 [14] and ErSi_2 [15]. We would like to point out that in the cases of NiSi_2 and CoSi_2 , interfacial impurities are unlikely to raise their formation temperatures or induce lateral nonuniformity. This is because the silicides are not the first one to form. On the basis that Ni or Co is the DMS in the initial phase (Ni_2Si or Co_2Si) formation, interfacial impurities will be swept out to the sample surface.

A higher bulk impurity concentration in Si^e than in Si^c can cause a lower silicide growth rate on the former Si substrate. We believe that it is one of the reasons causing slower growth rates of Co_2Si and CoSi on Si^e than on Si^c . However, the microstructural differences between the silicide formed on Si^e (small grain size, random grain orientation, and so on) and on Si^c can also cause different silicide growth rates. In general, the silicide formed on Si^e has small grain, therefore, more grain boundaries. If the grain boundary diffusion is dominant during silicide reaction, then the silicide may grow faster on Si^e than on Si^c . This result has been used to explain the faster growth rate of Ni_2Si [13] and Pd_2Si [16] on Si^e than on Si^c . On the other hand, if the bulk diffusion is dominant, then the growth rate can be slower or faster for silicide grown on Si^e than on Si^c depending on the the detailed structures of the silicide.

Positive formation energy of Si^e increases the driving force (more negative reaction free energy) for silicide formation. In general, larger driving force will only cause a higher growth rate. But in the case of thin silicides which are unstable at low temperature (NiSi_2 and CoSi_2), the positive formation energy of Si^e will decrease the silicide formation temperature. There are two possibilities to have an unstable silicide: In one case, the bulk phase silicide is considered to be nonexistent in thermal equilibrium at low temperatures [III]. In the other case, the bulk silicide barely exists, but the interface and strain energies make the thin silicide unstable at low temperature [18]. In both cases, the thin silicide is metastable on the Si^e substrate when the temperature is lower than a threshold temperature ($> 500^\circ\text{C}$ for CoSi_2 and $> 750^\circ\text{C}$

Silicides	Ref.	Comparison	Causes
NiSi	II	(1) No visible change	
Ni ₂ Si	II	(1) Grows a little faster on Si ^e than on Si ^c	(III), (IV), (I)
Pt ₂ Si	II		
PtSi ^a	II		
Pd ₂ Si	16		
Co ₂ Si	IV	(1) Grows slower on Si ^e than on Si ^c	(III)
CoSi	IV	(1) Grows slower on Si ^e than on Si ^c	(II), (III)
CrSi ₂	II	(1) Grows faster on Si ^e than on Si ^c	(I), (III), (IV)
TiSi ₂	14	(2) Reduced formation temperature on Si ^e	
ErSi ₂	15	(3) Improved silicide uniformity on Si ^e	
NiSi ₂	III	(1) Grows faster on Si ^e than on Si ^c	(IV), (III)
CoSi ₂	V	(2) Reduced formation temperature on Si ^e (3) Improved silicide uniformity on Si ^e (4) Threshold temperature for silicide on Si ^c	

a: The possible reasons for PtSi are (III) and (IV) only.

(I): The Si^e/M interface is cleaner than the Si^c/M interface.

(II): There are more impurities in Si^e than in Si^c.

(III): The silicides formed have different microstructures.

(IV): The Si^e has a positive formation energy.

Table 2

Differences between silicides formed on Si^e and Si^c and possible causes. The order of the causes represents their likelihood.

for NiSi₂). When the temperature exceeds that threshold, the growth can be very fast where the silicide nucleates. Such a growth controlled by heterogeneous nucleation then causes a laterally nonuniform silicide formation. The positive formation energy of Si^c can reduce the threshold temperature, i.e. the formation temperature. In the cases of NiSi₂ and CoSi₂, the threshold temperatures are reduced so much that the growth controlling processes are changed from this nucleation controlled processes to the diffusion controlled processes. Therefore, the silicide formed on Si^c becomes laterally uniform.

2.4 Conclusion

The formation of silicides: Ni₂Si, NiSi, NiSi₂, Co₂Si, CoSi, CoSi₂, Pt₂Si, PtSi, and CrSi₂ on the single crystalline (Si^c) and the evaporated amorphous Si (Si^e) were studied. The results are summarized in Table 1. Differences between the silicides formed on the Si^c and the Si^e are explained in terms of the different properties of Si^c/M system from those of Si^e/M system as shown in Table 2.

Chapter 3
Dominant Moving Species
during
Silicide Reactions

3.1 Introduction

In addition to the growth rates, another basic problem of silicide reactions is to identify the the dominant moving species (DMS)¹ of the reaction. We consider three kinds of silicide reactions [VI] (see Fig. 1): (1) silicide formation, (2) solid-phase-epitaxy (SPE) of Si^e through silicide, and (3) silicide oxidation. As shown in Fig. 1 the moving species can be either metal (from right to left) or Si (from left to right). It is interesting to identify and compare the DMS in the three reactions for a silicide.

Experimentally, the DMS identification can be approached with inert marker² studies. Elements that have been used as markers include noble gases such as Xe and Ar [21–24], reactive elements such as oxygen [10, X], thin inert metal layers [25, 11], and a metal with properties similar to that contained in the silicide [26–28]. All these experiments have the major disadvantage that foreign elements are introduced into the system. Those foreign atoms may affect the diffusing species. One way to improve the reliability of a result is use several different markers to do the experiments and check whether the results are all the same.

¹By “moving species” we mean the species that moves w.r.t. an inert marker².

²By “inert marker” we mean that the marker is fixed to the silicide lattice during the reaction and that it does not interfere with the reaction processes.

Another way is to compare the growth rates of samples with and without marker. If the growth rates are the same then the result may be reliable.

In this chapter, we study the DMS in thin film silicide reactions by marker (implanted Xe and ^{18}O) experiments. The DMS in a silicide during different silicide reactions (silicide formation, solid-phase-epitaxy (SPE) of Si^e through silicide, and silicide oxidation³) is studied. Most of the experiments are done for cases where the dominant moving species have not yet been reported. In some cases, we repeat previous experiments with different markers and compare our results with the published ones. In general, we find that the marker results are independent of what kind of marker is used, and that in all three silicide reactions the DMS in the silicide is the same.

3.2 Experimental Procedures

Si wafers were cleaned as in Chapter 2. Immediately after cleaning, the wafers were loaded into the evaporator described in Chapter 2. To prepare samples for the SPE study we evaporated metal (M) and Si films sequentially on top of the Si substrates (symbolized as $\text{Si}^e/\text{M}/\text{Si}^e$). The evaporation rate was about $30 \text{ \AA}/\text{s}$ with a pressure kept below 4×10^{-7} Torr during evaporation. The samples were then annealed in a vacuum furnace (pressure $\approx 5 \times 10^{-7}$ Torr) to form silicide (i.e., $\text{Si}^e/\text{silicide}/\text{Si}^e$). The thickness of the silicide and of the Si^e is in the range of few thousand \AA . After this annealing step, some of the samples were implanted at room temperature with either Xe or ^{18}O atoms as a marker. The energy of the implantation was adjusted so that the peak concentration of the ion profile lay in the silicide layer (symbolized as $\text{Si}^e/\text{silicide}(\text{Xe or }^{18}\text{O})/\text{Si}^e$) or in the Si^e layer (i.e., $\text{Si}^e/\text{silicide}/\text{Si}^e(\text{Xe or }^{18}\text{O})$). These are the as-prepared samples for SPE. The as-prepared

³The oxidation of silicides was performed by Dr. M. Bartur.

samples for oxidation had markers buried in the silicides. They were prepared using similar procedures and are designated Si^c/silicide (Xe or ¹⁸O). The as-prepared samples for silicide formation had markers buried in either the Si or in the metal film or in a thin precursor layer of the silicide formed by a brief pre-annealing step. The thicknesses of silicides were a few thousand Å.

The as-prepared samples were annealed in a vacuum furnace for silicide formation and SPE. The oxidation was conducted in a wet oxygen environment in an open tube furnace. The processes of SPE, formation and oxidation of silicide, and the movement of Xe marker were analyzed with MeV ⁴He⁺ RBS. The ¹⁸O profile was monitored by ¹⁸O(p,α)¹⁵N NRA.

3.3 Results

The DMS for several silicides in the reactions of the formation, oxidation, and SPE are listed in Table 3. The table lists other reported results (see the ref. column) as well as the results of this study (the reference is numbered by Roman numerals) for comparison. The table shows that, except for Pd₂Si, different markers give the same results for a silicide reaction. (The discrepancy in the Pd₂Si results may be due to the sensitivity of the formation of Pd₂Si to impurities (marker) in the sample or to the microstructures of the sample, as proven in Ref. 11). Another interesting consequence of the data is that, with the exception of CrSi₂, the DMS through a silicide is the same for all three kinds of silicide reactions. In the case of CrSi₂, Si is the DMS during formation, while Cr is the DMS in the cases of oxidation and SPE.

Generally, only noble gases and thin metal films are used as inert markers to determine moving species in solid state reactions. In this paper, we also use oxygen as a marker to monitor the DMS in some silicides. Table 3 shows that no matter which marker is used the results

(a) Silicide formation:

Si	$\Leftarrow J_M$ $M_\beta Si_{1-\beta}$ $J_{Si} \Rightarrow$	$M_\alpha Si_{1-\alpha}$
----	--	--------------------------

(b) SPE of Si^e through silicide:

Si ^e	$\Leftarrow J_M$ $M_\beta Si_{1-\beta}$ $J_{Si} \Rightarrow$	Si ^e
-----------------	--	-----------------

(c) Silicide oxidation:

Si	$\Leftarrow J_M$ $M_\beta Si_{1-\beta}$ $J_{Si} \Rightarrow$	SiO ₂
----	--	------------------

Figure 1

Three kinds of silicide ($M_\beta Si_{1-\beta}$) reactions are shown here. The positive direction of coordinate, x , is defined pointing from left to right. The fluxes of metal and Si are shown with arrows pointing to their respective positive directions.

Silicide	Formation			Oxidation			SPE		
	DMS	Marker or tracer	Ref.	DMS	Marker or tracer	Ref.	DMS	Marker or tracer	Ref.
NiSi	Ni	Pt	27	Ni	Xe	40	Ni ^a	Xe	VI
	Ni	¹⁸ O	10				Ni ^a	¹⁸ O	VI
NiSi ₂	Ni	Xe	39, III	Ni	Xe	37			
	Ni	W	VI	Ni	W	37			
Pd ₂ Si	Pd & Si	Ar	23	Pd & Si	¹⁸ O	VI			
	Si	W	11	Si ^b	W	37			
	Si	¹⁸ O	10						
Pd ₂ Si	Pd	I ^c	VII				Pd ^a	Xe, ¹⁸ O	VI
							Pd ^a	¹⁸ O	VI
							Pd	³¹ Si	41
PtSi	Pt	³¹ Si	42	Pt	¹⁸ O	VI	Pt ^a	¹⁸ O	VI
								Pt ^a	Xe
CoSi ₂	Co	Xe	VI	Co	Xe	37	Co	Xe	VI
	Co	¹⁸ O	VI	Co	W	37	Co	¹⁸ O	VI
							Co	W	VI
CrSi ₂	Si	Xe	43	Cr	¹⁸ O	VI	Cr	Xe	VI
	Si	¹⁸ O	XII				Cr	¹⁸ O	VI
TiSi ₂	Si	Xe	23	Si	³¹ Si	44	Si	Xe	VI
					¹⁸ O	VI	Si	¹⁸ O	VI

a: Silicide becomes Si riched after SPE.

b: Motion of marker can be due to interfacial drag.

c: Interface of epi-Pd₂Si/poly-Pd₂Si is used as a marker.

Table 3

Comparison of the dominant moving species (DMS) for formation of silicide, oxidation of silicide, and SPE of Si^c with that silicide.

are, in general, the same (except for Pd₂Si). This indicates that oxygen as well as other inert markers gives reliable data on moving species in these silicide reactions.

3.4 Discussions

It is not clear why the DMS in a silicide is the same in the three silicide reactions for most of the silicides studied here. One possible way to explain this is to postulate that the crystalline structure of a silicide has a much higher diffusivity for one species than for the other. This postulation, however, may be true for all silicides. Examination of the detailed motion of the atoms in the silicide, therefore, is needed to explain this phenomenon. In the following discussions, we will assume that all the silicide reactions occur at a fixed temperature. As shown in Fig. 1, there are, in general, two fluxes (metal flux, $J_M(x, t)$, and Si flux, $J_{Si}(x, t)$) in the silicide during the silicide reaction. It is interesting to know that if the stoichiometric range is very small (i.e., the difference of β in the silicide is much less than the average β) each flux is position independent [I]. With the above assumption and the assumption that new silicide molecules only form at the boundaries of the silicide, we can prove that the flux $J_\beta (\equiv (1 - \beta)J_M + \beta J_{Si})$ is the only physically important quantity in all three silicide ($M_\beta Si_{1-\beta}$) reactions. This can be seen from the following equations:

- (I) The total number of the molecular units $M_\beta Si_{1-\beta}$ per unit area, N_1 , (see Fig. 1 (a)) satisfies

$$dN_1/dt = \alpha/[(\alpha - \beta)\beta]J_\beta. \quad (3.1)$$

- (II) The total number of Si^e transported per unit area, N_2 , (see Fig. 1 (b)) satisfies

$$dN_2/dt = 1/\beta J_\beta. \quad (3.2)$$

(III) The total number of SiO_2 formed per unit area, N_3 , (see Fig. 1 (c)) satisfies

$$dN_3/dt = 1/\beta J_\beta. \quad (3.3)$$

We will assume that (A1)⁴ stoichiometric ranges of silicides are small (how true this is is unknown for almost all the silicides) and (A2) new silicide forms only at the boundaries of the silicide. Therefore to determine the DMS in the silicide during any silicide reaction, we just need to calculate the ratio $R \equiv (1 - \beta)J_M/[\beta J_{Si}]$ (i.e., if $1 \ll R$, then M is the DMS and if $R \ll 1$, then Si is the DMS). To compare the above-mentioned fluxes, we need to know the detailed expression of each flux, which is [17, 1]:

$$J_M(x, t) = J_M(t) = D_M \Delta C_M^{eq} / (X_{Ml} + X + X_{Mr}) \quad (3.4)$$

and

$$J_{Si}(x, t) = J_{Si}(t) = D_{Si} \Delta C_{Si}^{eq} / (X_{Sul} + X + X_{Sir}), \quad (3.5)$$

where D_A is the diffusion constant of A atoms in the silicide, ΔC_A^{eq} is the difference of the equilibrium concentration of A at the two interfaces, X is the thickness of the silicide, and X_{Al} and X_{Ar} are constants characterizing the rates of the interfacial reactions of A atoms at the left and right interfaces (see Fig. 1), respectively. From eqs. (3.4) and (3.5), we can roughly say that the magnitude of the flux of A atoms is the thermodynamical driving force (ΔC_A^{eq}) times the kinetics factor ($D_A/(X_{Al} + X + X_{Ar})$). We will assume that (A3) $\Delta C_M^{eq} \approx \Delta C_{Si}^{eq}$ in any silicide reaction so that the change of DMS from one reaction to another can only be due to the change of the kinetics factor. We also assume that (A4) the thicknesses of silicide, X , in all three reactions are similar during reaction. Therefore, the only factors that differ from one reaction to another are X_{Mr} and X_{Sir} (note that the left interfaces in all three reactions are very similar).

⁴(A_n) stands for the nth assumption.

In this case, the ratio R is

$$\begin{aligned} R &= [(1 - \beta)D_M / (X_{Ml} + X + X_{Mr})] / [\beta D_{Si} / (X_{Sil} + X + X_{Sir})] \\ &= R_0(1 + R_M) / (1 + R_{Si}), \end{aligned} \quad (3.6)$$

where $R_0 \equiv (1 - \beta)D_M / (\beta D_{Si})$ is constant for all three reactions and $R_A \equiv (X_{Al} + X_{Ar}) / X$ for atom A changes from one reaction to another. We therefore have the following cases:

If R_0 is very small or very large and the changes in R_M and R_{Si} from reaction to reaction are mild, the value of R will be dominated by that of R_0 so that the DMS is the same for all three reactions.

This explanation is, in fact, a generalization of the explanation given in the beginning in this section. Alternatively,

If R_0 is near 1 or the changes in R_M and R_{Si} from reaction to reaction are large, then the DMS will differ for the different reactions.

Experimentally, the silicide formation can be controlled either by the diffusion process or the interfacial reactions [1]. This is explained as $X_{Al} + X_{Ar} \ll X$ or $X_{Al} + X_{Ar} \ll X$, where A is the DMS in the case of silicide formation [17]. If the silicide formation is diffusion controlled, it is very likely that the R_0 dominates ((A5)). In that case the DMS is the same in all reactions, as the experiment data in Table 1 show. If the silicide formation is controlled by interfacial reaction, then it is quite possible that the R_0 is not dominant ((A6)). In that case the DMS will be different for the different silicide reactions. This is the case for CrSi_2 the formation of which is controlled by the interfacial reactions at the interfaces of CrSi_2 [1]. The DMS in CrSi_2 indeed changes from Si to Cr when the reaction changes from the formation to the SPE or oxidation.

If the activation energies of the physical quantities discussed here are different, a change in the temperature may have a different effect from one silicide reaction to another. The present treatment thus implicitly assumes that (A7) temperature has no effect over the range considered.

3.5 Conclusion

The DMS in the silicide during the silicide formation, during solid-phase-epitaxy of Si^e through silicide, and during silicide oxidation has been measured. The results are discussed in terms of the atomic fluxes that can flow through the silicide. It is concluded from this analysis (with several assumptions) that, if the silicide formation is diffusion controlled, all three reactions have the same DMS and that if the silicide formation is interfacial reaction controlled, different reactions may have different DMS.

Chapter 4
Tracer Profiles in Silicide
after
Silicide Formation

4.1 Introduction

As shown in the previous chapter, the DMS during silicide reactions can be measured by inert marker experiments. However, an inert marker experiment can not resolve the mechanism by which the DMS diffuses (interstitial (or grain boundary) or vacancy diffusion). One way to classify the diffusion mechanism of the moving species is to bury a thin layer of a radioactive isotope (tracer, e.g., ^{31}Si and ^{56}Ni) of the species in the sample and monitor the evolution of that tracer layer during the reaction [29–37]. Fig. 2 (a) shows an as-deposited sample for such a tracer study which has a thin layer of ^{31}Si deposited on top of the non-radioactive Si (Si^n) substrate, followed by a metal overlayer. Fig. 2 (b) shows a sample in which all the ^{31}Si is just consumed to form silicide. By annealing further, additional metal will be consumed to form silicide. We can then measure the ^{31}Si profile of the sample. Information about the atomic motion can be obtained from the tracer profile. However, theoretically it is much easier to calculate the tracer profile from an assumed atomic motion than to try to determine the mechanism of atomic motion from an experimental tracer profile. One therefore typically proposes a model and calculates tracer profiles from the assumed atomic mechanism. The calculated profiles are then compared with the experimental ones. Agreement between the two means that the assumed mechanism is consis-

(a) As deposited:

Si^n	^{31}Si	M
---------------	------------------	------------

(b) ^{31}Si is just consumed to form silicide:

Si^n	$\text{M-}^{31}\text{Si}$	M
---------------	---------------------------	------------

Figure 2

Schematics of the sample used for an ^{31}Si experiments: (a) initial tracer position, and (b) a sample when Si tracer is just consumed to form silicide.

tent with the data. Agreement does not prove, however, that the assumed mechanism is in fact present; it provides only one possible interpretation.

In this chapter, we will review the models which were proposed to calculate the tracer profiles and point out their deficiencies. We propose an improved model which offers good insight into what information can be obtained from the tracer experiments.

(i) Si is the DMS and moves interstitially:

Si^n	$\text{M-}^{31}\text{Si}$	M-Si^n
---------------	---------------------------	-----------------

(ii) Si is the DMS and moves by vacancy mechanism
or metal is the DMS:

Si^n	M-Si^n	$\text{M-}^{31}\text{Si}$
---------------	-----------------	---------------------------

Figure 3

Schematics for the model proposed by Pretorius et al. [29] to explain the profile of ^{31}Si when the metal is completely consumed.

4.2 Models

Several models have been used to predict the tracer profiles, assuming various mechanisms of atomic motion:

(I) Model 1: Pretorius et al. [29] proposed a model to interpret the Si tracer (^{31}Si) profile after silicide formation (see Fig. 3):

(a) If Si is the DMS which moves interstitially, the profile of tracer stays at the Si/silicide interface (see Fig. 3 (i)).

- (b) If Si is the DMS and moves by a vacancy mechanism, or if the metal is the DMS (whatever the mechanism), the tracer profile uniformly translates to the sample surface (see Fig. 3 (ii)).
- (c) If both mechanisms in (a) and (b) occur, the tracer profile is a combination of these two cases.

The deficiency of this model is that it ignores the self-diffusion of the tracer itself. This process cannot be neglected when Si (the DMS) diffuses through its sub-lattice of the silicide via a vacancy mechanism.

(II) Model 2: Pretorius et al. have used a computer simulation program to calculate ^{31}Si tracer profiles [36]. The calculated profile, in this case, contains a parameter that allows for an interchange of interstitial and substitutional Si ("exchange probability") [36]. Since the atomic mechanism in the silicide is not clearly specified in the simulation, we have reconsidered this problem and modeled it mathematically to reinterpret the simulation result [VIII]. In our model, we assume that Si is the DMS, that Si moves interstitially and convectively, and that the mobile interstitial Si can exchange position with the lattice Si which is assumed to be otherwise fixed in space. The tracer profiles are fitted by calculated profiles with the exchange probability as a parameter (see Fig. 4).

This model predicts that

- (a) If the exchange rate is zero, the profile of tracer stays at the initial position (see Fig. 4 (i)).
- (b) If the exchange rate is infinite, then the tracer profile uniformly translates to the sample surface (see Fig. 4 (ii)).
- (c) If the exchange rate is finite, then the tracer profile is the

(i) No exchange:

Si^n	$\text{M-}^{31}\text{Si}$	M-Si^n
---------------	---------------------------	-----------------

(ii) Exchange rate is infinite:

Si^n	M-Si^n	$\text{M-}^{31}\text{Si}$
---------------	-----------------	---------------------------

Figure 4

Schematics for a computer simulation proposed by Pretorius et al. [36] and a mathematical model by the author of this thesis [VIII] to explain the ^{31}Si profile (assuming that Si is the DMS, Si moves interstitially and convectively, and that the mobile interstitial Si can exchange position with the fixed lattice Si).

combination of the cases of Fig. 4 (i) and (ii).

Model 2 neglects the random motion of the mobile interstitial Si^1 ; i.e., the model assumes the mobile Si moves convectively. In the Ref. VIII, we

¹The author acknowledges T. Barwell who pointed out to me that the random motion of Si is not considered in the model.

(i) Si moves interstitially and does not exchange position with fixed Si:

Si^n	$\text{M-}^{31}\text{Si}$	M-Si^n
---------------	---------------------------	-----------------

(ii) Si moves by vacancy, or moves interstitially with an infinite exchange rate with fixed Si, or metal is the DMS with high Si mobility:

Si^n	M-Si^n
	$\text{M-}^{31}\text{Si}$

(iii) Metal is the DMS and the Si does not move:

Si^n	M-Si^n	$\text{M-}^{31}\text{Si}$
---------------	-----------------	---------------------------

Figure 5

Schematics for the Model 3 proposed in ref. IX to explain the profile of Si tracer (^{31}Si).

point out that the random motion of the mobile Si cannot be neglected.

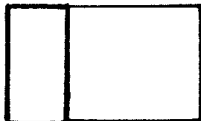



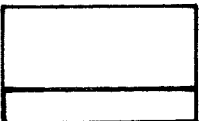
(III) Model 3: This model removes the deficiencies mentioned above [IX] (see Fig. 5):

- (a) If the interstitial Si is the DMS and does not exchange position with the lattice Si which is assumed to be fixed in space, the tracer profile then stays at the Si/silicide interface (see Fig. 5 (i)).
- (b) (1) If the lattice Si is the DMS, or (2) if the interstitial Si is the DMS and exchanges position with the fixed lattice Si at a very fast rate, or (3) if metal is the DMS and the lattice Si self-diffuses rapidly (note that (1) and (2) are, in fact, very similar), the tracer profile then is flat in the silicide (see Fig. 5 (ii)).
- (c) If the metal is the DMS and the Si can not diffuse, the tracer profile then uniformly translates to the sample surface (see Fig. 5 (iii)).
- (d) If the atomic motion is a combination of those mentioned above, the tracer profile then is the combination of the above cases.

The tracer profile in case (b) (1) and (2) is obtained in Ref. IX through a rigorous calculation. That a flat tracer profile will be observed can be seen from the fact that the diffusion length of the tracer must be comparable to or larger than the film thickness which grows as a result of this diffusion process. The detailed formulation and calculation are given in Ref. IX.

4.3 Discussion

From model 3, we observe that the assumption that there is a DMS (cases (1) and (2) described below) leads to the following conclusions (see also Table 4):

Tracer profiles	Information		
	DMS	Mechanism of DMS	Other
	Si	Purely interstitial or grain boundary	
	Si	Dominantly interstitial ^a or grain boundary	
	M	unknown	effective D_{Si} value
	M	unknown	negligible effective D_{Si}
	Si^i	Vacancy or interstitial ^b or any mechanism +	high D_{Si}
	M^i	unknown	high effective D_{Si}

a: Or purely interstitial + exchange with lattice Si.

b: Interstitially Si exchanges sites with lattice Si at a high exchange rate.

i: The DMS data are obtained from inert marker experiments.

Table 4

Information that can be obtained from the Si tracer profile after silicide formation.

- (1) If the tracer profile is not flat after silicide formation, the tracer experiments can be used to identify the DMS. For example, if the metal

is the DMS, the ^{31}Si atoms are located close to the sample surface; if Si is the DMS, the ^{31}Si atoms are located near the Si/silicide interface. In fact, the tracer here acts as an inert marker, because the tracer atoms are immobile. Additional information can also be obtained as follows:

- (a) If ^{31}Si is used as a tracer and if Si is found to be the DMS (i.e., the tracer is located at the Si/silicide interface after the reaction), the Si transport mechanism is dominated either by interstitial or by grain boundary diffusion.
 - (b) If ^{31}Si is used as a tracer and if metal is found to be the DMS (i.e., the tracer is located at the sample surface after the reaction), the effective diffusion constant of Si (D_{Si}) in the silicide can be estimated from the spreading of the tracer profile. However, this diffusivity value may only be true when reaction takes place.
- (2) If the tracer (e.g., ^{31}Si) profile is flat after reaction, we need an inert marker experiment to determine the DMS. With the DMS information, the following information is known:
- (a) If Si is the DMS, then either it diffuses in the silicide by a vacancy mechanism (or equivalently, it diffuses interstitially and during its movement, it exchanges sites with the lattice Si at a high exchange rate) or Si has a high diffusion constant in the Si sublattice (no matter what the mechanism of the DMS Si is).
 - (b) If metal is the DMS, then Si has a high diffusion constant in the Si sublattice. This case is, however, very unlikely due to the belief that the high diffusion constant species is, in general, the DMS.
- (3) If the fluxes of both atomic species are comparable, it is not easy to obtain information on the mechanisms of the atomic motion from tracer profiles.

4.4 Conclusion

- (1) Experimental Si tracer profiles are matched with the profile calculated from assumed atomic diffusion mechanism. However, the result obtained may not be unique.
- (2) If the Si tracer profile is not flat after silicide formation, the tracer experiments can be used to identify the DMS.
 - (a) If Si is found to be the DMS, the Si transport mechanism is dominated by interstitial or grain boundary diffusion.
 - (b) If metal is found to be the DMS, the effective diffusion constant of Si (D_{Si}) in the silicide can be estimated from the spreading of the tracer profile.
- (3) If the tracer (e.g., ^{31}Si) profile is flat after reaction, we need an inert marker experiment to determine the DMS.
 - (a) If Si is the DMS, then either it diffuses in silicide by a vacancy mechanism (or equivalently, it diffuses interstitially and during its movement, it exchange site with the lattice Si in a high exchange rate) or Si has a high diffusion constant in the Si sub-lattice (no matter what mechanism of the DMS Si is).
 - (b) If metal is the DMS, then Si has a high diffusion constant in the Si sub-lattice.

Chapter 5
Effect and Redistribution of Oxygen
in
Silicide Formation

5.1 Introduction

When we measure the growth rate and DMS of a silicide, we use samples which are as clean as possible. However, the reproducibility of the experimental results can be affected by the presence of impurities. Impurities can affect the properties of silicides directly by virtue of their presence; e.g., impurities in a silicide film may change the film's resistivity [46, 47], etching properties [55], stress [56], adhesion to the substrate [57], and many other parameters, such as grain size, thermal expansion coefficient, oxidation rate etc.. Impurities can also alter the properties of silicide indirectly by altering silicide formation processes; e.g., impurities in the sputtering gas can affect the stoichiometry of a deposited film [X, 48, 49], or they can modify the phase of a silicide formed by reaction of a metal film with an Si substrate [10, 50-54] or the DMS [11]. In this chapter, we will study the effect and redistribution of implanted ^{18}O in silicide formation, with atomic concentrations of oxygen of a few percent or less. The advantages and drawbacks for using ^{18}O (natural abundance $\approx 0.204\%$), instead of ^{16}O (natural abundance $> 99.7\%$), are discussed in ref. XI.

We can always classify an impurity as a bulk impurity when it is present in the bulk of a sample or as an interfacial impurity when it is present at the interface of a sample [X]. We can categorize a bulk impurity in terms of its redistribution during silicide formation as shown

in Table 5. The entries in the table identify the main mechanisms that are responsible for the redistribution of the impurity. Two limiting behaviors of the impurity are conceivable, depending on whether the diffusion rate of the impurity is much slower than (defined as immobile impurity) or comparable to or higher than (defined as mobile impurity) the silicide growth rate at an annealing temperature. The samples discussed here are a metal or silicide layer on the top of an Si substrate. The main questions here are how the impurity redistributes upon silicide formation and how this alters the growth rate of the silicide. For an immobile impurity, its redistribution is mostly determined by the kinetics of the silicide formation. We distinguish between two cases where the diffusion of the impurity is enhanced by the silicide formation (category II) and where it is not (category I). For mobile impurities (category III) the redistribution is determined by both the diffusion of the impurity and the kinetics processes of silicide formation.

In addition to bulk impurities, the interfacial impurities (only interfacial oxide is considered here) also have significant effects on silicide formation. Here, we will define the interfacial oxide layer as thin, thick, or nonuniform functionally by its effect on the silicide formation. For the thin interfacial oxide layer, the silicide reaction proceeds laterally uniformly, while for the thick interfacial oxide layer, the silicide formation is stopped completely. A nonuniform interfacial impurity layer is one which is thin in some places and thick in others. The redistribution of the interfacial oxide and its effect are similar to category I in Table 5.

5.2 Experimental Procedures

Generally, samples were prepared by evaporating a thin metal film either on a chemically cleaned Si substrate (to study bulk impurity effects) or a Si substrate with a thin oxide on the top (to study interfacial oxide effects). The sample cleaning and the evaporating procedures are

		Impurity redistributions	
		immobile	mobile
reacting silicide or metal film on Si	no diffusion enhancement	I kinetics of silicide formation	III diffusion + kinetics of silicide formation
	diffusion enhancement	II kinetics of silicide formation	

Table 5

Three categories of bulk impurity redistributions in media with different impurity diffusion rates during annealing. Entries in the table identify the main mechanisms for the impurity redistribution.

the same as described in Chapter 2. To study the effect of bulk oxygen in silicide formation, we have implanted ^{18}O either into the Si substrate or into the top (metal or silicide) layer. Unimplanted and implanted samples are then annealed in a vacuum furnace. To study the effect of the interfacial oxygen, we have prepared samples (of structure Si/SiO₂/M) with a thick interfacial oxide and used ion irradiation to break up the oxide. If the irradiation dose is low, the oxide is still thick. As the dose increases the oxide is thin in some places and thick otherwise. When the dose is further increased, the barrier becomes thin. Samples with thick, nonuniform, and thin interfacial oxide are annealed in vacuum together and then measured. The experimental techniques used to study the silicides and the distribution of impurities are RBS, $^{18}\text{O}(p,\alpha)^{15}\text{N}$ NRA, X-ray diffractions, secondary ion mass spectrometry (SIMS), and optical microscopy.

5.3 Results and Discussion

5.3.1 Bulk oxygen

The redistribution and the effect of impurities in samples whose initial structure consists of a reacting film on an Si substrate are listed in Table 6. We have classified the bulk impurities into immobile (category I and II) and mobile (category III) impurities during silicide formation, as defined in Table 5. The immobile case is subdivided into groups with (I) or without (II) enhanced impurity redistribution. For the mobile impurities, we cannot in general distinguish between a redistribution process with or without enhancement; therefore, only one category (III) is used here.

Scott has proposed a model [10] to explain the redistribution and the effect of oxygen and nitrogen in silicide formation in terms of two parameters, viz., the moving species during silicide formation and the reactivity of the impurity with the metal and the Si. The model is generalized in ref. [X] by the author of this thesis for all the immobile impurities (category I) and uses only the moving species parameter to explain the redistribution and the effect of impurities. The modified model (see Fig. 6) assumes that there is a dominant moving species during the silicide formation (say metal (M)) and a stationary species (say Si) (i.e., M atoms dissociate at silicide/M interface, migrate through the silicide and form silicide with Si atoms at Si/silicide interface). If the immobile impurity (I) is initially present in the stationary species layer (see Fig. 6 (a)), then the impurity will stay stationary with respect to the stationary species during silicide formation due to its immobility. Therefore the impurity will be uniformly diluted and incorporated in the silicide. In this case impurities may slow down the growth rate of silicide but the effect is generally small.

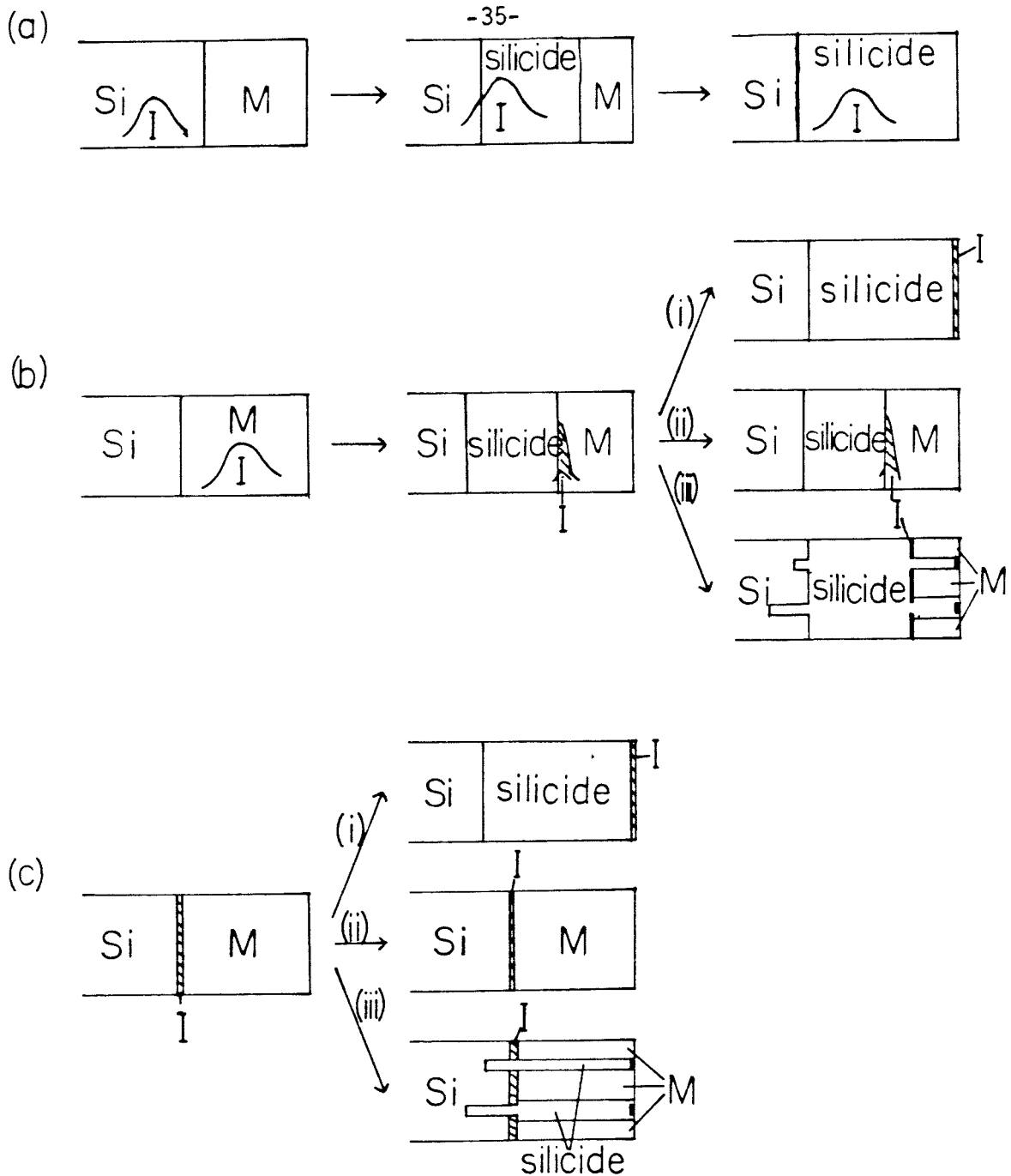


Figure 6

A model is proposed to explain the redistribution of the immobile impurity during silicide formation. The impurity is initially located either (a) in the stationary species layer, or (b) in the moving species layer, or (c) at the Si/metal interface [10, X]. In all cases, the metal (M) is assumed to be the moving species and Si to be the stationary species.

If the impurity is initially present in the layer of the moving species (see Fig. 6 (b), which assumes that metal is the DMS), then as the metal atoms leave the silicide/M interface and migrate through silicide, the impurity is left behind and accumulates at the silicide/M interface during silicide formation. Therefore either (i) the impurity is ultimately accumulated at the silicide surface (similar to the thin interfacial impurity, see next section), or (ii) the impurity that accumulates at the silicide/metal interface interferes with the reaction so much that the silicide formation is stopped uniformly with an unreacted metal film remaining (similar to the case of thick interfacial barrier, see next section). A parallel combination of these two cases (see Fig. 6 (b) (iii)) can lead to laterally nonuniform layers (similar to the nonuniform interfacial impurity case, see next section). An immobile impurity initially present in the moving species layer therefore has more of an effect on growth rate than when it is initially located in the stationary species layer.

For our cases of NiSi_2 , Co_2Si , CoSi , Pt_2Si , and CrSi_2 , oxygen is immobile in the sample (see Table 6) and the experimental results are as predicted by the model described in Fig. 6. For the case of oxygen initially in the Pd or Ta film, the previous model can not explain the profile of oxygen during silicide formation. Two possibilities can happen: The first is that a large number of point defects are generated in the vicinity of the Si/silicide interface during the formation of silicides and these defects enhance the diffusivity of oxygen (category II) [58]. The second is that the oxygen is mobile during silicide formation (category III). The oxygen redistribution then is a net result of both its own diffusion and the silicide formation processes.

5.3.2 Interfacial oxide

Interfacial impurities can drastically affect the stability of a contact. Immobile impurities present at the Si/M interface can be charac-

silicide	Location of ^{18}O		Growth rate	Conservation of ^{18}O	Refs.	Category (table 1)
	as-prepared	annealed				
NiSi_2^*	NiSi	NiSi_2	slow	yes (^{18}O)	III	I
	NiSi	NiSi_2	slow	yes (Xe)	III	I
Co_2Si	Co	$\text{Co}_2\text{Si}/\text{Co}$	same	yes	XIII	I
	Si	Co_2Si	fast	yes	XIII	I
CoSi	Co	$\text{Co}_2\text{Si}/\text{Co}$	same	yes	XIII	I
	Si	$\text{CoSi}/\text{Co}_2\text{Si}$	slow	yes	XIII	I
Pd_2Si	Pd	Pd_2Si	same	loss	XV	II or III
	Si	$\text{Si}/\text{Pd}_2\text{Si}$	slow		XV	I
Pt_2Si	Pt	$\text{Pt}_2\text{Si}/\text{Pt}$		yes	XI	I
CrSi_2	Cr	CrSi_2	slow	yes	XII	I
	Si	Si/CrSi_2	slow	yes	XII	I
TaSi_2	Ta	$\text{Ta}+\text{TaSi}_2$	slow	loss	XIV	II or III
	Si	Si/TaSi_2	slow	yes	XIV	I

*: Xe as well as ^{18}O were implanted as an impurity

Table 6

Redistribution and effect of implanted ^{18}O in samples: Si/M or Si/silicide.

terized as thin, thick, or nonuniform interfacial barriers and are defined as follows (see Fig. 6 (c)):

- (I) Thin barrier: The interfacial impurity is not able to stop the uniform silicide formation and is therefore pushed to the silicide/moving species layer interface (see Fig. 6 (c) (i), and compare this with Fig. 6 (b) (i)).
- (II) Thick barrier: The impurity stops the silicide formation completely (see Fig. 6 (c) (ii), and compare this

Metal	Impurity	Temperature annealed (°C)	Rough interface	Silicide Formation	Location of impurity	Refs.
Ni	O ^a	250 (20min)		stopped		59
	O ⁱ	400 (1h)		stopped		XVI
	O ^{i,j}	400 (1h)	yes	NiSi ?	NiSi	XVI
	O ^{i,k}	400 (1h)	no	NiSi	surface	XVI
Pd	O ⁱ	400 (1h)		stopped		XVI
	O ^{i,j}	400 (1h)	yes	Pd ₂ Si	Pd ₂ Si	XVI
	O ^{i,k}	400 (1h)	no	Pd ₂ Si	Si/Pd ₂ Si	XVI
Pt	O ^a	250 (20min)		stopped		60
	O ⁱ	400 (1h)		stopped		XVI
	O ^{i,j}	400 (1h)	yes	PtSi ?	PtSi	XVI
	O ^{i,k}	400 (1h)	no	PtSi	surface	XVI
Cr	O ^a	450 (45min)	yes			60

a: Si oxidized in solution : NH₄OH: H₂O₂: H₂O = 1: 1: 5.

i: Si oxidized in an ¹⁸O plasma (thick interfacial barrier).

j: Sample was implanted with few × 10¹⁵ Si/cm² (nonuniform barrier).

k: Sample was implanted with 5 × 10¹⁵ Si/cm² (thin barrier).

Table 7

Redistribution and effect of interfacial impurities in samples consisting of a Si substrate and a metal overlayer.

with Fig. 6 (b) (ii)).

(III) Nonuniform barrier: The barrier is thin in some places and thick in others. From the above definition, silicide forms only at the thin part of barrier (see Fig. 6 (c) (iii), and compare this with Fig. 6 (b) (iii)).

Note that the definition for an interfacial barrier depends on the sample (i.e., the same interfacial oxide can be thin for some silicides and

thick for others), the annealing temperature (e.g., a barrier which is thick at low temperature can be thin at high temperature), and so on. In the case of a nonuniform barrier, the silicide formed has a rough Si/silicide interface and a nonuniform surface morphology (compare with Fig. 6 (b) (iii)). The effect and redistribution of an interfacial impurity are listed in Table 7.

Examples of thin, thick, and nonuniform interfacial oxides are given in Ref. XVI in which a near-noble metal (Ni, Pt, or Pd) film was evaporated on an ^{18}O plasma-oxidized Si substrate. Si was then implanted through the interfacial oxide. Implanted and unimplanted samples were annealed at 400°C for 1 hr.. RBS spectra show that after a high dose (5×10^{15} Si/cm 2) implantation, the silicide forms very uniformly (i.e., thin barrier); an unimplanted sample does not react at all (i.e., thick barrier); after a low dose (few $\times 10^{15}$ Si/cm 2 or less) implantation, a nonuniform silicide forms (i.e., nonuniform barrier). The profiles of ^{18}O measured with $^{18}\text{O}(p,\alpha)^{15}\text{N}$ nuclear reaction show that the locations of ^{18}O are consistent with the predictions of the model shown in Fig. 6 (c): the ^{18}O profile in the high dose implanted sample is very narrow and locates at the silicide/moving species interface; the ^{18}O profile in the low dose implanted sample is broad and located in the silicide; for the unimplanted sample, the ^{18}O stays at the Si/metal interface and the silicide reaction is stopped (an example of Si-Pt system is shown in Fig. 7).

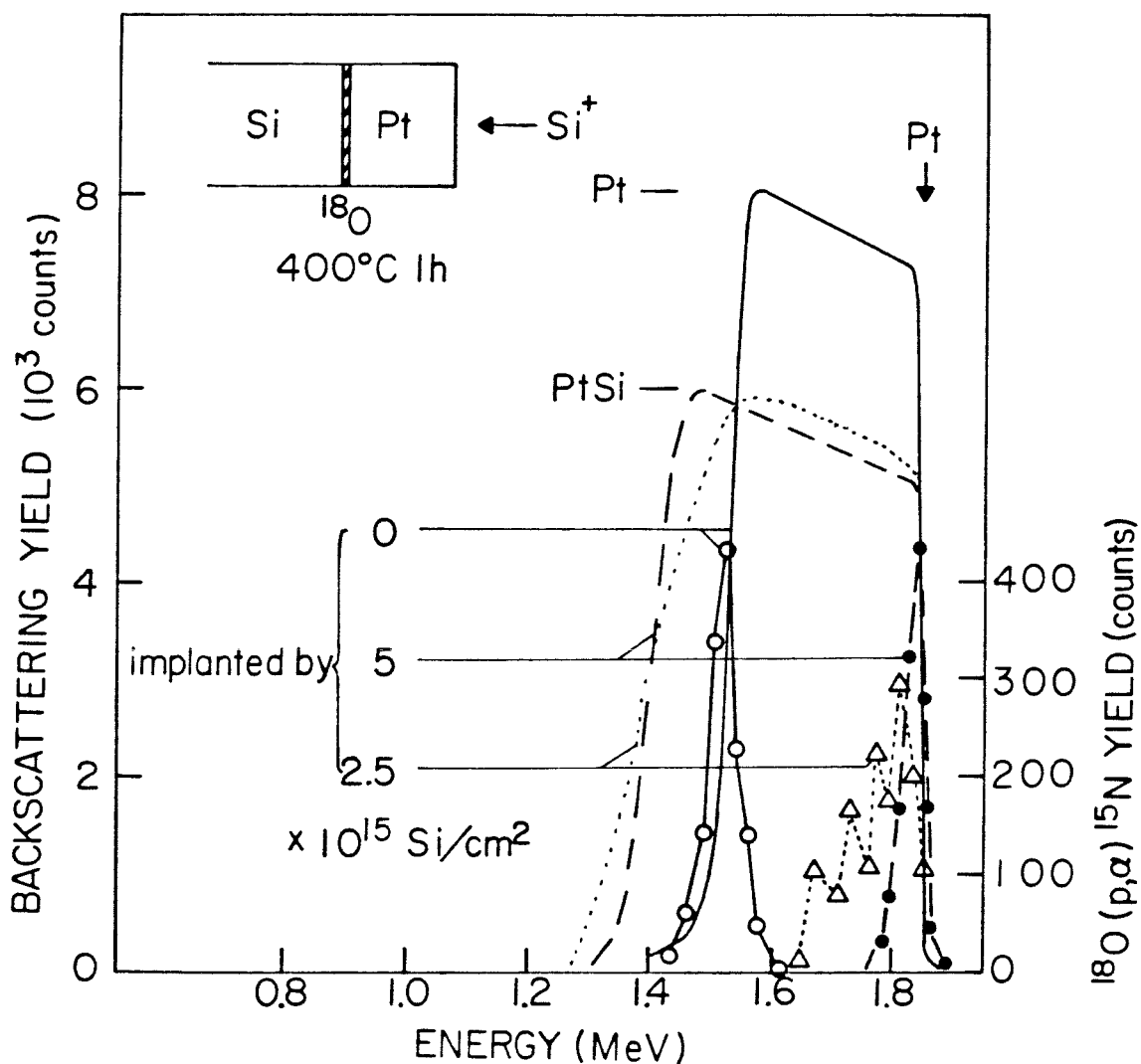


Figure 7

2 MeV RBS spectra (Pt signal only) of Si-Pt samples annealed at 400°C for 1 hr.. Solid line shows the spectrum of the unimplanted sample. Dotted-lines and dashed-lines show the spectra of 2.5×10^{15} and 5×10^{15} Si/cm² implanted samples, respectively. The ¹⁸O signals of the unimplanted sample (open circles), the low dose implanted sample (triangles), and the high dose implanted sample (full circles) are also shown here [XVI].

Chapter 6
Electrical Properties
of
Thin Co Silicides

6.1 Introduction

The electrical properties of silicides are as important as other properties studied in the previous chapters. However, to get reliable electrical data, we need a clean and uniform silicide. In this chapter, we study the Schottky barrier height and electrical resistivity of Co silicides formed from Si^c.

6.1.1 Schottky Barrier Height

With the trend toward smaller geometries, it is important to consume small amounts of Si from the Si substrate in forming silicides, [8, 9], to use low temperature processing for the silicide formation, and to have a uniform Si/silicide interface. We have shown that CoSi₂ can be formed at 400°C from Si^c, while temperatures > 500°C are required when formed from Si^v. The disilicide thus formed is laterally more uniform than that formed from Si^c, while consuming only a limited amount of Si from the substrate. Therefore a CoSi₂ contact formed from Si^c is preferable, in those respects, to a contact of CoSi₂ formed from Si^v. The advantages of using CoSi₂, instead of Co₂Si or CoSi, are that CoSi₂ is the final phase in the Co-Si reaction and therefore is stablest in subsequent high temperature processes, and that CoSi₂ has the lowest resistivity (about 18 Ωcm) which minimizes the lateral resistance of a small contact.

In the first part of this chapter, we investigate Schottky barrier height of Co silicides formed on an n-type Si^c substrate from a Co-Si^c or Co-Si^e reaction. The Schottky barrier heights of Co silicides were measured by using forward and reverse I-V methods.

6.1.2 Resistivity

Silicides have been studied with increasing interest as low resistivity interconnections for integrated circuits [1, 2]. As the dimensions of integrated circuits scale down, it is important to minimize the resistivity because line scaling increases the sheet resistance, therefore the propagation delay. Knowledge of the electrical characteristics of these films is therefore important. The mobility and carrier concentrations of thin-film silicides are typically unknown [63].

In the second part of this chapter, we investigate the electrical transport properties of Co₂Si, CoSi, and CoSi₂ formed by solid phase reaction between Co and evaporated Si (Si^e) films on SiO₂ substrates. Si^e instead of crystalline Si (Si^c) was chosen because CoSi₂ films can be formed from Si^e at lower temperature than from Si^c [v]. This procedure considerably improves the control of the thickness and the uniformity of the resulting disilicide [v].

6.2 Experimental Procedures

6.2.1 Schottky Barrier Height

Samples were cleaned as described in Chapter 2. Immediately after cleaning, the wafers were loaded into an oil-free e-beam evaporator. Half of each wafer was covered with a thin Ni mask with holes of 1 mm

diameter. After evaporation, the masked parts of the wafers had circular dots for measuring the barrier height. The unmasked parts of the wafers were used to monitor the silicide formation.

Three kinds of samples were prepared by consecutive evaporation of Co and B-doped Si ($\text{Si}^e(\text{B})$) with resistivity 0.005–0.015 Ωcm , resulting in the following configurations:

sample I: $\text{Si}^e(100)/\text{Co}$ ($\approx 370 \text{ \AA}$),

sample II: $\text{Si}^e(100)/\text{Co}$ ($\approx 370 \text{ \AA}$)/ $\text{Si}^e(\text{B})$ ($\approx 1800 \text{ \AA}$),

sample III: $\text{Si}^e(100)/\text{Co}$ ($\approx 50 \text{ \AA}$)/ $\text{Si}^e(\text{B})$ ($\approx 1200 \text{ \AA}$)/ Co ($\approx 320 \text{ \AA}$).

The p^+ $\text{Si}^e(\text{B})$ was used so that in the I–V measurement the diodes had low series resistance and the silicide/ Si^e interface was an ohmic contact. The evaporation rates of Si and Co were about 25 and 40 $\text{\AA}/\text{s}$, respectively. During evaporation, the pressure was kept below 4×10^{-7} Torr. The samples were subsequently annealed in vacuum (pressure $\approx 5 \times 10^{-7}$ Torr) at temperatures ranging from 350°C to 550°C

6.2.2 Resistivity

Thermally grown SiO_2 wafers were organically cleaned as described in Chapter 2. Samples were then blown dry with nitrogen and loaded into an oil-free electron-beam evaporation system. An Si film (about 2000–4000 \AA thick) followed by a Co film (about 450–1000 \AA) was evaporated at rates of 25 $\text{\AA}/\text{s}$ and 35 $\text{\AA}/\text{s}$, respectively. During evaporation, the pressure was kept below 4×10^{-7} Torr. The samples were subsequently annealed in vacuum (pressure $\approx 5 \times 10^{-7}$ Torr) at temperatures ranging from 450°C to 500°C for different durations.

2 MeV $^4\text{He}^+$ RBS and Read camera X-ray diffractions were used to identify the thicknesses and phases of the silicides formed. The sheet resistance and the Hall coefficient of the silicide layers were measured with

	temp.	350°C	400°C	450°C	450°C	500°C	550°C
	time	30 min	30 min	30 min	180 min	30 min	30 min
	silicide	?	CoSi	CoSi	CoSi ^a	CoSi ₂	CoSi ₂
I	F I-V ^b	0.66(1.25)	0.67(1.13)	0.67(1.07)	0.67(1.06)	0.65(1.06)	0.64(1.07)
	R I-V ^b	0.67	0.67	0.66	0.66	0.64	0.62
II	F I-V	0.66(1.24)	0.67(1.14)	0.67(1.07)	0.66(1.08)	0.65(1.06)	0.65(1.05)
	R I-V	0.67	0.67	0.66	0.65	0.65	0.66
III	F I-V	0.69(1.08)	0.67(1.08)	0.67(1.07)	0.65(1.07)	0.65(1.07)	0.66(1.03)
	R I-V	0.69	0.67	0.67	0.65	0.65	0.66

a: silicide formed in sample II and III is CoSi₂, not CoSi.

b: F I-V and R I-V stand for forward and reverse I-V, respectively.

Table 8

The table lists Schottky barrier heights (in eV) of Co silicides on an n-type (100) Si in samples whose configurations prior to annealing were I (Si^c/Co), II (Si^c/Co/Si^c(B)), and III (Si^c/Co/Si^c(B)/Co) [xvii].

Van der Pauw method at room temperature. In general, the samples used were cleaved squares (≈ 1 cm on side). The magnetic field (B) used was about 4kG.

6.3 Results and Discussion

6.3.1 Schottky Barrier Height

During annealing, Co₂Si and CoSi start to form simultaneously at the Si^c/Co and Co/Si^c (if there is any) interfaces and the Co₂Si transforms into CoSi once all the Co is consumed. The Co-Si^c reaction is

slightly slower than the $\text{Si}^c\text{-Co}$ reaction, as reported in Chapter 2 and Ref. IV. When all the Co_2Si is transformed into CoSi , CoSi_2 starts to grow only at the CoSi/Si^c interface if there is one [v]. There is no reaction at the Si^c/CoSi interface, except when the annealing temperature is higher than 500°C . When the CoSi_2 reaction is completed, the thicknesses of the Si^c consumed in samples I, II, and III are about 1340 \AA , 360 \AA , and 140 \AA , respectively. The final sample configuration for sample I or III is $\text{Si}^c/\text{CoSi}_2$ and that for sample II is $\text{Si}^c/\text{CoSi}_2/\text{Si}^c(\text{B})$ ($\approx 820 \text{ \AA}$).

The barrier height in each kind of samples after heat treatment are shown in Table 8. The barrier height was measured with forward I-V (the ideality factor is indicated in the parenthesis) and reverse I-V characteristics. The uncertainty of the measured barrier height is about 0.01 eV . After annealing at 350°C for 30 min, the phase of the silicide formed is not identified (as shown by a question mark in Table 8). When annealed at 400°C and 450°C for 30 min, the phase formed in each sample is CoSi . To form CoSi_2 , a 500°C annealing is needed for sample I (Si^c/Co), while a 450°C annealing (with long enough annealing time) is enough for samples II ($\text{Si}^c/\text{Co}/\text{Si}^c(\text{B})$) and III ($\text{Si}^c/\text{Co}/\text{Si}^c(\text{B})/\text{Co}$). RBS spectra show that the CoSi_2 formed in samples II and III has a more uniform Si/CoSi_2 interface than that formed in sample I.

For sample I (Si^c/Co), the barrier height of CoSi is $0.66\text{--}0.67 \text{ eV}$ (annealing temperatures ranging from 350°C to 450°C), but that of CoSi_2 is lower and is about $0.64 \pm 0.1 \text{ eV}$ (annealing temperatures higher than 500°C). The results are the same as reported by van Gurp [62]. For samples II and III, the barrier height of CoSi is the same as that of sample I but this is not so for CoSi_2 . In samples II and III, the barrier height of CoSi_2 is close to that of CoSi ($0.65\text{--}0.66 \text{ eV}$).

The differences between barrier heights of CoSi_2 in sample I and samples II and III are most probably due to the laterally nonuniform Si/CoSi_2 interface in sample I [XVII]. A laterally nonuniform interface has at least two effects on the barrier height measured from the I-V charac-

teristics. The first effect is that the interface has a larger effective area than what is assumed in calculating the barrier height. This error will result in a barrier height that is lower than the real one as indeed observed. The second effect is that a nonuniform interface creates a nonuniform electrical field in the vicinity of the interface. The relationship between current (I) and voltage (V) thus requires a two or three-dimensional model instead of the one-dimensional model used in the conventional analysis [61]. Even without an accurate model, it is physically evident that sharp protrusions in an otherwise uniform interface will create paths of enhanced current without materially reducing the total area. Such an effect also tends to lower the apparent barrier height of the contact. We thus believe that the true barrier height of CoSi₂ on n-type Si is 0.65–0.66 eV instead of 0.64 eV as measured from a laterally nonuniform diode.

6.3.2 Resistivity

As stated above, Co₂Si and CoSi initially always form together in a Si/Co sample. After Co is completely consumed, the CoSi forms at the expense of Co₂Si. It is, therefore, not easy to form a single layer of Co₂Si. To measure the electrical properties of Co₂Si, we adopted a model which assumes that the two layers of silicides are laterally uniform and electrically connected in parallel; i.e., electrical field in the sample depends only on the planar coordinates of the sample. With this assumption, we can show [XVII] that σ_s/t_0 is a linear function of $R \times \sigma_s^2/t_0$, where σ_s is the measured sheet conductance of the sample, t_0 is the thickness of the as-deposited Co film, and R is the measured sheet Hall coefficient defined as

$$R[\text{cm}^2/\text{Coulomb}] = 10^8 \times V_H[\text{volt}]/(B[\text{Gauss}] \times I[\text{Amper}]). \quad (6.1)$$

The relationship between σ_s/t_0 and of $R \times \sigma_s^2/t_0$ does not depend on the thickness of the Co deposited. Figure 8 shows the relations between the

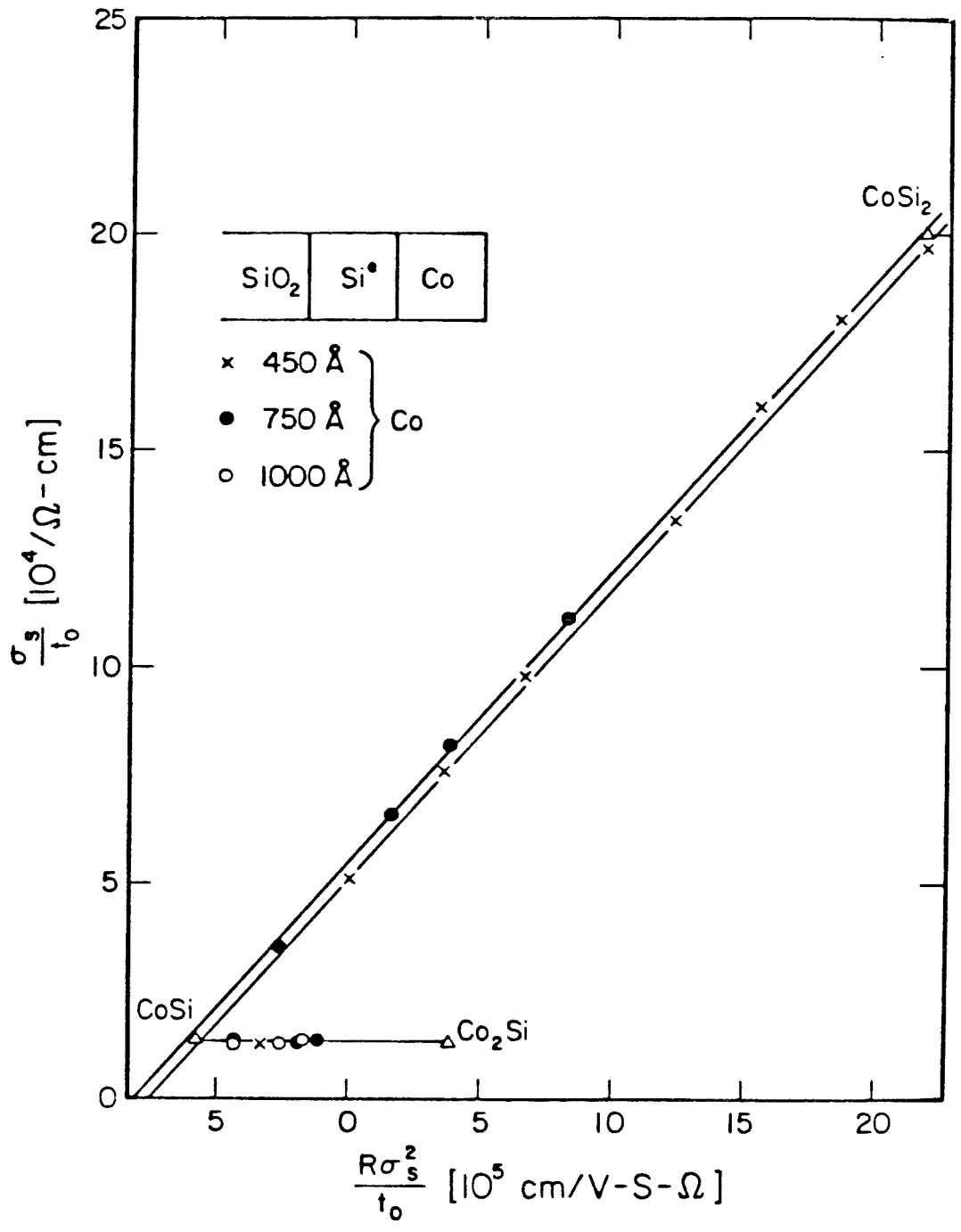


Figure 8

Data of $(\sigma)_s/t_0$ versus $R\sigma_s^2/t_0$ for samples containing two silicide phases [XVIII].

	Resistivity [$\mu\Omega cm$]	Carrier Concentration [$10^{22}/cm^3$]	Hall Mobility [$cm^2/V - s$]	Ref.
Co ₂ Si	40	0.20±0.04	28±5	3 ^a
	66.2			67 ^b
	110±5			XVIII ^f
CoSi	120	0.10±0.02	-43 ± 7 ^e	3 ^a
	150			66 ^b
	86			67 ^b
	147±5			XVIII ^f
CoSi ₂	18-20	2.5	11 ± 1	3 ^c
	25			3 ^d
	64.8			65 ^b , 66 ^b
	18			67 ^b
	18±1			XVIII ^f

- a*: Co on <100> Si
b: bulk silicides
c: Co on poly Si
d: cosputtered alloy
e: negative mobility for electron
f: Co on Si^e

Table 9

Electrical Properties of Co₂Si, CoSi, and CoSi₂ [XVIII].

measured values of σ_s/t_0 and of $R \times \sigma_s^2/t_0$. Crosses, open circles, and full dots are data from samples with Co thicknesses (t_0) of about 450 Å (annealed at 500°C), 750 Å (annealed at 490°C), and 1000 Å (annealed at 450°C), respectively. One straight line was fitted to the data measured from samples with both Co₂Si and CoSi phases (see Fig. 8: Co₂Si — CoSi). Another line was fitted to the data measured from samples with both CoSi and CoSi₂ phases (CoSi—CoSi₂). These two straight lines fit the data very well. This implies that the assumption of two silicide layers

connected in parallel electrically is consistent with the observations. The intersection of these two lines corresponds to a sample consisting of only CoSi. The points corresponding to the single phases of Co₂Si and CoSi₂ were calculated from the data after accounting for the known contribution of the CoSi layer when two phases are present. For clarity, these single phase data points are represented by triangles. Note that Co₂Si and CoSi₂ are p-type ($R \times \sigma_v^2/t_0 > 0$) and CoSi is n-type ($R \times \sigma_v^2/t_0 < 0$). Values measured here and reported before are listed in Table 9. Except for the resistivity of Co₂Si and the carrier concentration of CoSi, the agreement between the data measured here and those reported in references is quite good. The final phase of Co silicide (CoSi₂) has the lowest resistivity ($\approx 18 \mu\Omega cm$) and, in this respect, is the best of the three Co silicides for VLSI interconnection material. In fact, the resistivity of CoSi₂ is one of the lowest among the transition metal silicides.

6.4 Conclusion

1. True barrier height of CoSi₂ is 0.65–0.66eV.
2. That CoSi₂ is the final phase of the Co–Si reaction and that Co–Si system has high eutectic temperature make the CoSi₂ phase stable with respect to high temperature processing.
3. CoSi₂ formed from Si^c is laterally uniform and has low resistivity, and therefore is a good candidate for shallow contact material.
4. The low resistivity of CoSi₂ (one of the silicides with lowest resistivity) makes it a good candidate for VLSI interconnection material.

Chapter 7

Further Work

7.1 Ion Irradiation Improved Contact

As reported in many studies, a refractory silicide (e.g., TiSi_2 , MoSi_2 , TaSi_2 , WSi_2 , and so on) has a nonuniform Si^c /silicide interface when formed from a solid phase reaction between a refractory metal and Si^c . In practice, one needs a very uniform Si^c /silicide interface. One way to reduce the nonuniformity of a contact is to deposit a slightly metal-rich refractory disilicide on Si^c and then anneal the sample. The problems with this method are that the Si^c /silicide interface is as dirty as the original Si surface, which can induce a nonuniform reaction, and that it is not easy to control the stoichiometry of silicide during deposition. Therefore, we suggest another method to form a uniform silicide Schottky contact:

- (1) Depositing metal or metal rich silicide on a Si^c substrate.
- (2) Irradiating inert ion beam into the sample to break up the interfacial impurity and possibly to relax the stress in the film.
- (3) Annealing samples at low temperatures to form stoichiometric silicide.
- (4) Annealing samples at high temperatures (e.g., 900°C for 1 hr.) to anneal out the implantation damage.

Uniform refractory silicides can be formed from this method (see, e.g., Chapter 5). In fact, this method has been used to form a uniform refractory silicide (e.g., WSi_2 [71] and MoSi_2 [72]) ohmic contact if dopant atoms are used to break up the interfacial impurity and at the same time dope the Si substrate. However, the contact resistance value of

an ohmic contact will not be jeopardized by the presence of the defects generated by the ion irradiation, while those defects can be very harmful to the Schottky barrier height and ideality factor of a Schottky contact. It would be interesting to find out whether ion irradiation can be used to improve the electrical property of a refractory silicide contact. If it can, then what kind of implantation dose and energy are needed for this application? Of course, for the purpose of this experiment, we need to choose those silicide contacts which can be annealed at high temperature without degrading their Schottky barrier height.

7.2 Diffusion of Ni and Co in Si

Both Ni and Co have large diffusion constants in Si [69] but Ni has much higher solid solubility in Si than Co does [69]. Tu et al. [73] have shown that Ni atoms, which were evaporated on top of an Si wafer, can go through that wafer when Al was deposited at the back of the Si wafer and annealed at 540°C. We have done the similar experiments for both Ni and Co to compare the diffusion of Ni and Co in Si and to study their effects on the Schottky barrier of Ni or Co silicide contacts:

(1) A thin Ni or Co layer (about 300 Å) is evaporated on top of a (100) N-type Si wafer of resistivity 2–4 Ω-cm and of about 150 μm thick. Half of the wafer is reloaded and 1000 Å of Al was deposited on the reverse side of the Si. We therefore have four kinds of samples:

(i) Si^c/Ni,

(ii) Al/Si^c/Ni,

(iii) Si^c/Co,

(iv) Al/Si^c/Co.

Following the described experimental techniques, part of each sample was made with small circular dots of Ni or Co for Schottky barrier height measurement.

(2) All the samples are annealed in forming gas at 540°C for different durations (from 1 to about 10 days).

- (3) Forward and reverse I-V characteristics are measured to obtain the Schottky barrier heights of the circular dots of silicide. MeV RBS is used to monitor the phase of the silicide formed, the uniformity of the silicide interface, and the amount of Ni or Co transported to the back side of the Si.

The results show that

- (1) The silicides formed on the Si are NiSi (in samples (i) and (ii)) and CoSi₂ (in samples (iii) and (iv)) as expected.
- (2) Some Ni is transported from the top to the back of the Si when there is Al on the back of Si (sample (ii)). This long range transport is not observed in samples (i), (iii), and (iv).
- (3) The Schottky barrier contacts in all the samples (regardless of the duration of annealing) have very good ideality factor; i.e., the contacts are electrically good.
- (4) The Schottky barrier contacts have similar I-V curves whether Al is on the back of the Si or not.
- (5) DLTS¹ results show that there is no electrically active metal defects in Si (within several micron from the Si/silicide contact).

Comparing samples (i) with (ii), the long range transport of Ni in sample (ii) is due to the fact that Al acts as a sink for the Ni in Si. Comparing samples (ii) with (iv), the lack of Co transport in sample (iv) is either because that Co has too low "solid solubility times diffusivity" in Si or because that Al is not a sink for Co. The first suggestion is consistent with the reported result [69] that Co has comparable diffusivity as Ni but has much lower solid solubility than Ni. The formation of stable NiSi Schottky contacts, in spite of the fact that Ni atoms can diffuse across the Si substrate, is possibly because the Ni defects or precipitates in Si

¹The DLTS experiments were done by A. Prabhakar.

are not electrically active. The similarity between the I–V curves of the samples with or without Al sink is an interesting phenomenon.

7.3 Strange Behavior of CrSi_2

We have found that uniform CrSi_2 can be formed from the sample $\text{SiO}_2/\text{Si}^\epsilon/\text{Cr}$. However, if the order of Si and Cr is switched (i.e., $\text{SiO}_2/\text{Cr}/\text{Si}^\epsilon$), the silicide is uniform initially and becomes more and more nonuniform as the thickness of silicide increases. With the latter sample configuration, but with a thin Si layer of few hundred Å added at the SiO_2/Cr interface (i.e., $\text{SiO}_2/\text{thin Si}/\text{Cr}/\text{Si}$), we can improve the uniformity of CrSi_2 a lot. The explanation for such an unexpected behavior of Si–Cr reaction is still unknown.

7.4 Nucleation Controlled Silicides Formed from Si^ϵ

There are two characteristic temperatures for a silicide formation, viz., the lowest temperature that the silicide can nucleate (we will name it ‘nucleation temperature,’ T_n) and the lowest temperature that the silicide can grow with a reasonable rate (say, 200 Å/h) (we will name it ‘kinetics temperature,’ T_k). If a silicide has its T_n much lower than its T_k , the silicide formation is controlled by its kinetics mechanism (e.g., Ni_2Si and NiSi). If the reverse is true, the silicide formation is controlled by its nucleation process (e.g., NiSi_2). If T_n is a little higher than T_k , the silicide formation is controlled by the nucleation process initially and then controlled by the kinetics mechanism (e.g., CoSi_2). It would be very interesting if one could change the relative magnitude of the T_n and T_k of a silicide and observe the controlling process changing from one to another. In Chapter 2, We have observed that reaction between a metal and evaporated Si (Si^ϵ , which is amorphous) has a lower T_n than that between the metal and single crystalline Si (Si°). In

fact, the T_n 's of NiSi_2 and CoSi_2 formed from Si^e are reduced so much that the formation of either silicide on Si^e does not show any nucleation phenomenon. It would be very interesting to do the similar experiments for other nucleation-controlled silicides such as PdSi , HfSi_2 , Rh_4Si_5 , and IrSi_3 for their properties such as kinetics, moving species, impurity effect, and electrical properties.

7.5 Different amorphous Si

Here we give a few examples to point out that there are different kinds of amorphous Si:

- (1) It is known that PdSi is unstable at low temperatures ($< 800^\circ\text{C}$) [1] but it can be formed from ion beam amorphized Si at 400°C [70]. We have tried to form PdSi on Si^e (which is also amorphous) but the result is negative.
- (2) NiSi_2 can be formed from NiSi and Si^e reaction at low temperatures (e.g., 400°C). However, when we annealed the sample further, we found that the NiSi_2 dissociates into NiSi and Si. This dissociation will not take place if the Si^e is implanted with Xe or oxygen first [III].
- (3) It is reported that a low temperature annealing of ion beam amorphized Si can change the permittivity of the implanted Si even though the Si stays amorphous.

REFERENCES I - General

1. M-A. Nicolet and S. S. Lau, in *VLSI Electronics: Microstructure Science*, N. G. Einspruch, treatise Ed., Vol. 6, *Materials and Process Characterization*, N. G. Einspruch and G. B. Larrabee, volume Eds. (Academic Press, New York, 1983), Ch. 6.
2. S. P. Murarka, *Silicides for VLSI Applications* (Academic Press, New York, 1983).
3. S. P. Murarka, *J. Vac. Sci. Technol.* **17**, 775 (1980).
4. J. L. Vossen, *J. Vac. Sci. Technol.* **19**, 761 (1981).
5. F. Mohammadi, *Solid State Technol.*, Jan., 65 (1981).
6. G. Ottaviani, *J. Vac. Sci. Technol.* **16**, 1112 (1979).
7. S. P. Murarka, M. H. Read, C. J. Doherty, and D. B. Fraser, *J. Electrom. Sco.* **129**, 293 (1982).
8. K. N. Tu, W. N. Hammer, and J. O. Olowolafe: *J. Appl. Phys.* **51**, 1663 (1980).
9. B-Y. Tsaur, D. J. Silversmith, R. W. Mountain, L. S. Hung, S. S. Lau, and T. T. Sheng: *J. Appl. Phys.* **52**, 5243 (1981).
10. D. M. Scott, Ph.D. thesis, California Institute of Technology (1982).
11. K. T. Ho, C.-D. Lien, U. Shreter, M-A. Nicolet, *J. Appl. Phys.* (in press).
12. K. Nakamura, J. O. Olowolafe, S. S. Lau, M-A. Nicolet, J. W. Mayer, and R. Shima, *J. Appl. Phys.* **47**, 1278 (1976).
13. J. O. Olowolafe, M-A. Nicolet and J. W. Mayer, *Thin Solid Films* **38**, 143 (1976).

14. L. S. Hung, J. Gyulai, J. W. Mayer, S. S. Lau, and M-A. Nicolet, *J. Appl. Phys.* **54**, 5076 (1983).
15. C. S. Wu, S. S. Lau, T. F. Kuech, and B. X. Liu, *Thin Solid Films* **104**, 175 (1983).
16. N. Cheung, S. S. Lau, M-A. Nicolet, J. W. Mayer, and T. T. Sheng, in *Proceedings of the Symposium on Thin Film Interfaces and Interactions*, J. E. E. Baglin and J. M. Poate, Eds., Vol. 80-2 (Electrochemical Society, Princeton, 1980) p. 494.
17. U. Gösele and K. N. Tu, *J. Appl. Phys.* **53**, 3252 (1982).
18. J. Baglin, F. d'Heurle, and S. Petersson: in *Proceedings of the Symposium on Thin Film Interfaces and Interactions*, J. E. Baglin and J. M. Poate, Eds., Vol. 80-2 (Electrochemical Society, Princeton, 1980) p. 341.
19. E. P. Donovan, F. Spaepen, D. Turnbull, J. M. Poate, and D. C. Jacobson, *Appl. Phys. Lett.* **42**, 693 (1983).
20. J. C. C. Fan and H. Anderson, *J. Appl. Phys.* **52**, 4003 (1981).
21. W. K. Chu, H. Krautle, J. W. Mayer, H. Müller, M-A. Nicolet and K. N. Tu, *Appl. Phys. Lett.* **25**, 454 (1974).
22. S. S. Lau, J. S. Feng, J. O. Olowolafe and M-A. Nicolet, *Thin Solid Films* **25**, 415 (1975).
23. W. K. Chu, S. S. Lau, J. W. Mayer, M. Müller and K. N. Tu, *Thin Solid Films*, **25**, 393 (1975).
24. G. J. Van Gorp, W. F. van der Weg and D. Sigurd, *J. Appl. Phys.* **49**, 4011 (1978).
25. G. J. Van Gorp, D. Sigurd and W. F. van der Weg, *Appl. Phys. Lett.* **23**, 159 (1976).
26. J. E. E. Baglin, F. M. d'Heurle, W. N. Hammer and S. Petersson, *Nucl. Instr. Meth.* **168**, 491 (1980).

27. T. G. Finstad, J. W. Mayer and M-A. Nicolet, *Thin Solid Films*, **51**, 391 (1978).
28. J. Baglin, F. M. d'Heurle and S. Petersson, *Appl. Phys. Lett.* **33**, 237 (1978).
29. R. Pretorius, C. L. Ramiller and M-A. Nicolet, *Nucl. Instr. Meth.* **149**, 629 (1978).
30. R. Pretorius, C. L. Ramiller, S. S. Lau and M-A. Nicolet, *Appl. Phys. Lett.* **30**, 501 (1977).
31. R. Pretorius, *J. Electrochem. Soc.* **128**, 107 (1981).
32. A. P. Botha, R. Pretorius, and S. Kritzinger, *Appl. Phys. Lett.* **40**, 412 (1982).
33. R. Pretorius, J. O. Olowolafe and J. W. Mayer, *Philosophical Magazine A* **37**, 327 (1978).
34. A. P. Botha and R. Pretorius, in *Proceedings of MRS Symposium on Thin Films and Interfaces*, P. S. Ho and K. N. Tu, Eds., Vol. 10 (North-Holland, New York, 1981) p. 129.
35. J. E. E. Baglin, H. A. Atwater, D. Gupta and F. M. d'Heurle, *Thin Solid Films* **93**, 255 (1982).
36. R. Pretorius and A. P. Botha, *Thin Solid Films* **91**, 99 (1982).
37. M. Bartur and M-A. Nicolet, *J. Appl. Phys.* **54**, 5497 (1983).
38. S. S. Lau, Z. L. Liao, and M-A. Nicolet, *Thin Solid Films* **47**, 313 (1977).
39. F. d'Heurle, S. Petersson, L. Stolt, and B. Strizker, *J. Appl. Phys.* **53**, 5678 (1982).
40. F. d'Heurle, *Thin Solid Films* **105**, 285 (1983).
41. R. Pretorius, Z. L. Liao, S. S. Lau, and M-A. Nicolet, *Appl. Phys. Lett.* **29**, 598 (1976).

42. R. Pretorius, A. P. Botha, and J. C. Lombard, *Thin Solid Films* **79**, 61 (1981).
43. A. Martinez, D. Esteve, A. Guivarc'h, P. Auvray, P. Henoc, and G. Pelous, *Solid State Electron.* **23**, 55 (1980).
44. J.-R. Chen, Y.-C. Liu, and S.-D. Chu, *Appl. Phys. Lett.* **42**, 263 (1982).
45. R. Pretorius and A. P. Botha, *Thin Solid Films* **93**, 127 (1982).
46. S. Schiller, U. Heisig, K. Steinfeld, and Chr. Korndorfer, *Thin Solid Films* **96**, 279 (1982).
47. F. Neppel, G. Menzel, and U. Schwabe, *J. Electrochem. Soc.* **130**, 1174 (1983).
48. G. Beensh-Marchwicka, L. Król-Stepniewska, and W. Posadowski, *Thin Solid Films* **82**, 313 (1981).
49. M. Hill, *Solid State Technol.*, Jan., 53 (1980).
50. L. S. Hung, L. R. Zheng, and J. W. Mayer, *J. Appl. Phys.* **54**, 792 (1983).
51. N. W. Cheung, M.-A. Nicolet, M. Wittmer, C. A. Evans, Jr. and T. T. Sheng, *Thin Solid Films* **79**, 51 (1981).
52. M. Wittmer, C.-Y. Ting, I. Ohdomari, and K. N. Tu, *J. Appl. Phys.* **53**, 6781 (1982).
53. C. A. Crider, J. M. Poate, J. E. Rowe, and T. T. Sheng, *J. Appl. Phys.* **52**, 2860 (1981).
54. M. Wittmer, *J. Appl. Phys.* **54**, (1983).
55. M. Y. Tsai, H. H. Chao, L. M. Ephrath, B. L. Crowder, A. Cramer, R. S. Bennett, C. J. Lucchese, and M. R. Wordeman, *J. Electrochem. Soc.* **128**, 2207 (1981).
56. S. P. Murarka and D. B. Fraser, *J. Appl. Phys.* **51**, 342 (1980).

57. J. N. Ramsey, *J. Vac. Sci. Technol.* **A1(2)**, 721 (1983).
58. M. Wittmer and K. N. Tu, *Phys. Rev. B* (unpublished).
59. L. S. Wieluński, C.-D. Lien, B. X. Liu, and M-A. Nicolet, *J. Vac. Sci. Technol.* **20**, 182 (1982).
60. L. S. Wieluński, C.-D. Lien, B.-X. Liu, and M-A. Nicolet, in *Proceedings of MRS Symposium on Metastable Materials of Formation by Ion Implantation*, edited by S. T. Picraux and W. J. Choyke, Vol. 7 (North-Holland, New York, 1982), p. 139.
61. S. M. Sze: *Physics of Semiconductor Devices*, 2nd edn. (Wiley-Interscience, New York, 1982).
62. G. J. van Gorp: *J. Appl. Phys.* **46**, 4308 (1975).
63. M. Wittmer, D. L. Smith, P. W. Lew, and M-A. Nicolet, *Solid State Electron* **21**, 573 (1978).
64. E. G. Colgan, M. Mäenpää, M. Finetti, and M-A. Nicolet, *J. of Electronic Materials* **12**, 413 (1983).
65. P. T. B. Shaffer, *Handbook of High-Temperature Materials, No. 1 Materials Index* (Plenum Press, New York, 1984).
66. R. Guidoth, *Evaluation of MHD Materials for Use in High Temperature Fuel Cells*, Montana Energy & MHD Res. and Dev. Inst., Butte, Montana (U. S. Dept. of Energy 6/15/78).
67. G. V. Samsonov and I. M. Vinitskii, *Handbook of Refractory Compounds* (IFI/Plenum Press, New York, 1983).
- 68.

$$\frac{1}{\lambda\rho} = \left(\frac{8\pi}{3}\right)^{1/3} \frac{e^2 n^{2/3}}{h}$$

λ = mean free path, ρ = resistivity, e = electron charge, n = carrier concentration, and h = Planck's constant, *Thin film Phenomena*, K. L. Chopra (McGraw-Hill, New York, 1969), p. 345.

69. E. R. Weber, Appl. Phys. A **30**, **1** (1983).
70. B. Y. Tsaur, S. S. Lau, and J. W. Mayer, Appl. Phys. Lett. **35**, **225** (1979).
71. B. Y. Tsaur and C. H. Anderson, Appl. Phys. Lett. **41**, **877** (1982).
72. E. Nagasawa, H. Okabayashi, and M. Morimoto, Jap. J. Appl. Phys. **22**, **L57** (1983).
73. K. N. Tu (private communication).

REFERENCES II - Work published by Chuen-Der Lien

Kinetics

- I. C.-D. Lien and M-A. Nicolet, *A modified model for a planar compound formation* (see Appendix A).
- II. C.-D. Lien, M-A. Nicolet, and S. S. Lau, *Kinetics of silicides on (100) Si and evaporated Si* (see Appendix B).
- III. C.-D. Lien, M-A. Nicolet, and S. S. Lau, *Low temperature formation of NiSi₂ from evaporated silicon*, phys. stat. sol. (a) **81**, 123 (1984).
- IV. C.-D. Lien, M-A. Nicolet, C. S. Pai, and S. S. Lau, *Growth of Co-silicides from single crystal and evaporated Si* (see Appendix C).
- V. C.-D. Lien, M-A. Nicolet, and S. S. Lau, *Kinetics of CoSi₂ from evaporated silicon*, Appl. Phys. A (1984) (in press).

Marker and Tracer

- VI. C.-D. Lien, M. Bartur, and M-A. Nicolet, *Marker experiments in silicides during solid phase epitaxy of evaporated silicon*, in THIN FILM AND INTERFACES II, edited by J. E. E. Baglin, D. R. Campbell, and W. K. Chu (Elsevier Science Pub. Co., New York, 1984), Mat. Res. Soc. Symp. Proc. Vol. 25, p. 51.
- VII. C.-D. Lien, M-A. Nicolet, and C. S. Pai, *Structure marker experiment for Pd₂Si formation*, J. Appl. Phys. (in press).
- VIII. C.-D. Lien and M-A. Nicolet, *Mathematical model for radioactive tracer in silicide formation*, J. Appl. Phys. **55**, 4187 (1984).
- IX. C.-D. Lien and M-A. Nicolet, *Profile of Si* in silicide when Si diffuses by vacancy mechanism or by interstitial with high exchange rate*, J. Appl. Phys. (submitted).

Impurity Effect

- X. C.-D. Lien and M-A. Nicolet, *Impurity effects in transition metal silicides*, J. Vac. Sci. Technol. B, Oct/Dec (1984).
- XI. C.-D. Lien, L. S. Wieluński and M-A. Nicolet, *Comparison of the nuclear reactions $^{18}\text{O}(p,\alpha)^{15}\text{N}$ and $^{16}\text{O}(d,\alpha)^{14}\text{N}$ to study the oxygen effects in Pt silicide formation*, Nucl. Instr. Meth. **213**, 463 (1983).
- XII. C.-D. Lien, L. S. Wieluński, Marc-A. Nicolet, and J. M. Stika, *Behavior and influence of oxygen in chromium silicide formation*, Thin Solid Films **104**, 235 (1983).
- XIII. C.-D. Lien and M-A. Nicolet, *Oxygen effect and redistribution in cobalt silicide formation*, in THIN FILM AND INTERFACES II, edited by J. E. E. Baglin, D. R. Campbell, and W. K. Chu (Elsevier Science Pub. Co., New York, 1984), Mat. Res. Soc. Symp. Proc. Vol. 25, p. 131.
- XIV. K. T. Ho, C.-D. Lien, M-A. Nicolet, and D. M. Scott, *Effect of nitrogen and oxygen impurities on tantalum silicide formation*, in THIN FILM AND INTERFACES II, edited by J. E. E. Baglin, D. R. Campbell, and W. K. Chu (Elsevier Science Pub. Co., New York, 1984), Mat. Res. Soc. Symp. Proc. Vol. 25, p. 123.
- XV. K. T. Ho, C.-D. Lien, and M-A. Nicolet, *Palladium silicide formation under the influence of nitrogen and oxygen impurities*, J. Appl. Phys. (in press).
- XVI. C.-D. Lien, M-A. Nicolet, and P. William, *Effects of ion irradiation on thermally formed silicides in the presence of interfacial oxide* (see Appendix D).

Electrical Property

- XVII. C.-D. Lien, M. Finetti, and M-A. Nicolet, *Comparison of Schottky barrier heights of cobalt disilicide formed from evaporated silicon or from crystalline Si*, Appl. Phys. A (1984) (in press).

- XVIII. C.-D. Lien, M. Finetti, M.-A. Nicolet and S. S. Lau, *Electrical properties of thin Co_2Si , CoSi , and CoSi_2 layers grown on evaporated Si*, J. Elec. Mat. **13**, 95 (1984).
- XIX. C.-D. Lien, F. C. T. So, and M.-A. Nicolet, *An improved forward I-V method for non-ideal Schottky diodes with high series resistance*, IEEE Trans. Electron Devices **ED-31**, No. 10, Oct. (1984).

Appendix A -
A Modified Model
for
a Planar Compound Formation

C.-D. Lien and M.-A. Nicolet
California Institute of Technology
Pasadena, CA 91125 U.S.A.

Abstract

It is shown that the application of Fick's laws, a modified coordinate, and a modified interfacial reaction formula to a single compound formation in a binary system leads to a simple solution for the thickness of the compound even if the interdiffusion constant is atomic concentration dependent. Experimental data of an amorphous phase formation are fitted to the model.

1. Introduction

With assumptions of continuous chemical potential (therefore no interfacial reaction barriers), concentration dependent interdiffusion constant, and no volume change during reaction, Kidson proposed a model which predicted that all the equilibrium phases of a binary A/B system should be present with thicknesses proportional to the square root of time when it is annealed at a constant temperature [1]. Experimentally, some of the thicknesses of

phases formed are linear function of time (e.g., formation of CrSi_2) or a combination of both square root and linear function of time (e.g., formation of SiO_2) and not all the equilibrium phases are present in thin film reaction (e.g. Si-thin Ni film system). Assuming a constant diffusion coefficient of oxygen in SiO_2 , position independent oxygen flux in SiO_2 , and reaction barriers at the interfaces of SiO_2 , Deal et al. proposed a model [2] which explained the non-square root of time growth of SiO_2 very successfully. In most cases of single compound formations, this model fit the experimental results very well. Also a similar model was used to explain the multi-phase formation in a binary system [3]. However, that the flux is position independent is true only when the film thickness is much less than the diffusion length (see Appendix).

In this paper, we will solve a single compound formation problem by using a similar model as proposed by Deal et al. with the following modifications:

- (1): A modified coordinate is introduced so that there is no "volume" change during reaction.
- (2): A modified interfacial reaction is used. This modified interfacial reaction renders a simple solution for the problem and has a similar physical meaning as the original interfacial reaction.
- (3): A concentration dependent, instead of constant, interdiffusion diffusion constant is assumed.
- (4): The position independent atomic flux is not assumed.

Similarity between the modified and previous interfacial reaction formulas will be discussed.

2. Models for a single compound formation in a binary system

We consider a binary system as shown in Fig. 1 (a): A compound ($A_\beta B_{1-\beta}$ (β phase)) layer grows between two phases $A_\alpha B_{1-\alpha}$ (α phase) and

$A_\gamma B_{1-\gamma}$ (γ phase) where the subscripts $\alpha > \beta > \gamma$ (each value is between 0 and 1) characterize the composition of the compounds. We will assume α and γ are constant and β is a function of position and time. We will introduce a modified coordinate x , which is a function of the ordinary spatial coordinate y , defined as

$$x = \int_0^y N(y, t) dy / N_0, \quad (1)$$

where $N(y, t)$ is the total atomic concentration at position y and time, t and N_0 is a chosen constant concentration. The modified position x , instead of y , will be used for the position coordinate in later discussion. The merits of using this modified coordinate are that there is no "volume" change during reaction and that the total atomic "concentration" is constant everywhere at any time ($= N_0$). In the absence of interfacial reaction barriers, the concentrations of A at the interfaces of β phase are given by the corresponding equilibrium values $C_{\beta\alpha}^{eq}$ ($\equiv N_0\beta_1^*$) and $C_{\beta\gamma}^{eq}$ ($\equiv N_0\beta_2^*$) (see Fig. 1) [1]. In this case, the thickness of $A_\beta B_{1-\beta}$ is known to be proportional to the square root of time [1]. In the presence of interfacial reaction barriers, the concentrations of A at the interfaces are $C_{\beta\alpha}$ ($\equiv N_0\beta_1 < C_{\beta\alpha}^{eq}$) and $C_{\beta\gamma}$ ($\equiv N_0\beta_2 > C_{\beta\gamma}^{eq}$) [2, 3].

A. A general diffusion problem

From the conservation of atoms, The "concentration" of A, $C(x, t)$ ($\equiv N_0\beta(x, t)$), satisfies the following equation:

$$\frac{\partial C(x, t)}{\partial t} = -\frac{\partial J(x, t)}{\partial x} \quad (2)$$

in the β phase, where $J(x, t)$ is the flux of A atoms at x and time t . We assume that the flux $J(x, t)$ is proportional to the "gradient" of $C(x, t)$; i.e.,

$$J = -D(C(x, t)) \frac{\partial C(x, t)}{\partial x}, \quad (3)$$

where the "interdiffusion coefficient" D ($D \equiv (1-\beta)D_A(\beta) + \beta D_B(\beta)$, where D_A and D_B are "diffusion constants" of A and B atoms in $A_\beta B_{1-\beta}$, respectively) depends on the concentration of A only; i.e., $D = D(C)$. The $C(x, t)$ then satisfies the following diffusion equation

$$\frac{\partial C(x, t)}{\partial t} = \frac{\partial}{\partial x} \left[D(C(x, t)) \frac{\partial C(x, t)}{\partial x} \right] \quad (4)$$

in the β phase. From the conservation of atoms, we can calculate the change of the position of the two interfaces (see Fig. 1 (a)) with time [1, 3]:

$$\frac{dx_{\beta\alpha}}{dt} = -\frac{J_{\beta\alpha}}{(\alpha - \beta)N_0} = \frac{1}{(\alpha - \beta)N_0} D(C_{\beta\alpha}) \left(\frac{\partial C}{\partial x} \right)_{\beta\alpha} \quad (5)$$

and

$$\frac{dx_{\beta\gamma}}{dt} = \frac{J_{\beta\gamma}}{(\beta 2 - \gamma)N_0} = -\frac{1}{(\beta 2 - \gamma)N_0} D(C_{\beta\gamma}) \left(\frac{\partial C}{\partial x} \right)_{\beta\gamma}. \quad (6)$$

The thickness of the $A_\beta B_{1-\beta}$ layer X_β is equal to $x_{\beta\gamma} - x_{\beta\alpha}$. To complete the formulation, we still need two interfacial reaction formulas to characterize the the interfacial reaction flux at each boundary. A general expression for an interfacial reaction flux would be a function of C^{eq} and C and the flux is flowing out of the boundary when $C^{eq} - C$ is positive. For simplicity, we suggest that the function has a positive constant to characterize the interfacial reaction flux. A first order approximation of the interfacial reaction flux would be

$$\begin{aligned} J_{\beta\alpha} &= k_{\beta\alpha} (C_{\beta\alpha}^{eq} - C_{\beta\alpha}) \\ J_{\beta\gamma} &= k_{\beta\gamma} (C_{\beta\gamma} - C_{\beta\gamma}^{eq}), \end{aligned} \quad (7)$$

where two positive reaction constants $k_{\beta\alpha}$ and $k_{\beta\gamma}$ are used to characterize the interfacial reaction fluxes [2, 3].

B. Constant D and first order approximated interfacial reaction formula

For the case of a constant interdiffusion coefficient, i.e., $D(C) = D$, one can define $X_1 \equiv D/k_{\beta\alpha}$ and $X_2 \equiv D/k_{\beta\gamma}$, so that the approximated interfacial reaction flux equation can be rewritten as

$$\begin{aligned} J_{\beta\alpha} &= D(C_{\beta\alpha}^{eq} - C_{\beta\alpha})/X_1 \\ J_{\beta\gamma} &= D(C_{\beta\gamma} - C_{\beta\gamma}^{eq})/X_2. \end{aligned} \quad (8)$$

Mathematically, the interfacial reaction flux, $J_{\beta\alpha}$ say, is equivalent to a flux through a $A_\beta B_{1-\beta}$ layer of thickness X_1 in which $C(x, t)$ is a linear function x and the boundary values of $C(x, t)$ are $C_{\beta\alpha}^{eq}$ and $C_{\beta\alpha}$ (see Fig. 1 (b)). Therefore, the problem is equivalent to (see Fig. 1 (b)) a diffusion problem in the three layers of $A_\beta B_{1-\beta}$ of which thicknesses are X_1 , $X_\beta(t)$, and X_2 , respectively. The concentration $C(x, t)$ is a linear function of x in the first and the third layers and satisfies the diffusion equation; i.e., eq. (4), in the second layer. $C(x, t)$ is fixed at the equilibrium values at the boundaries of the first and the third layers, i.e., $C(x_{\beta\alpha}, t) = C_{\beta\alpha}^{eq}$ and $C(x_{\beta\gamma}, t) = C_{\beta\gamma}^{eq}$ (see Fig. 1 (b)). The motion of the $x_{\beta\alpha}$ and the $x_{\beta\gamma}$ are determined by eqs. (5) and (3). Even though the interdiffusion constant is concentration independent, the problem defined in Fig. 1 (b) is still not easy to solve.

C. Special case of B when $X_\beta/\sqrt{Dt} \ll 1$

Case (B) can be easily solved if $X_\beta/\sqrt{Dt} \ll 1$ is assumed which is true when $\Delta C_\beta^{eq} (\equiv C_{\beta\alpha}^{eq} - C_{\beta\gamma}^{eq}) \ll C_{\beta\gamma}^{eq}$ (see Appendix). With this additional assumption (see Appendix), one can assume that $C(x, t)$ is a linear function of x in the β phase; therefore, J is position independent. Note that in all three layers of $A_\beta B_{1-\beta}$, $C(x, t)$ is a linear function of x . In this case, instead of solving eq. (4), we can use

$$J(x, t) = J(t) = D(C_{\beta\alpha} - C_{\beta\gamma})/X_{\beta}. \quad (9)$$

Using eqs. (5-8), we can easily show that [2, 3]

$$J(t) = D\Delta C_{\beta}^{eq}/(X_1 + X_{\beta} + X_2), \quad (10)$$

$$C(x, t) = C_{\beta\alpha}^{eq} - \Delta C_{\beta}^{eq}(X_1 + x)/(X_1 + X_{\beta} + X_2), \quad (11)$$

and

$$dX_{\beta}(t)/dt = \left[\frac{(1-\alpha)\beta_1}{(\alpha-\beta_1)C_{\beta\alpha}} + \frac{(1-\gamma)\beta_2}{(\beta_2-\gamma)C_{\beta\gamma}} \right] J(t) \approx K J(t), \quad (12)$$

where

$$K = \left[\frac{(1-\alpha)\beta_1^*}{(\alpha-\beta_1^*)C_{\beta\alpha}^{eq}} + \frac{(1-\gamma)\beta_2^*}{(\beta_2^*-\gamma)C_{\beta\gamma}^{eq}} \right] \quad (13)$$

Therefore

$$X_{\beta}^2 + 2(X_1 + X_2)X_{\beta} = 2D\Delta C_{\beta}^{eq}Kt. \quad (14)$$

D. Apply a modified interfacial reaction formula to the general diffusion problem

In some cases, however, the condition $X_{\beta}/\sqrt{Dt} \ll 1$ is not true and/or D is concentration dependent, we need go back to solve the problem in the Fig. 1 (a). Since this problem is not easy to solve, we would like to avoid the difficulty by modifying the problem slightly. One possibility is using a modified interfacial reaction formula instead of the first order approximation one. In fact, the three-layer concept used in case (B) (see Fig. 1 (b)) can

be modified for a new interfacial reaction formula; i.e., we can assume that the concentration $C(x, t)$ in all the three layers satisfies the diffusion equation (4) with a concentration dependent diffusion constant. The thicknesses of the two artificial layers X_1 and X_2 are used to characterize the interfacial reaction fluxes. In addition, we will use the equations

$$dx_{\beta\alpha}/dt = -\frac{J_{\beta\alpha}}{(\alpha - \beta 1^*)N_0} \quad (15)$$

and

$$dx_{\beta\gamma}/dt = \frac{J_{\beta\gamma}}{(\beta 2^* - \gamma)N_0} \quad (16)$$

instead of eqs. (5) and (6) to calculate $x_{\beta\alpha}$ and $x_{\beta\gamma}$. The solution of this problem coincides with that of the problem in Fig. 1 (b) when $D(C) = D$, and $X_1 + X_2$ is much smaller than \sqrt{Dt} (e.g., when t is large). The solution of this problem also coincides with that of the problem in Fig. 1 (c) when $D(C) = D$ and when $X_1 + X_\beta + X_2$ are much smaller than \sqrt{Dt} (e.g., when $\Delta C_\beta^{eq}/C_{\beta\gamma} \ll 1$)

The solution of the problem defined in Fig. 1 (d) is solved in the Appendix. The concentration $C(x, t)$ is a function of a single variable λ ($\equiv x/(t + t_0)$ see Appendix), i.e., $C(x, t) = C(\lambda)$. The thickness X_β is a simple function of time t

$$X_\beta = \lambda_\beta \sqrt{t + t_0} - (X_1 + X_2), \quad (17)$$

where λ_β is a constant defined in the Appendix and $t_0 = [(X_1 + X_2)/\lambda_\beta]^2$. This is equivalent to

$$X_\beta^2 + 2(X_1 + X_2)X_\beta = \lambda_\beta^2 t. \quad (18)$$

Therefore, we have proven that the equation (18) is a very general equation for the thickness of a growing film.

E. Fitting the experimental data

As shown in the Appendix, the "modified " thickness of the γ phase consumed, X_γ , during the reaction is also a simple function of time:

$$X_\gamma = \lambda_{\beta\gamma}\sqrt{t+t_0} - \lambda_{\beta\gamma}\sqrt{t_0}. \quad (19)$$

This implies

$$X_\gamma + 2\lambda_{\beta\gamma}\sqrt{t_0} = \lambda_{\beta\gamma}^2 t / X_\gamma. \quad (20)$$

Figure 2 shows a plot of Y_γ vs. t/Y_γ for an amorphous Ni-Hf film growth measured in Ref. 4 (where Y_γ is the real thickness of the γ phase consumed). Using the least mean square method, the data are fitted by a straight line:

$$Y_\gamma + 270.9 [\text{\AA}] = 705.9 [\text{\AA}^2/\text{min}] t/Y_\gamma.$$

This is equivalent to

$$X_\gamma + 270.9[\text{\AA}]N_\gamma/N_0 = 705.9[\text{\AA}^2/\text{min}](N_\gamma/N_0)^2 t/X_\gamma. \quad (21)$$

Comparing eqs. (20) and (21), we have

$$(1) t_0 = 25.98 \text{ min and}$$

$$(2) (\lambda_{\beta\gamma}N_0/N_\gamma)^2 = 705.9 \text{ \AA}^2/\text{min}.$$

If we assume $D(C) = D$ and $N_0 = 7 \times 10^{22} \text{ cm}^{-3}$, then we have (see Table 1)

$$(1) X_1 + X_2 = 206.7 \text{ \AA and}$$

$$(2) D = 1.1 \times 10^{-15} \text{ cm}^2/\text{s}.$$

3. Summary

We have proposed a modified formula for interfacial reaction barriers. With this formula, we have obtained a simple formula for the thickness of a single film growth. Experimental data of amorphous Ni-Hf formation were fitted by this model.

Acknowledgments

The authors are grateful to Dr. M. Bartur and T. Banwell for helpful discussions. We also thank Dr. M. Van Rossum for offering Ni-Hf data.

Appendix

In this appendix, we will solve the problem in Fig. 1 (d) and discuss the validity of using position-independent flux as assumed in Fig. 1 (c).

When $X_1 + X_2 = 0$ in the problem defined in Fig. 1 (d), we can rewrite the eq. (4) in terms of the variable $\lambda \equiv x/\sqrt{t}$ [1]

$$t \frac{\partial C(\lambda, t)}{\partial t} = \frac{\partial}{\partial \lambda} \left[D(C(\lambda, t)) \frac{\partial C(\lambda, t)}{\partial \lambda} \right] + \frac{\lambda}{2} \frac{\partial C(\lambda, t)}{\partial \lambda}. \quad (22)$$

In this case, as shown in Ref. 1, we have

- (1): The solution $C(\lambda, t)$ depends only on λ , i.e., $C(\lambda, t) = C(\lambda)$.
- (2): The positions of the interfaces $x_{\beta\alpha}$ and $x_{\beta\gamma}$ are proportional to the square root of time; i.e.,

$$x_{\beta\alpha}(t) = \lambda_{\beta\alpha} \sqrt{t} \quad (23)$$

and

$$x_{\beta\gamma}(t) = \lambda_{\beta\gamma} \sqrt{t}, \quad (24)$$

where constants $\lambda_{\beta\alpha}$ and $\lambda_{\beta\gamma}$ are calculated from

$$\lambda_{\beta\alpha} = \frac{2D(C(\lambda_{\beta\alpha}))}{(\alpha - \beta 1^*)N_0} \frac{dc(\lambda_{\beta\alpha})}{d\lambda} \quad (25)$$

and

$$\lambda_{\beta\gamma} = \frac{2D(C(\lambda_{\beta\gamma}))}{(\beta 2^* - \gamma)N_0} \frac{dc(\lambda_{\beta\gamma})}{d\lambda}. \quad (26)$$

(3): The thickness of the β phase, $X_\beta(t)$, is proportional to the square root of time as proven in Ref. 1:

$$X_\beta(t) = (\lambda_{\beta\gamma} - \lambda_{\beta\alpha})\sqrt{t} \equiv \lambda_\beta\sqrt{t}. \quad (27)$$

For the case of $X_1 + X_2 > 0$, we still use the constants $\lambda_{\beta\alpha}$, $\lambda_{\beta\gamma}$, and λ_β defined in eqs. (25-27) but redefine λ as

$$\lambda \equiv \frac{x}{\sqrt{t + t_0}},$$

where $t_0 \equiv (X_1 + X_2)/\lambda_\beta$; then we have

(1): $C(\lambda, t) = C(\lambda)$.

(2): The positions of the interfaces $x_{\beta\alpha}$ and $x_{\beta\gamma}$ are

$$x_{\beta\alpha}(t) = \lambda_{\beta\alpha}\sqrt{t + t_0} \quad (28)$$

and

$$x_{\beta\gamma}(t) = \lambda_{\beta\gamma}\sqrt{t + t_0}. \quad (29)$$

(3): The thickness of the β phase, $X_\beta(t)$ is

$$X_\beta(t) = \lambda_\beta\sqrt{t + t_0} - (X_1 + X_2). \quad (30)$$

The rate change of the modified thickness of $A_\gamma B_{1-\gamma}$ consumed, X_γ , is

$$dX_\gamma/dt = dx_{\beta\gamma}/dt \quad (31)$$

which results in

$$X_\gamma = \lambda_{\beta\gamma} \sqrt{t + t_0} - \lambda_{\beta\gamma} \sqrt{t_0}. \quad (32)$$

Similarly, the modified thickness of $A_\alpha B_{1-\alpha}$ consumed, X_α , is

$$X_\alpha = \lambda_{\beta\alpha} \sqrt{t + t_0} - \lambda_{\beta\alpha} \sqrt{t_0}. \quad (33)$$

For more detailed information, we need to know the function $D(C)$. As an example, we will solve the problem for the constant interdiffusion constant case; i.e., $D(C) = D$ which gives

$$\begin{aligned} C(\lambda) &= C_{\beta\alpha}^{eq} - \Delta C_{\beta}^{eq} / (A\sqrt{\pi}) \int_{-k_1}^{\lambda/\sqrt{D}} \exp(-y^2/4) dy \\ &= C_{\beta\alpha}^{eq} - (\Delta C_{\beta}^{eq} / A) [\operatorname{erf}(\lambda/\sqrt{4D}) + \operatorname{erf}(k_1/2)], \end{aligned} \quad (34)$$

where

$$A = 1/\sqrt{\pi} \int_{-k_1}^{k_2} \exp(-y^2/4) dy = \operatorname{erf}(k_2/2) + \operatorname{erf}(k_1/2), \quad (35)$$

$$k_1 \exp(k_1^2/4) A = \frac{2}{(\alpha - \beta_1^*)} \frac{\Delta C_{\beta}^{eq}}{N_0 \sqrt{\pi}} = 2/\sqrt{\pi} \frac{\beta_1^* - \beta_2^*}{\alpha - \beta_1^*}, \quad (36)$$

$$k_2 \exp(k_2^2/4) A = \frac{2}{(\beta_2^* - \gamma)} \frac{\Delta C_{\beta}^{eq}}{N_0 \sqrt{\pi}} = 2/\sqrt{\pi} \frac{\beta_1^* - \beta_2^*}{\beta_2^* - \gamma}, \quad (37)$$

$$\lambda_{\beta\alpha} = -k_1 \sqrt{D},$$

and

$$\lambda_{\beta\gamma} = k_2\sqrt{D}.$$

This gives

$$X_\beta = k_\beta \sqrt{Dt + (X_1 + X_2)^2/k_\beta^2} - (X_1 + X_2), \quad (38)$$

where $k_\beta = k_2 + k_1$.

From eqs. (34) and (38) we can see that (by expanding the eq. (34) in terms of Taylor series) $X_\beta/\sqrt{Dt} \ll 1$ if and only if (iff) k_1 and $k_2 \ll 1$ iff $C(\lambda, t)$ can be approximated by a linear function of λ , i.e., a linear function of x . Also from eqs. (35-37), we can see that $\Delta C_\beta^{c_q}/N_0 \ll 1$ iff k_1 and $k_2 \ll 1$. Therefore, in the case of $D(C) = D$, we can conclude that

$C(\lambda, t)$ can be approximated by a linear function of λ ,

iff $X_\beta/\sqrt{Dt} \ll 1$, and

iff $\Delta C_\beta^{c_q}/N_0 (= \beta_1^* - \beta_2^*) \ll 1$.

Note that if $k_\beta \ll 1$ (which is equivalent to $\beta_1^* - \beta_2^* \ll 1$), then $C(\lambda, t)$ is a linear function of λ and $k_\beta = \sqrt{2\Delta C_\beta^{c_q}/N_0} \sqrt{1/(\alpha - \beta_1^*) + 1/(\beta_2^* - \gamma)}$. This solution is the same as that of the problem in Fig. 1 (c).

References

1. G. V. Kidson, *J. Nucl. Mater.* **3**, 21 (1961).
2. B. E. Deal and A. S. Grove, *J. Appl. Phys.* **36**, 3770 (1965).
3. U. Gösele and K. N. Tu, *J. Appl. Phys.* **53**, 3252 (1982).
4. M. Van Rossum, M-A. Nicolet, and W. L. Johnson, *Phys. Rev. B* **29**, 5498 (1984).

A	B	α	$\beta 1^*$	$\beta 2^*$	γ	$N_0[10^{22}/\text{cm}^3]$	$N_{Hf}[10^{22}/\text{cm}^3]$
Ni	Hf	1	0.7	0.45	0	7	4.52
$\beta 1^* - \beta 2^*$	$\alpha - \beta 1^*$	$\beta 2^* - \gamma$	k1	k2	k_β	$X_1 + X_2 [\text{Å}]$	$D[\text{cm}^2/\text{s}]$
0.25	0.3	0.45	0.909	0.666	1.575	206.7	1.1×10^{-15}

Table 1

The data for the amorphous Ni-Hf formation [4] with the assumption that $D(C) = D$.

Figure Captions

- Figure 1 (a) Concentration profile of A in an $A_\alpha B_{1-\alpha} / A_\beta B_{1-\beta} / A_\gamma B_{1-\gamma}$ diffusion couple. The interdiffusion constant, D , is assumed to depend on the atomic concentration of A, $C(x, t)$, i.e., $D = D(C)$. We assume that $\alpha = \text{constant} > \beta > \gamma = \text{constant}$.
- (b) A special case of (a) (when $D(C) = D$) with two first order interfacial reactions (eq. 7) expressed as linear profiles of A atoms in two layers of $A_\beta B_{1-\beta}$ of thicknesses X_1 and X_2 inserted at the original boundaries.
- (c) A special case of (b) with the assumption that the concentration of A atoms is a linear function of position in the original β phase. This is the model proposed by Deal et al. [2].
- (d) A problem modified from (a) with the assumption that the concentration of A atoms satisfies the diffusion equation (4) in all three layers of β phase.
- Figure 2 The real thickness of Hf consumed Y_γ vs. t/Y_γ during amorphous Ni–Hf formation by annealing at 340°C in vacuum [4]. The straight line shown was fitted by the least mean square method.

Fig.1

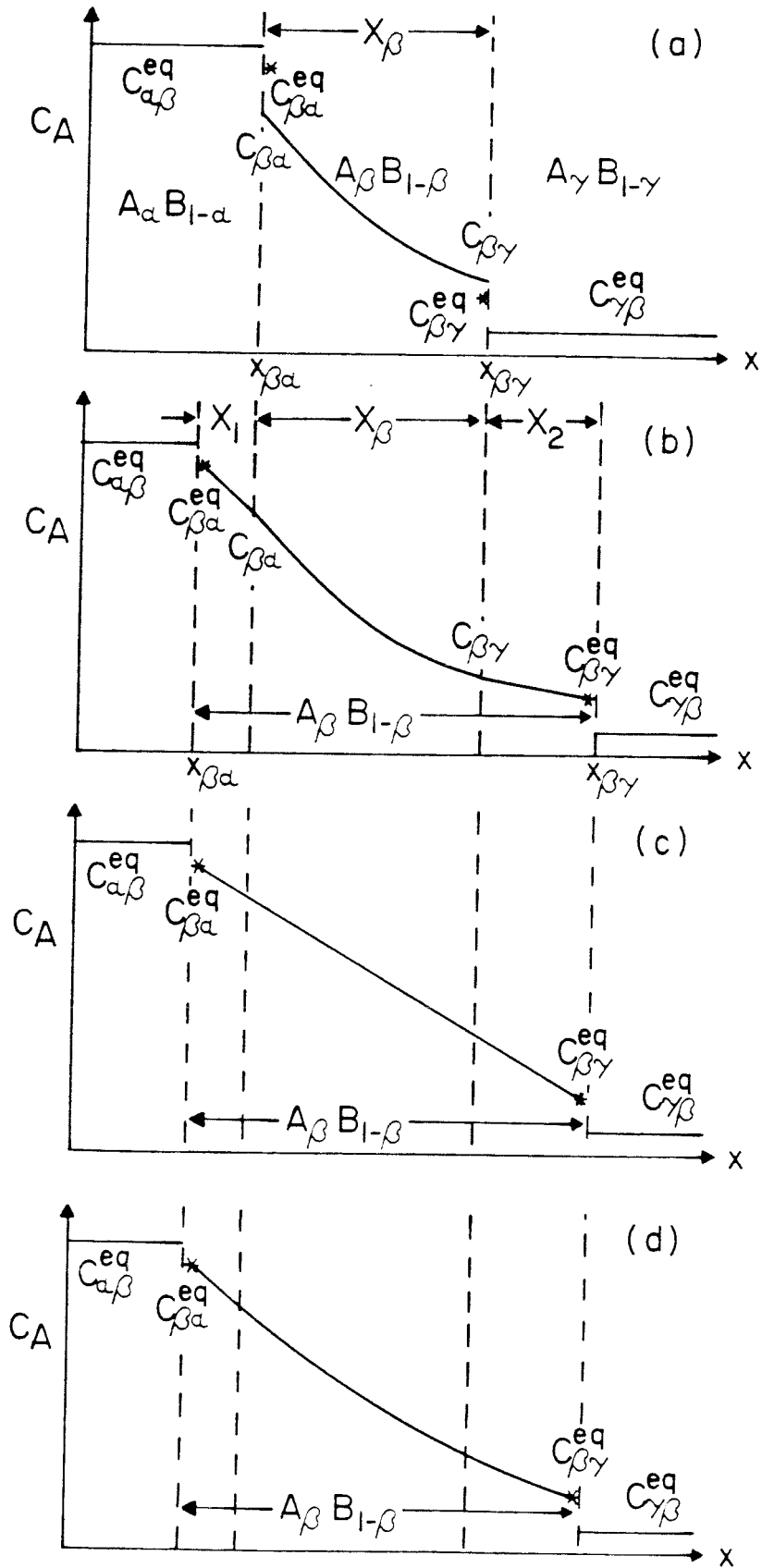
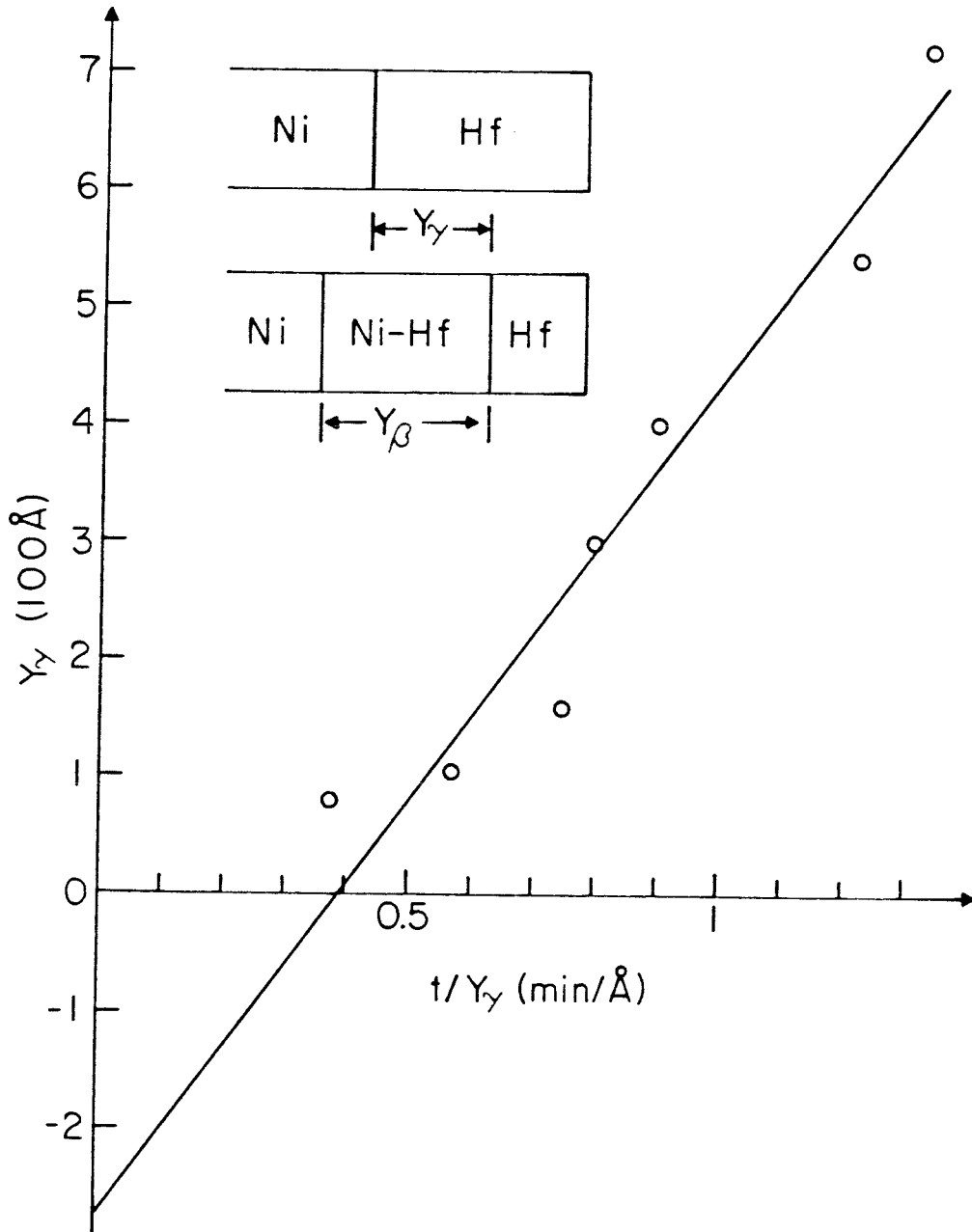


Fig.2



Appendix B –
Kinetics of Silicides
on
(100) Si and Evaporated Si Substrates

C.-D. Lien and M.-A. Nicolet
California Institute of Technology
Pasadena, California 91125
and
S. S. Lau
University of California at San Diego
La Jolla, California 92093

Abstract

We investigate the growth rates of Ni_2Si , NiSi , Pt_2Si , PtSi , and CrSi_2 formed on a (100) Si (Si^c) or an evaporated Si (Si^e , which is amorphous) substrate during thermal annealing. The same phases of silicides were found on Si^c and on Si^e . Also the growth rates of the silicides formed on Si^c is similar to that formed on Si^e . The formation temperature of CrSi_2 is about 50°C lower on Si^e than on Si^c . Also the CrSi_2 formed on Si^e is laterally more uniform than that formed on Si^c .

Introduction

Metal silicides are important in the manufacture of semiconductor devices. There has been much activity in the study of growth kinetics [1]. As the packing density of discrete elements in integrated circuits increases, the junctions below the contacts become shallow, the silicides used for contact are not allowed to consume too much Si from the substrate. Silicides formed from the evaporated Si (Si^e) are very good candidates for these shallow junction contacts [2, 3]. The properties of silicides formed from Si^e are therefore important. There has been much activity in the study of the growth kinetics of silicides on Si^c [1], but, only few have been reported for silicide formation on Si^e [4–9].

There are several differences between samples with Si^c substrate (Si^c/M) or Si^e substrate (Si^e/M):

- (I) There is more impurity at the Si^c/M interface than at the Si^e/M interface. This is because the Si^e evaporation is followed by the metal evaporation without breaking the vacuum.
- (II) Si^c may contain less impurity than Si^e which getters impurities during evaporation.
- (III) The Si substrates, and therefore the silicides results, have different microstructures.
- (IV) The Si^a has a positive formation energy (about 2.8 kcal/mol for noble gas implanted Si^a [11] or about 2.4 kcal/mol for sputtered Si^a [12]), and so does Si^e .

Impurities at the metal/ Si^c interface have been said to raise the metal– Si^c reaction temperature and to cause a laterally nonuniform silicide reaction in TiSi_2 [6] and ErSi_2 [7]. Microstructural differences in the silicide have been invoked to explain the faster growth of Pd_2Si on Si^e than on Si^c , but impurities in the bulk of Si^e reduce the growth rate [5]. Formation energy arguments have been advanced to explain why NiSi_2 [8] and CoSi_2 [9] form at low temperatures on Si^e , but not on Si^c . The question here is how these differences might affect the formation of Ni_2Si , NiSi , Pt_2Si , PtSi , and CrSi_2 .

Experimental Procedures

Commercially prepared p-type (100) Si wafers of resistivity 1.5–2.5 Ωcm were cleaned ultrasonically with TCE, acetone and methanol and then etched in a 20% HF solution. After a 5 min etch, the wafer was rinsed in deionized water, oxidized in RCA solution ($\text{H}_2\text{O}_2:\text{NH}_4\text{OH}:\text{H}_2\text{O} = 1:1:5$) for 5 min, and then etched in a 6% HF solution for another 5 min.

Immediately after cleaning, the wafers were loaded into an oil-free e-gun evaporator. Silicon films of various thicknesses (1 kÅ to 10 kÅ) were evaporated on half of each wafer; several metal films (Ni, Pt, Cr) of different thicknesses (500 Å to 4000 Å) were then deposited on the top of the full wafers. This procedure assures that the metal used on Si^c and on Si^e have the same evaporation conditions and, therefore, have similar properties. During evaporation, the pressure was kept below 3×10^{-7} Torr and the evaporation rates of metal and Si are about 35–45 Å/s and 20–30 Å/s, respectively.

Samples were then annealed in a vacuum furnace. During isothermal annealing, samples of both Si^c and Si^e substrates were placed side-by-side in the same boat and annealed for the same length of time. The vacuum during annealing was about 5×10^{-7} Torr. Annealing temperatures ranged from 200°C to 500°C.

The thicknesses and atomic ratio in the silicides were measured by MeV Rutherford backscattering spectrometry (RBS). Read camera X-ray diffraction films were used to establish the phases of silicides present in the sample.

Results

A. Formation of Ni Silicides

Olowolafe et al. reported that when the sample with a thin evaporated

Ni film on Si^c was annealed in vacuum, there were two phases, namely, Ni_2Si and NiSi , present simultaneously [4]. By doing a similar experiment, we have found that Ni_2Si is the only phase present when Ni is not completely consumed. Fig. 1 (a) shows the thicknesses of Ni_2Si versus \sqrt{t} at different temperatures. Results show that the growth of Ni_2Si on Si^c (100) and on Si^c are diffusion-controlled. Fig. 1 (b) shows the Arrhenius plot for the Ni_2Si formation. The open circles and full circles are data points of Ni_2Si formed from Si^c and Si^c , respectively. The growth rate of Ni_2Si is a little faster on Si^c than on (100) Si^c . The activation energy of Ni_2Si grown on Si^c and on Si^c are about 1.5 ± 0.1 eV and 1.4 ± 0.1 eV, respectively. The result of Ni_2Si grown on (100) Si^c is similar to those reported by Tu et al. (— — —) [13] and Olowolafe et al. (- - -) [4] as shown in Fig. 1 (b).

When NiSi grows on (100) Si, two kinds of kinetics have been reported: Coe et al. claimed that the thickness of NiSi is proportional linearly to time [14], while Scott et al. reported that the thickness is proportional to \sqrt{t} [15, 16]. Here we find the results similar to that reported by Scott et al.. Figure 2 (a) shows the square of the NiSi thicknesses versus t . The growth rates are the same for NiSi grown on either substrate. Figure 2 (b) shows the Arrhenius plot of NiSi (circles) and data from Scott (crosses). The activation energy of NiSi is about 1.55 ± 0.1 eV.

B. Formation of Pt Silicides

Platinum silicides, in contrast with Ni silicides, were reported to have a similar growth rate on (100) Si or (111) Si [17, 18]. We also find that Pt silicides have similar rates on both Si^c and Si^c substrates. Figure 3 (a) shows the thicknesses of Pt_2Si versus \sqrt{t} . Results show that in both cases the growth is controlled by the diffusion process. Figure 3 (b) shows the Arrhenius plot for Pt_2Si . As for the case of Ni_2Si , the formation temperature of Pt_2Si is a little lower on the Si^c than on the (100) Si^c ; the growth rate of Pt_2Si on Si^c is a little faster than that on Si^c , and both have a similar activation energy of about 1.4

± 0.1 eV. Data of Pt₂Si grown on (100) Si from Canali et al. (— -) [18], Poate et al. (- - -) [17], and Crider et al. (— — —) [19] are also shown in the Fig. 3 (b). That the growth rates of this silicide scatter a lot, as shown in the figure, may imply that Pt₂Si is sensitive to the impurity in the film. In fact, the rate of Pt₂Si formed in UHV [19] is much faster than that of Pt₂Si formed in the ordinary vacuum.

Figure 4 (a) shows the square of the PtSi thicknesses versus \sqrt{t} . The growth of PtSi is also diffusion-controlled. Just as in the Pt₂Si case, the growth rate of PtSi is a little faster when formed on Si^e than when formed on Si^c. The Arrhenius plot of PtSi (see Fig. 4 (b)) shows a similar activation energy of about 1.5 ± 0.1 eV. As in the Pt₂Si case, other reported results are also shown in Fig. 4 (b). The data of PtSi are also scattered as those of Pt₂Si. This seems to suggest that PtSi is also sensitive to impurities. In fact, PtSi formed in UHV [19] has a very fast rate.

C. Formation of CrSi₂

In contrast to the silicides reported above, CrSi₂ has a constant initial growth rate. However, the growth rate decreases when the CrSi₂/Cr interface approaches the surface. This slowing down effect was believed due to the penetration of oxygen during annealing [20, 21]. To reduce this interference of oxygen, we used samples with a 3000 Å thick Cr film to study the kinetics of CrSi₂. Also as reported by Olowolafe et al. [20], the formation temperature of CrSi₂ is about 450°C; by inserting a thin Pd film in Cr/Si interface, the formation temperature of CrSi₂ decreases to 400°C. However, the growth rate of CrSi₂ at 450°C or higher is very similar regardless of the presence of Pd. They suggested that the absence of CrSi₂ below 450°C was due to the presence of interfacial impurities. Here by evaporating Si and subsequent Cr films, the Cr/Si^e interface has much less impurity than the Cr/Si^c interface. We find that the formation temperature of CrSi₂ from Si^e is also about 400°C. The linear growth rate of CrSi₂ is a little faster on Si^e than on Si^c. Also from the

RBS spectra and optical microscope results, the CrSi_2 film on Si^e is much more uniform and has a better surface morphology than that on Si^c . This is the same result as reported for ErSi_2 [7] and TiSi_2 [6]. These facts can be explained by the presence of the interfacial impurity at the Cr/Si^c interface, but not at the Cr/Si^e interface. Figure 5 (a) shows the thicknesses of CrSi_2 versus time. The subsequent slowing down of CrSi_2 growth is again observed here. The Arrhenius plot of the initial growth rate of CrSi_2 shown in Fig. 5 (b) gives the activation energy of about 2.0 ± 0.1 eV. This activation energy given here is higher than that of CrSi_2 on (100) Si reported by Olowolafe et al. (about 1.7 eV) [20] (see Fig. 5 (b)).

Discussion

The silicides formed, their formation temperatures, activation energy, and the time dependence of thickness, are listed in table 1. The results show that:

- (1) Some silicides have a lower formation temperature on Si^e than on Si^c (namely, NiSi_2 , CoSi_2 , and CrSi_2).
- (2) Some silicides are more uniform on Si^e than on Si^c (namely, NiSi_2 , CoSi_2 , and CrSi_2).
- (3) Most silicides have a faster growth rate on Si^e than on Si^c (namely, Ni_2Si , NiSi_2 , CoSi_2 , Pt_2Si , PtSi , and CrSi_2), but Co_2Si and CoSi show the reverse phenomenon.
- (4) If the formation of a silicide on Si^c is diffusion-controlled (i.e., \sqrt{t} dependent) or interfacial reaction-controlled (i.e., t dependent), then that time dependence remains the same on Si^e .
- (5) On Si^c , the formation of NiSi_2 or CoSi_2 has a threshold temperature [22], but not on Si^e .

Those silicides that form on Si^c and Si^e and have different properties can be attributed to various causes. Four have been mentioned in the introduction of this chapter and are listed in Table 2. We do not know which of these applies to any particular case. We nevertheless list those that we believe apply in each case. They are listed in Table 2 in order of their likelihood.

The impurities at the Si^c/M interface can stop the silicide formation at a temperature which is sufficient for silicide formation at the clean Si^e/M interface. When the temperature increases, silicide forms first on the weak spots of a contaminated interface. The silicide thus grows is laterally nonuniform. If the annealing temperature further increases, the effect of the interfacial impurities is much reduced. Therefore the interfacial impurities can explain why the CrSi_2 (1) has a lower formation temperature when formed on Si^e than on Si^c substrates and (2) is more uniform when formed on Si^e than on Si^c . The above results are also observed for the cases of TiSi_2 [6] and ErSi_2 [7]. We would like to point out that in the cases of NiSi_2 and CoSi_2 , interfacial impurities are unlikely to raise their formation temperatures or induce lateral nonuniformity. This is because the silicides are not the first ones to form. On the basis that Ni or Co is the DMS in the initial phase (Ni_2Si or Co_2Si) formation, interfacial impurities will be swept out to the sample surface.

A higher bulk impurity concentration in Si^e than in Si^c can cause a lower silicide growth rate on the former Si substrate. We believe that it is one of the reasons that cause the slower growth rates of Co_2Si and CoSi on Si^e than on Si^c . However, the microstructural differences between the silicide formed on Si^e (small grain size, random grain orientation, and so on) and on Si^c can also cause different silicide growth rates. In general, the silicide formed on Si^e has a small grain size, and therefore, more grain boundaries. If the grain boundary diffusion is dominant during silicide reaction, then the silicide may grow faster on Si^e than on Si^c . This result has been used to explain the faster growth rate of Ni_2Si [4] and Pd_2Si [5] on Si^e than on Si^c . On the other hand, if the bulk diffusion is dominant, then the growth rate can be slower or faster for the silicide grown on Si^e than on Si^c , depending on the the detailed structures

of the silicide.

The positive formation energy of Si^e increases the driving force (more negative reaction free energy) for silicide formation. In general, the larger driving force will only cause a higher growth rate. But in the case of thin silicides which are unstable at low temperature (NiSi_2 and CoSi_2), the positive formation energy of Si^e will decrease the silicide formation temperature. There are two possibilities for having an unstable silicide: In one case, the bulk-phase silicide is considered to be nonexistent in thermal equilibrium at low temperatures [8]. In the other case, the bulk silicide barely exists, but the interface and strain energies make the thin silicide unstable at a low temperature [22]. In both cases, the thin silicide is metastable on the Si^e substrate when the temperature is lower than a threshold temperature ($> 500^\circ\text{C}$ for CoSi_2 and $> 750^\circ\text{C}$ for NiSi_2). When the temperature exceeds that threshold, the growth can be very fast where the silicide nucleates. Such a growth, controlled by heterogeneous nucleation, then causes a laterally nonuniform silicide formation. The positive formation energy of Si^e can reduce the threshold temperature, i.e. the formation temperature. In the cases of NiSi_2 and CoSi_2 , the threshold temperatures are reduced so much that the growth controlling processes are changed from the nucleation controlled processes to the diffusion controlled processes. Therefore, the silicide formed on Si^e becomes laterally uniform.

Conclusion

In contrast to Pd_2Si , ErSi_2 , CoSi_2 , and NiSi_2 , the differences between the Si^e (100) and the evaporated Si have little effect on the kinetics of Ni_2Si , NiSi , Pt_2Si , PtSi , and CrSi_2 . However, in the case of CrSi_2 , we find the lowering of formation and improvement of surface morphology when the silicide is grown from Si^e . These results may imply that CrSi_2 is much more sensitive to the interfacial impurity than Ni and Pt silicides are.

Acknowledgments

The authors acknowledge B. X. Liu and Dr. M. Van Rossum for making X-ray diffractions, R. Fernandez for assisting sample preparation.

References

1. M-A. Nicolet and S. S. Lau, in *VLSI Electronics: Microstructure Science*, N. G. Einspruch, treatise Ed., Vol. 6, *Materials and Process Characterization*, N. G. Einspruch and G. B. Larrabee, volume Eds. (Academic Press, New York, 1983), Ch. 6.
2. B.-Y. Tsaur, D. J. Silversmith, R. W. Mountain, L. S. Hung, S. S. Lau, T. T. Sheng, *J. Appl. Phys.* 52, 5243 (1981).
3. S. Kritzinger and K. N. Tu, *J. Appl. Phys.* 52, 305 (1981).
4. J. O. Olowolafe, M-A. Nicolet and J. W. Mayer, *Thin Solid Films* 38, 143 (1976).
5. N. Cheung, S. S. Lau, M-A. Nicolet, and J. W. Mayer, in *Proc. Symp. on Thin Film Interfaces and Interactions*, J. E. E. Baglin and J. M. Poate, Eds., (Electrochemical Society, Princeton, NJ, 1980) Vol. 80-2, p. 494.
6. L. S. Hung, J. Gyulai, J. W. Mayer, S. S. Lau, and M-A. Nicolet, *J. Appl. Phys.* 54 5076 (1983).
7. C. S. Wu, S. S. Lau, T. F. Kuech, and B. X. Liu, *Thin Solid Films* 104 175 (1983).
8. C.-D. Lien, M-A. Nicolet, and S. S. Lau, *phys. stat. sol. (a)* 81, 123 (1984).
9. C.-D. Lien, M-A. Nicolet, and S. S. Lau, *Appl. Phys. A* (1984) (in press).
10. C.-D. Lien, M-A. Nicolet, C. S. Pai, and S. S. Lau (in preparation).
11. E. P. Donovan, F. Spaepen, D. Turnbull, J. M. Poate, and D. C. Jacobson, *Appl. Phys. Lett.* 42 698 (1983).
12. J. C. C. Fan and H. Anderson, *J. Appl. Phys.* 52 4003 (1981).

13. K. N. Tu, W. K. Chu, and J. W. Mayer, *Thin Solid Films* 25, 403 (1975).
14. D. J. Coe and E. H. Rhoderick, *J. Phys. D* 9, 965 (1976).
15. D. M. Scott and M–A. Nicolet, *Nucl. Instr. Meth.* 182/183, 655 (1981).
16. D. M. Scott and M–A. Nicolet, *phys. stat. sol. (a)* 66, 733 (1981).
17. J. M. Poate and T. C. Tisone, *Appl. Phys. Lett.* 24, 391 (1974).
18. C. Canali, C. Catellani, M. Prudenziati, W. H. Wadlin, and C. A. Evans, Jr., *Appl. Phys. Lett.* 31, 43 (1977).
19. C. A. Crider and J. M. Poate, *Appl. Phys. Lett.* 36, 417 (1980).
20. J. O. Olowolafe, M–A. Nicolet, and J. W. Mayer, *J. Appl. Phys.* 47, 5182 (1976).
21. C.–D. Lien, L. S. Wieluński, M–A. Nicolet, and K. M. Stika, *Thin Solid Films* 104, 235 (1983).
22. J. Baglin, F. d'Heurle, and S. Petersson: in *Proceedings of the Symposium on Thin Film Interfaces and Interactions*, J. E. Baglin and J. M. Poate, Eds., Vol. 80–2 (Electrochemical Society, Princeton, 1980) p. 341.

Silicide	Time Dependence	silicon substrate	Activation Energy(eV)	Temperature Range(°C)	Ref.
Ni ₂ Si ^a	\sqrt{t}	(100)	1.5±0.1	210-335	II
	\sqrt{t}	Si ^e	1.4±0.1	210-335	II
NiSi ^b	\sqrt{t}	(100)	1.55±0.1	250-400	II
	\sqrt{t}	Si ^e	1.55±0.1	250-400	II
NiSi ₂ ^{d,i}	N. C. ^f	(100)		> 750	8
	\sqrt{t}	Si ^e	1.65±0.2	350-425	8
Co ₂ Si ^g	\sqrt{t}	(100)	1.7±0.1	385-490	10
	\sqrt{t}	Si ^e	1.85±0.1	385-490	10
CoSi ^g	\sqrt{t}	(100)	1.8±0.1	385-490	10
	\sqrt{t}	Si ^e	1.9±0.1	385-490	10
CoSi ₂ ^{d,i}	\sqrt{t}	(100)		> 500	9
	\sqrt{t}	Si ^e	2.3±0.1	405-500	9
Pt ₂ Si ^a	\sqrt{t}	(100)	1.4±0.1	194-305	II
	\sqrt{t}	Si ^e	1.4±0.1	194-305	II
PtSi ^a	\sqrt{t}	(100)	1.5±0.1	250-370	II
	\sqrt{t}	Si ^e	1.5±0.1	250-370	II
CrSi ₂ ^{a,h,i}	t	(100)	2.0±0.1	455-505	II
	t	Si ^e	2.0±0.1	400-505	II

a: Silicide grows faster on Si^e than on Si^c.

b: No visible difference in growth rates of the silicide on Si^e and Si^c.

d: Silicide will not form on Si^c below some threshold temperature.

f: Growth of the silicide is controlled by the silicide nucleation [22].

g: Silicide grows faster on Si^e than on Si^c.

h: Formation temperature of the silicide is lower on Si^e than on Si^c.

i: The silicide is more uniform on Si^e than on Si^c.

Table 1

Results on the reaction kinetics of silicides formed on Si^c (100) and the Si^e substrates.

Silicides	Ref.	Comparison	Causes
NiSi	II	(1) No visible change	
Ni ₂ Si	II	(1) Grows a little faster on Si ^e than on Si ^c	(III), (IV), (I)
Pt ₂ Si	II		
PtSi ^a	II		
Pd ₂ Si	5		
Co ₂ Si	10	(1) Grows slower on Si ^e than on Si ^c	(III)
CoSi	10	(1) Grows slower on Si ^e than on Si ^c	(II), (III)
CrSi ₂	II	(1) Grows faster on Si ^e than on Si ^c	(I), (III), (IV)
TiSi ₂	6	(2) Reduced formation temperature on Si ^e	
ErSi ₂	7	(3) Improved silicide uniformity on Si ^e	
NiSi ₂	8	(1) Grows faster on Si ^e than on Si ^c	(IV), (III)
CoSi ₂	9	(2) Reduced formation temperature on Si ^e (3) Improved silicide uniformity on Si ^e (4) Threshold temperature for silicide on Si ^c	

a: The possible reasons for PtSi are (III) and (IV) only.

(I): The Si^e/M interface is cleaner than the Si^c/M interface.

(II): There are more impurities in Si^e than in Si^c.

(III): The silicides formed have different microstructures.

(IV): The Si^e has a positive formation energy.

Table 2

Differences between silicides formed on Si^e and Si^c and possible causes. The order of the causes represents their likelihood.

Figure Captions

- Figure 1**
- (a) Thicknesses of Ni₂Si against \sqrt{t} . The Ni₂Si is formed between a thin Ni film and a (100) Si^c (full circles) or an Si^e (open circles) substrate. The annealing temperature (°C) is used as a parameter for the data.
 - (b) Arrhenius plot of Ni₂Si which gives the activation energy of about 1.5 ± 0.1 eV for both substrates. Open and full circles are data points from Si^e and Si (100) substrates, respectively. Data by Olowolafe et al. (- - -) [4] and Tu et al. (— — —) [13] are also shown here.
- Figure 2**
- (a) Thickness square of NiSi against time. The NiSi is formed between an Ni₂Si film and a (100) Si^c (full circles) or an Si^e (open circles) substrate. For simplicity, some of the fitting lines are not shown here. The annealing temperature (°C) is used as a parameter for the data.
 - (b) Arrhenius plot of NiSi which gives the activation energy of about 1.55 ± 0.1 eV. Open circles are data points from Si^e as well as Si (100) substrates. Crosses are data reported by Scott et al. [15, 16].
- Figure 3**
- (a) Thicknesses of Pt₂Si against \sqrt{t} . The Pt₂Si is formed between a thin Pt film and a (100) Si^c (full circles) or an Si^e (open circles) substrate. The annealing temperature (°C) is used as a parameter for the data.
 - (b) Arrhenius plot of Pt₂Si which gives the activation energy of about 1.4 ± 0.1 eV for both substrates. Data of Pt₂Si grown on (100) Si^c from Canali et al. (— - —) [18], Poate et al. (- - -) [17], and Crider et al. (— — —) [19] are also shown here.
- Figure 4**
- (a) Thickness square of PtSi against time. The PtSi is formed

between a Pt₂Si film and a (100) Si^c (full circles) or an Si^c (open circles) substrate. The annealing temperature (°C) is used as a parameter for the data.

- (b) Arrhenius plot of PtSi which gives the activation energy of about 1.5 ± 0.1 eV for both substrates. Data of PtSi grown on (100) Si^c from Canali et al. (— - —) [18], Poate et al. (- - -) [17], and Crider et al. (— — —) [19] are also shown here.

Figure 5

- (a) Thicknesses of CrSi₂ against time. The CrSi₂ is formed between a Cr film and a (100) Si^c (full circles) or an Si^c (open circles) substrate. The annealing temperature (°C) is used as a parameter for the data.
- (b) Arrhenius plot of CrSi₂ initial growth rate which gives the activation energy of about 2.0 ± 0.1 eV. Data of CrSi₂ grown on (100) Si^c by Olowolafe et al. (— — —) [20] (activation energy is about 1.7 ± 0.1 eV) are also shown here.

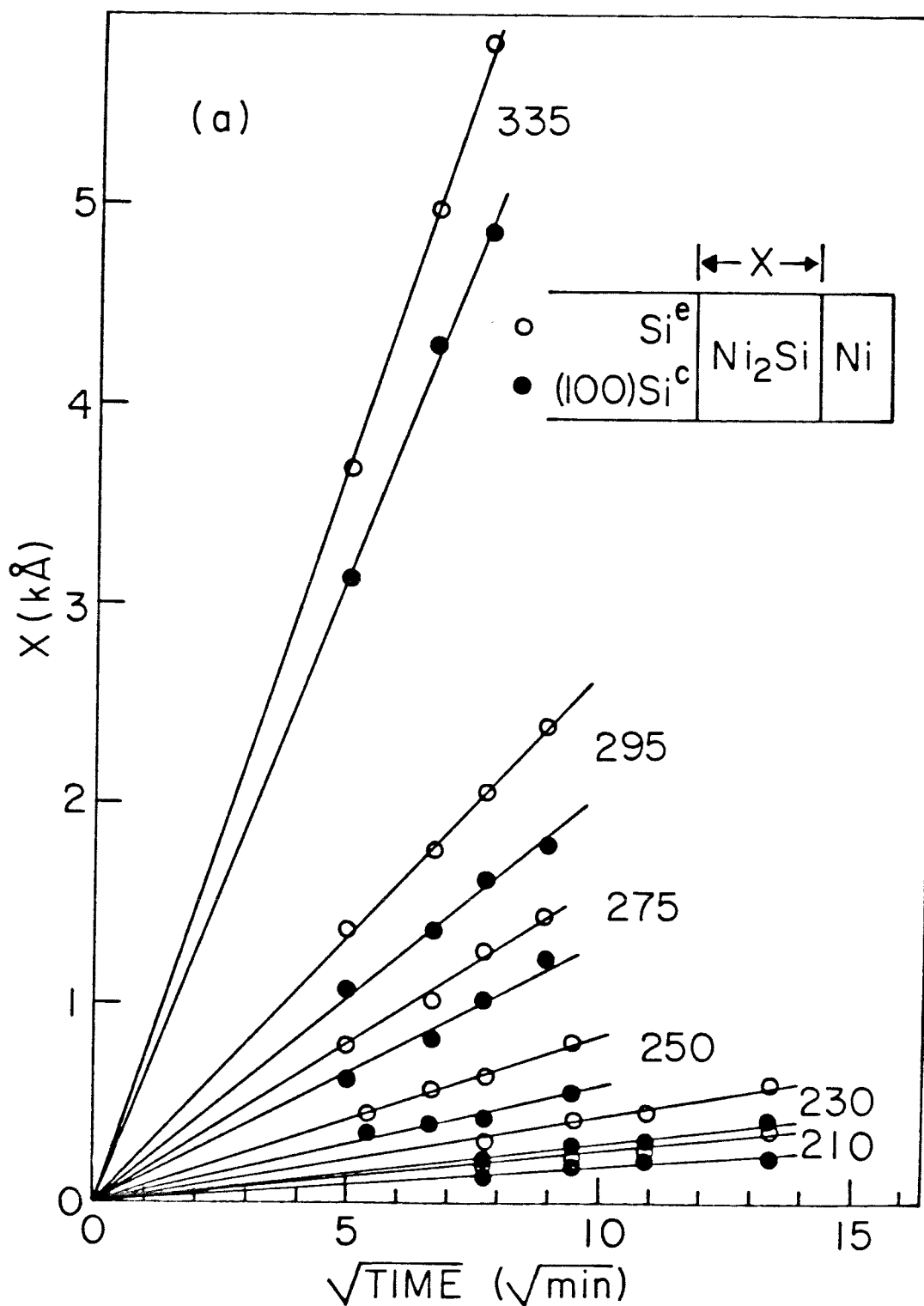


Fig.1

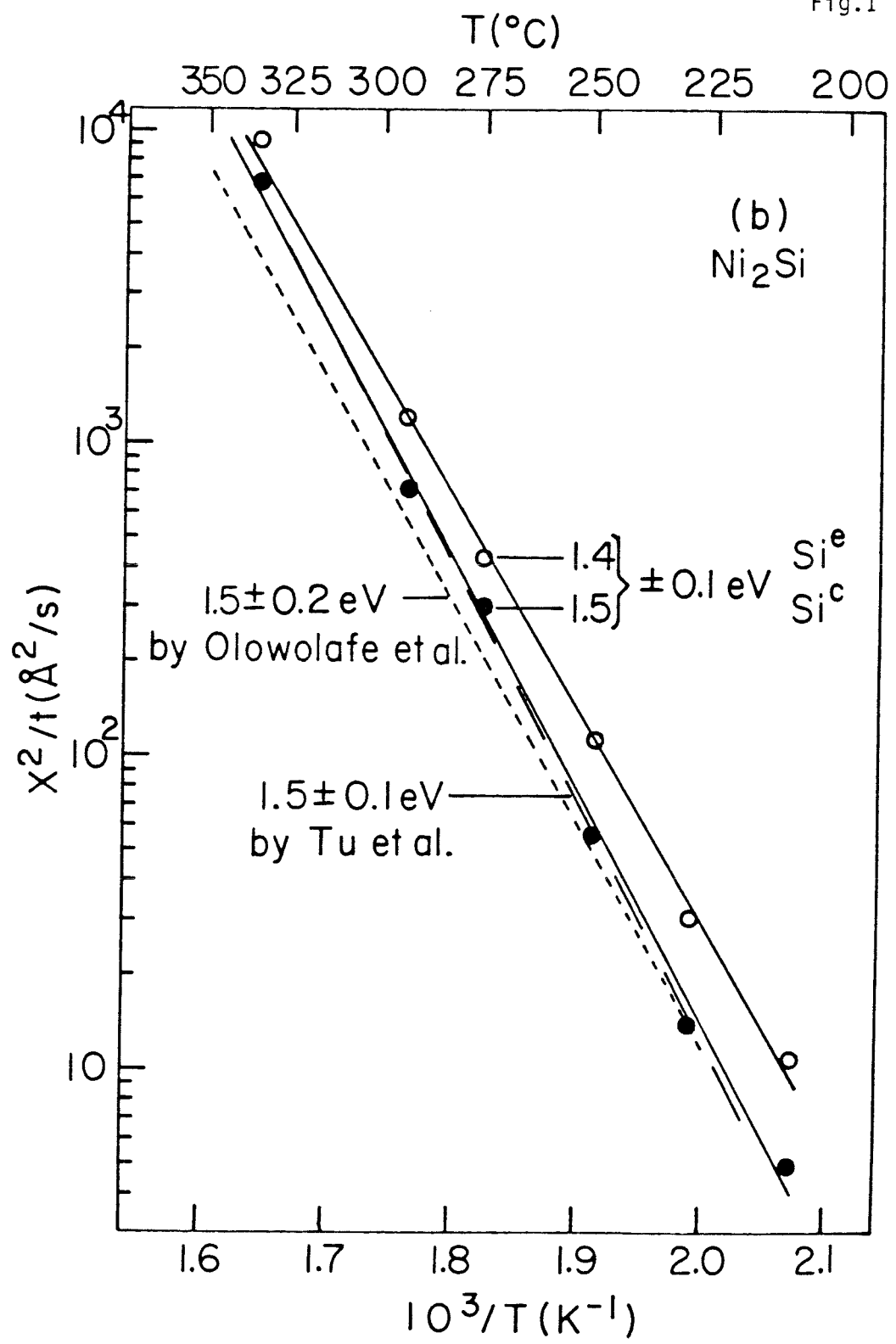
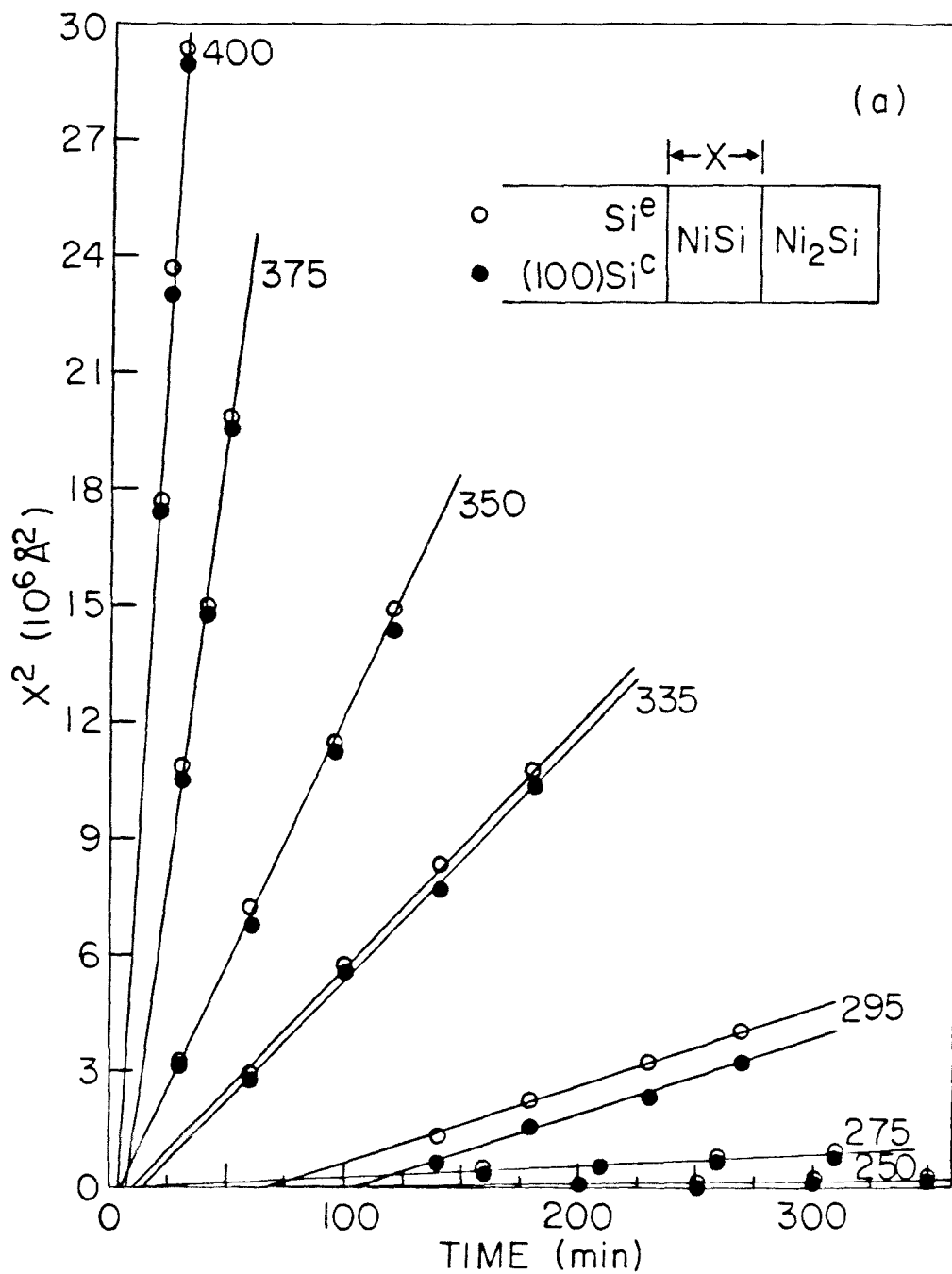
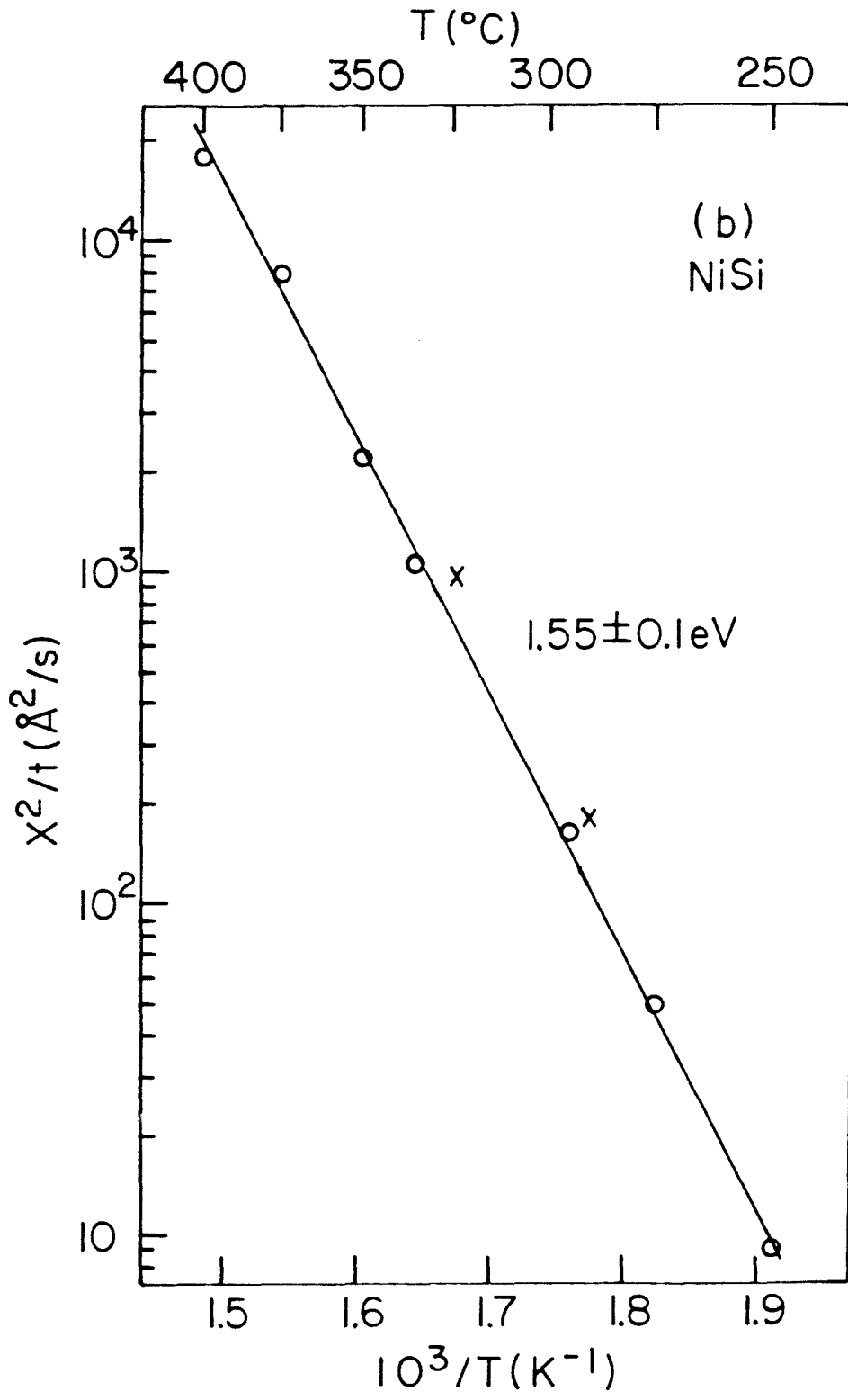


Fig.2





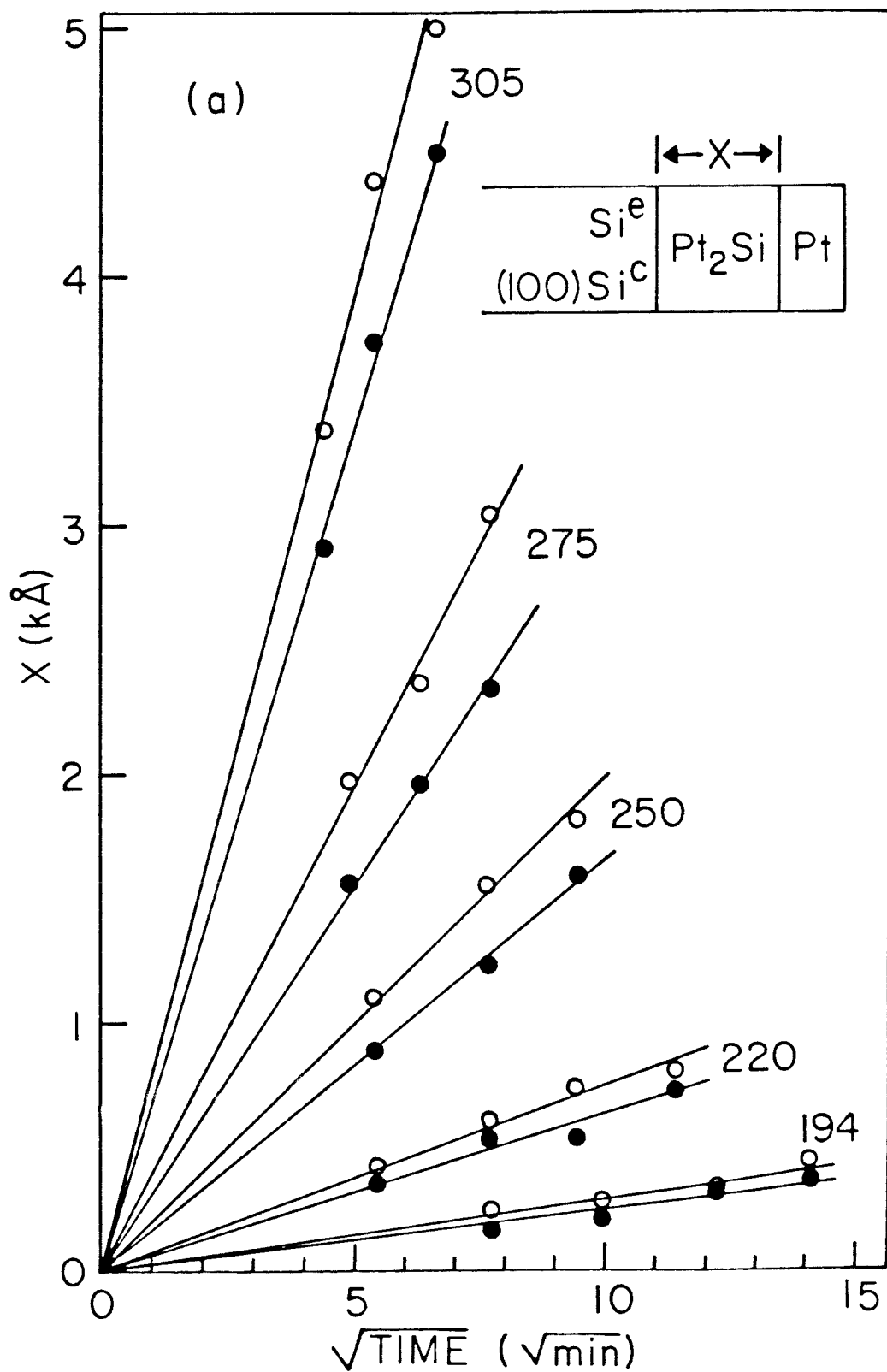


Fig.3

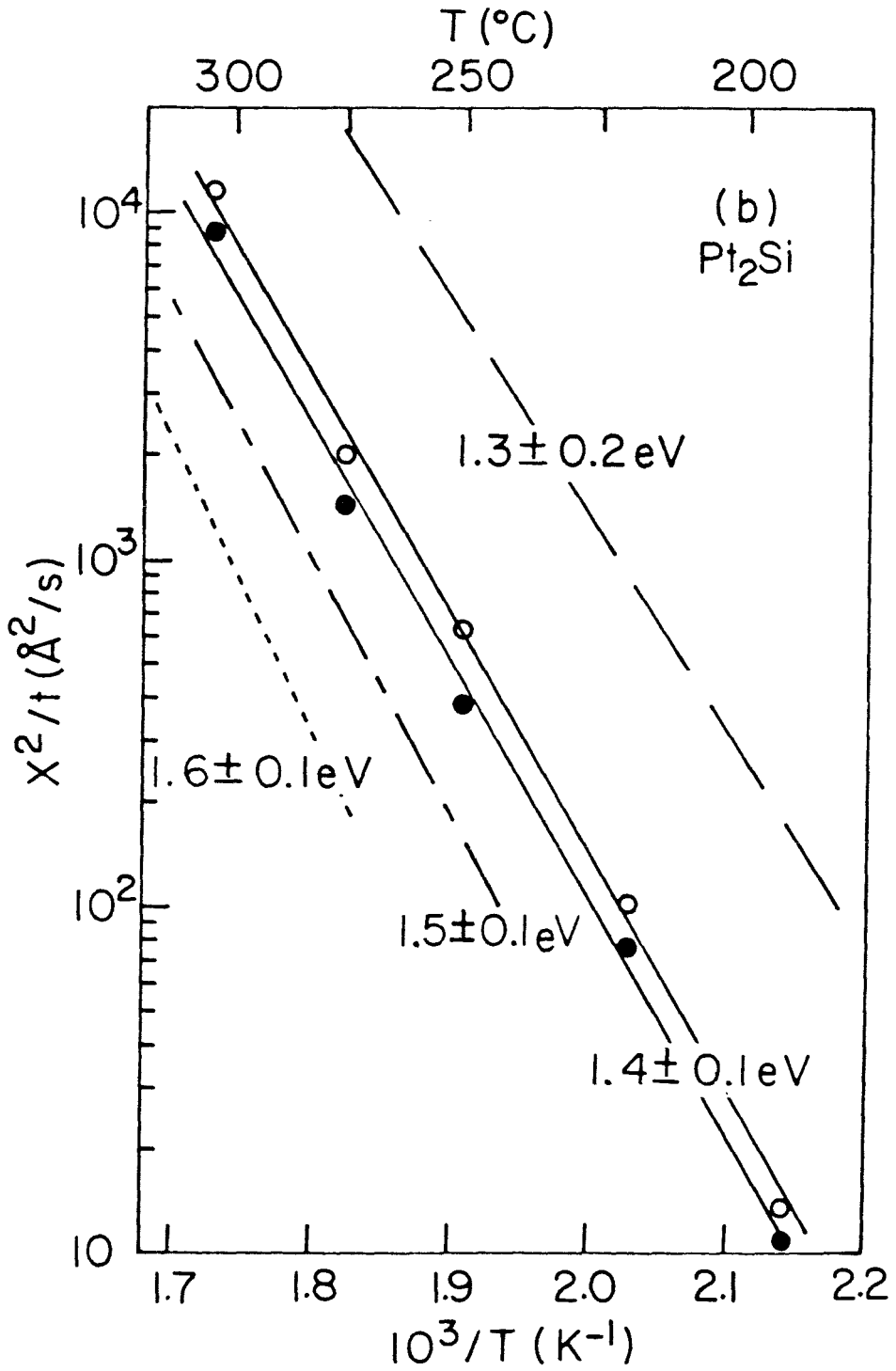


Fig.4

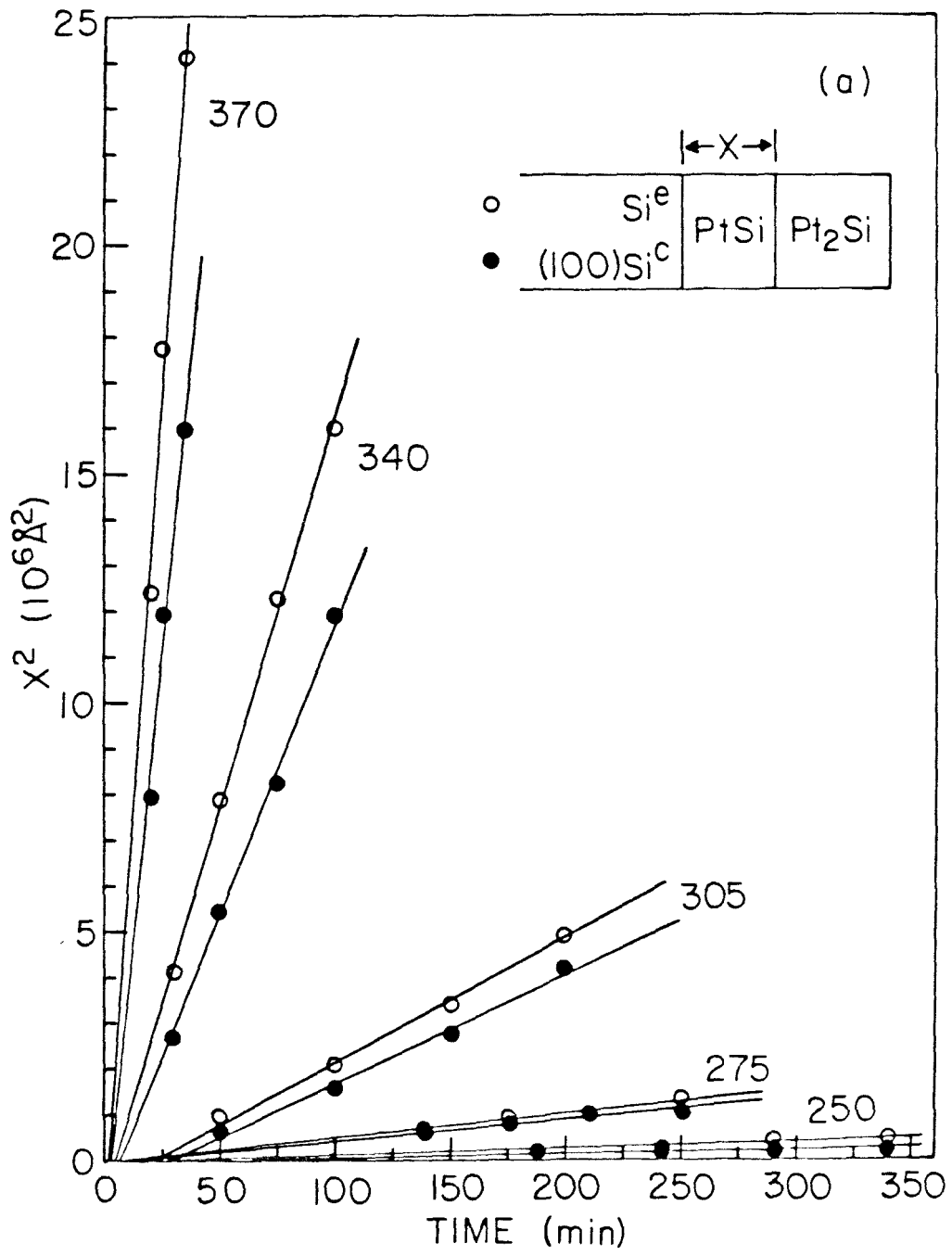


Fig.4

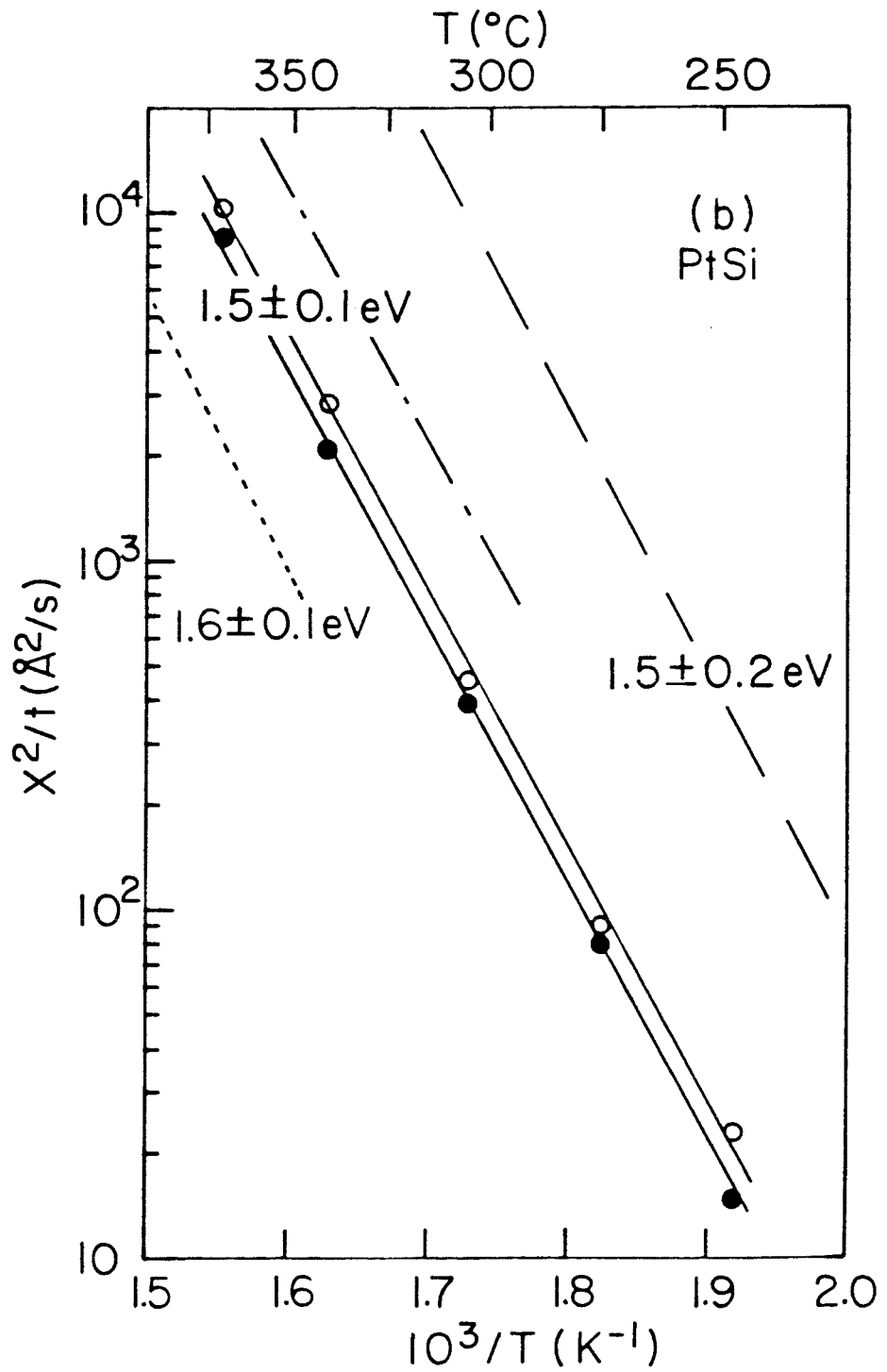


Fig.5

-105-

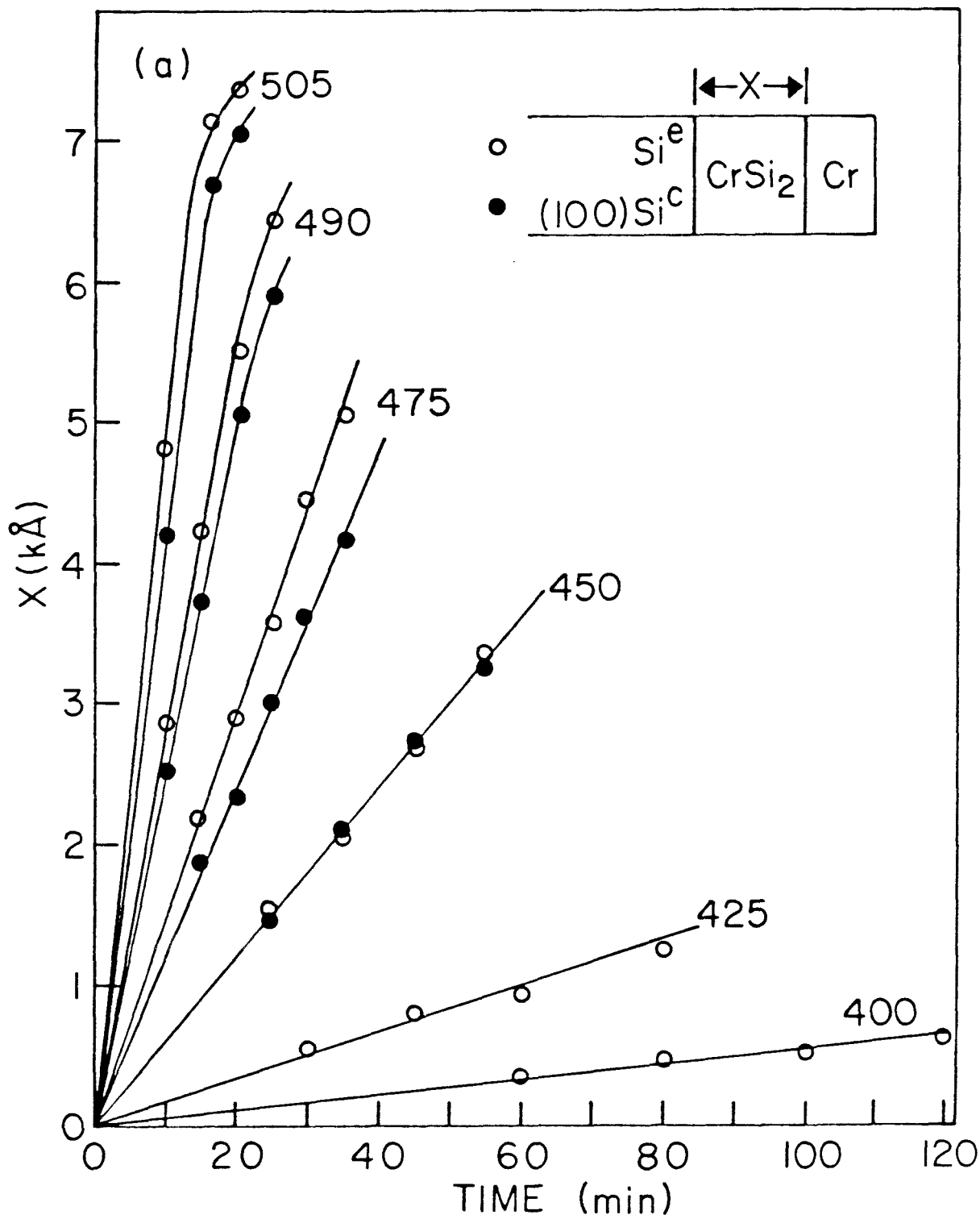
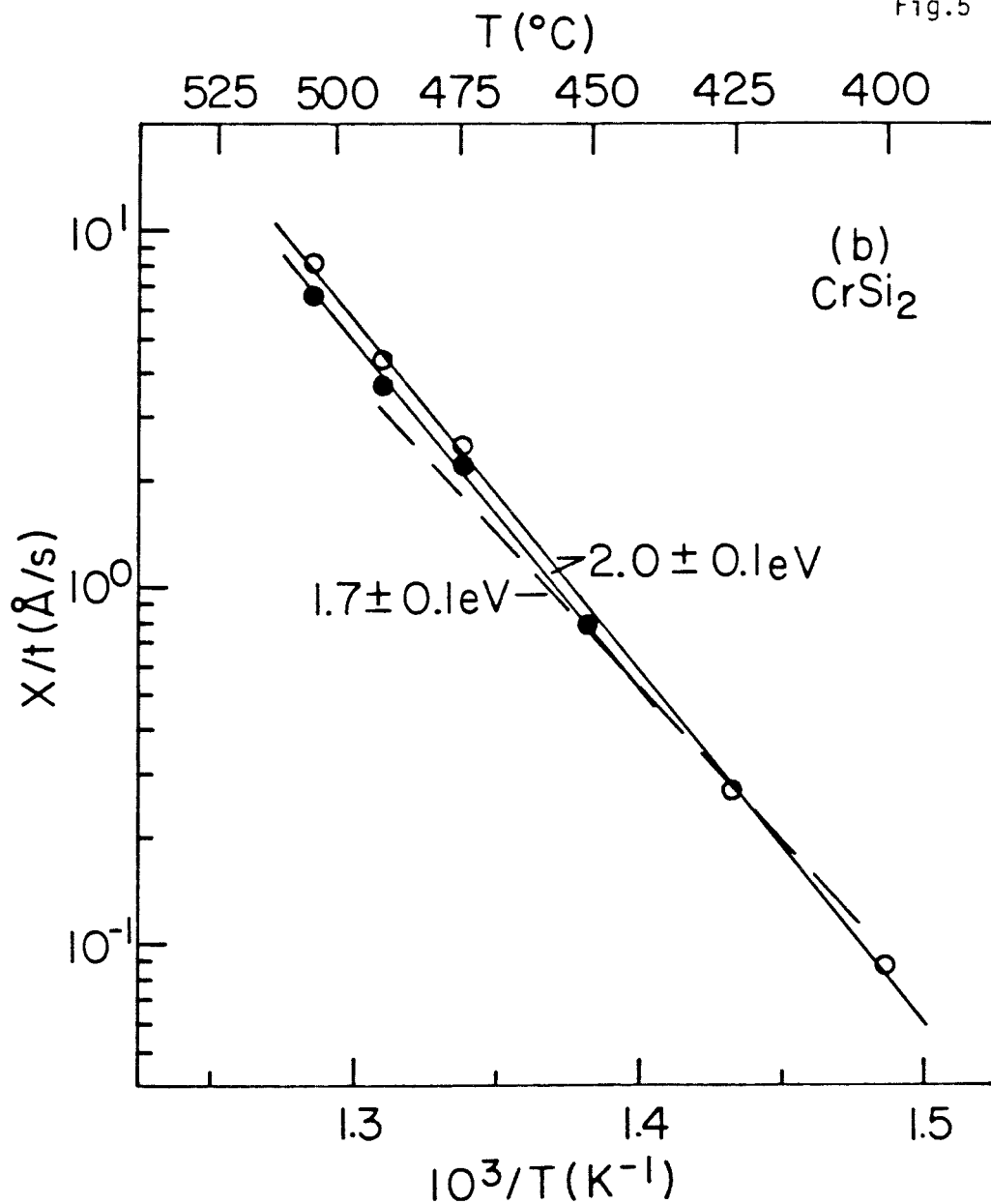


Fig.5



Appendix C –
Growth of Co–Silicides
from
Single Crystal and Evaporated Si

C.-D. Lien and M.-A. Nicolet
California Institute of Technology
Pasadena, California 91125

and

C. S. Pai and S. S. Lau
University of California at San Diego
La Jolla, California 92093

Abstract

We have investigated reactions of a thin Co film with a (100) Si (Si°) or an evaporated Si (Si^e , which is amorphous) substrates during thermal annealing. On either substrate, Co_2Si and CoSi form simultaneously and the growth of each phase has a square root of time dependence. A model was proposed to calculate the effective diffusion constant in each silicide from the growth data of the silicides. The activation energies of the effective diffusion constants in Co_2Si and CoSi grown on Si° were 1.7 eV and 1.8 eV, respectively, while those on Si^e were 1.85 eV and 1.9eV, respectively. Either silicide formed on Si^e grows faster than the corresponding silicide formed on Si° .

Introduction

Metal silicides are important in the manufacture of semiconductor devices. There has been much activity in the study of growth kinetics [1]. Lau et al. have reported that when a thin Co film begins to react with a (100) Si substrate, Co_2Si and CoSi grow side-by-side first and that Co_2Si transforms to CoSi once all the Co is consumed [2]. The thicknesses of both Co_2Si and CoSi are proportional to the square root of annealing time. The activation energies of growth for Co_2Si and CoSi are 1.5 and 1.9 eV, respectively [2]. In this two-phase formation case, the growth of each silicide depends on a mixed result of fluxes in Co_2Si and CoSi . Therefore the activation energy of silicide growth is physically less meaningful than that of the flux in each silicide. Another result of the Co-Si (100) reaction is that only Co_2Si is formed initially and that CoSi started to form only when the Co was totally consumed [3]. If this is the case, the activation energy of the growth will be physically meaningful. However, ref. 3 does not show any activation energy data.

In this paper, we study and compare the silicide formation during thermal annealing of the Co/Si system with either the Si^c or the Si^e substrate. We also give a simple model to calculate the effective diffusion constant (proportional to the diffusion constant, as defined in the Appendix) in each silicide from the measured growth data.

Experimental Procedures

Commercially prepared p-type Si (100) wafers of resistivity 1.5–2.5 Ωcm were cleaned ultrasonically with TCE, acetone and methanol and then etched in a 20% HF solution. After a 5 min etch, the wafer was rinsed in deionized water, oxidized in RCA solution ($\text{H}_2\text{O}_2:\text{NH}_4\text{OH}:\text{H}_2\text{O} = 1:1:5$) for 5 min, and then etched in a 6% HF solution for another 5 min.

Immediately after cleaning, the wafers were loaded into an oil-free

e-gun evaporator. Silicon films of thickness about 5000 Å were evaporated on half of each wafer. Cobalt films of thickness about 2200 Å were then deposited on the top of the full wafers. This procedure assures that the Co used on Si^c and on Si^e have the same evaporation conditions and, therefore, have similar properties. The evaporation rates of Si and Co were about 40 Å/s and 25 Å/s, respectively, with pressure kept below 3×10^{-7} Torr during evaporation.

Samples were then annealed in a vacuum furnace. During isothermal annealing, samples of both Si^c and Si^e substrates were placed side-by-side in the same boat and annealed for the same length of time. The vacuum during annealing was about 5×10^{-7} Torr. Annealing temperatures ranged from 380°C to 490°C.

The thicknesses and atomic ratio in the silicides were measured by MeV Rutherford backscattering spectrometry (RBS).

Results

Figure 1 shows RBS spectra of (a) Co/Si^c and (b) Co/Si^e samples annealed at 440°C. The spectra show that Co₂Si and CoSi form simultaneously for either Si substrate. The two-phase formation in the Co/Si^c sample is the same as that reported by Ref. 2. The thicknesses of (a) Co₂Si and (b) CoSi vs. \sqrt{t} were shown in Fig. 2 at different temperatures. Open and full symbols show data of silicides formed on Si^e and Si^c, respectively. On either substrate, we can see that the growth of each silicide has a square root of time dependence. From Fig. 2, it is clear that the growth rate of either silicide is slower on Si^e than on Si^c.

During a thin silicide film reaction, it is known that [4, 5], if the fluxes in silicides are controlled by the diffusion processes, the thickness of each silicide is proportional to the square root of the isothermal annealing time. In this case, the square of a silicide thickness divided by time (defined as growth

rate of that silicide) is constant for a fixed temperature. If there is only one silicide formed during reaction, the growth rate of the silicide is proportional to the effective diffusion constant (see Appendix) of the silicide. Therefore, the activation energy of the silicide growth rate is just that of the effective diffusion constant of the silicide. However, if there are several silicides formed simultaneously during reaction, the growth of each silicide is due to the mixed results of several fluxes [5]. Therefore, in this case, the activation energy of a silicide growth rate is not physically meaningful.

Thus, in the case of the two-phase formation studied here, the activation energy of the silicide growth rate is not as meaningful as in the single compound formation case. However, we can obtain the effective diffusion constant data from the silicide growth rate data as shown in the Appendix. Figure 3 shows the Arrhenius plots of the effective diffusion constants in Co_2Si and CoSi for either substrate. As in the case of Fig. 2, the open and full symbols are used to represent the data from Si^e and Si^c , respectively. The circles show the data of Co_2Si and the triangles show those of CoSi . The activation energies of the effective diffusion constants in Co_2Si and CoSi grown on Si^e are 1.7 eV and 1.8 eV, respectively, while those on Si^c are 1.85 eV and 1.9 eV, respectively. In the same figure, we also present the effective diffusion constant data calculated from the growth rate data in Ref. 2. These data show that the activation energies of the effective diffusion constants in Co_2Si and CoSi are 1.65 eV and 1.9 eV, respectively. The effective diffusion constants for Co_2Si (cross) and CoSi (square) at 460°C calculated from Ref. 3 are also shown in this plot.

Discussion

There are several differences between samples with an Si^e substrate (Si^e/M) or an Si^c substrate (Si^c/M). These differences are:

- (I) There is more impurity at the Si^c/M interface than at the Si^e/M interface. This is because the Si^e evaporation is followed by the metal evaporation

without breaking the vacuum.

- (II) Si^c may contain less impurity than Si^e which getters impurities during evaporation.
- (III) The Si substrates, and therefore the silicides results, have different microstructures.
- (IV) The Si^a has a positive formation energy (about 2.8 kcal/mol for noble gas implanted Si^a [6] or about 2.4 kcal/mol for sputtered Si^a [7]), and so does Si^c .

These differences do not have a big effect on the formation of Ni_2Si , NiSi , Pt_2Si , and PtSi [8]. However, they do affect the formation of some other silicides: Impurities at the metal/ Si^c interface have been said to raise the metal- Si^c reaction temperature and to cause a laterally nonuniform silicide reaction in TiSi_2 [9], ErSi_2 [10], and CrSi_2 [3]. Formation energy arguments have been advanced to explain why NiSi_2 [11] and CoSi_2 [12] form at low temperatures on Si^e , but not on Si^c . Microstructural differences in the silicide have been invoked to explain the faster growth of Pd_2Si on Si^e than on Si^c , but impurities in the bulk of Si^e reduce the growth rate [13].

In the present case of Co_2Si and CoSi , we found that the growth rates of silicides grew slower on Si^e than on Si^c . This can be either due to the impurity in the Si^e which hinders the growth of silicide or due to the microstructural difference of the silicides which alters the effective diffusion constants in the silicides. The impurity in the Si substrate indeed can decrease the flux in the CoSi ; however, the impurity cannot change the flux in Co_2Si [14]. The observation here shows that the flux in either silicide is reduced on the Si^e substrate. We thus believe that the microstructural differences in the silicide have reduced the flux in Co_2Si . Whether the flux in CoSi is reduced by the presence of the impurity in the Si^e or by the different microstructures of the silicide is not known from the study here.

Conclusion

The growth of Co_2Si and CoSi on Si^c and Si^e has been investigated. The results show that on either substrate the Co_2Si and CoSi formed simultaneously during annealing. The growth rates of either silicide is slower on Si^e than on Si^c . A simple model was used to calculate the effective diffusion constants out of the growth rate data. The activation energies of the effective diffusion constants in Co_2Si and CoSi grown on Si^c were 1.7 eV and 1.8 eV, respectively, while those of the fluxes in Co_2Si and CoSi grown on Si^e were 1.85 eV and 1.9 eV, respectively.

Acknowledgments

The authors acknowledge A. Ghaffari and R. Gorris for technical assistance.

Appendix

In this Appendix, we will find a relation between a film thickness and the fluxes in the film and its adjacent compounds. When a compound A_qB_{1-q} is sandwiched by another two compounds, A_pB_{1-p} and A_rB_{1-r} , (assuming $p > q > r$) the thickness of the sandwiched compound will change due to the fluxes in these three compounds (see Fig. 4 (a)). In the silicide reaction, we will assume that p , q , and r are essentially constant so that the fluxes in each phase are position independent. We will use J_A^α and J_B^α to designate the magnitudes of the fluxes of A and B, respectively, in the phase $A_\alpha B_{1-\alpha}$ (α equals p or q or r). The positive direction of each flux is shown in Fig. 4. For later usage, we define

$$J^\alpha = (1 - \alpha)J_A^\alpha + \alpha J_B^\alpha. \quad (1)$$

The conservation law of atoms at the A_pB_{1-p}/A_qB_{1-q} interface gives:

$$A + \frac{1-p}{p-q}A_qB_{1-q} = \frac{1-q}{p-q}A_pB_{1-p} \quad (2)$$

and

$$-B + \frac{p}{p-q}A_qB_{1-q} = \frac{q}{p-q}A_pB_{1-p}. \quad (3)$$

These two equations imply that the number of A_qB_{1-q} molecular per unit area formed at the A_pB_{1-p}/A_qB_{1-q} interface is equal to

$$(J_A^q - J_A^p)\frac{1-p}{p-q} + (J_B^q - J_B^p)\frac{p}{p-q} = J_A^q\frac{1-p}{p-q} + J_B^q\frac{p}{p-q} - J^p\frac{1}{p-q}. \quad (4)$$

Similarly, the number of A_qB_{1-q} molecular per unit area formed at the A_qB_{1-q}/A_rB_{1-r} interface is

$$(J_A^q - J_A^r) \frac{1-r}{q-r} + (J_B^q - J_B^r) \frac{r}{q-r} = J_A^q \frac{1-r}{q-r} + J_B^q \frac{r}{q-r} - J^r \frac{1}{q-r}. \quad (5)$$

The total number of A_qB_{1-q} molecular per unit area formed is the sum of eqs. (4) and (5); i.e.,

$$C_q \frac{dx_q}{dt} = -J^p \frac{1}{p-q} + J^q \frac{p-r}{(p-q)(q-r)} - J^r \frac{1}{q-r}, \quad (6)$$

where x_q is the thickness of A_qB_{1-q} and C_q is the molecular density of A_qB_{1-q} .

Figure 4 (b) shows that a schematic plot for the Co/Co₂Si/CoSi/Si system, for $\alpha = 1$, $\beta = 2/3$, $\gamma = 1/2$, and $\delta = 0$ with A = Co and B = Si. From eq. (6), we have (with $p = \alpha$, $q = \beta$, and $r = \gamma$)

$$\begin{aligned} C_\beta \frac{dx_\beta}{dt} &= \frac{\alpha - \gamma}{(\alpha - \beta)(\beta - \gamma)} J^\beta - \frac{1}{\beta - \gamma} J^\gamma \\ &= 9J^\beta - 6J^\gamma \end{aligned} \quad (7)$$

and (with $p = \beta$, $q = \gamma$, and $r = \delta$)

$$\begin{aligned} C_\gamma \frac{dx_\gamma}{dt} &= \frac{\beta - \delta}{(\beta - \gamma)(\gamma - \delta)} J^\gamma - \frac{1}{\beta - \gamma} J^\beta \\ &= -6J^\beta + 8J^\gamma. \end{aligned} \quad (8)$$

If a flux J_E^p , for any phase p and atom E (i.e., A or B) is controlled by the diffusion process, it can be expressed as [5]

$$J_E^p = \frac{D_{Ep} \Delta C_{Ep}^{eq}}{x_p}, \quad (9)$$

where D_{Ep} is the diffusion constant of atom E in the phase p ; ΔC_{Ep}^{eq} is the difference of the equilibrium concentrations of atom E at the two interfaces of

the phase p . In our case of Co/Si reaction, the fluxes are controlled by the diffusion processes. From eqs. (7) and (8), we have

$$\frac{dx_\beta}{dt} = 9D_\beta^{eff}/x_\beta - 6\frac{C_\gamma}{C_\beta}D_\gamma^{eff}/x_\gamma \quad (10)$$

and

$$\frac{dx_\gamma}{dt} = -6\frac{C_\beta}{C_\gamma}D_\beta^{eff}/x_\beta + 8D_\gamma^{eff}/x_\gamma, \quad (11)$$

where

$$D_\beta^{eff} = (1 - \beta)D_{A\beta}\Delta C_{A\beta}^{eq}/C_\beta + \beta D_{B\beta}\Delta C_{B\beta}^{eq}/C_\beta \quad (12)$$

and

$$D_\gamma^{eff} = (1 - \gamma)D_{A\gamma}\Delta C_{A\gamma}^{eq}/C_\gamma + \gamma D_{B\gamma}\Delta C_{B\gamma}^{eq}/C_\gamma. \quad (13)$$

We would like to mention two things about the effective diffusion constant D^{eff} : (1) If there is a dominant moving species (say A) in a phase (say phase β), then physically D^{eff} has a well-defined activation energy. (2) If $\Delta C_A^{eq} = \Delta C_B^{eq}$ (say for phase β), then

$$D_\beta^{eff} = \frac{C_B D_{A\beta} + C_A D_{B\beta}}{C_\beta} \frac{\Delta C_{A\beta}^{eq}}{C_\beta}.$$

The solutions of the eqs. (10) and (11) are

$$x_\beta = k_\beta \sqrt{t} \quad (14)$$

and

$$x_\gamma = k_\gamma \sqrt{t}, \quad (15)$$

where the constants k_β and k_γ are solutions of the following eqs.:

$$k_\beta = 18D_\beta^{eff}/k_\beta - 12\frac{C_\gamma}{C_\beta}D_\gamma^{eff}/k_\gamma \quad (16)$$

and

$$k_\gamma = -12\frac{C_\beta}{C_\gamma}D_\beta^{eff}/k_\beta + 16D_\gamma^{eff}/k_\gamma. \quad (17)$$

From these two equations, we can express the effective diffusion constants as

$$D_\beta^{eff} = k_\beta(k_\beta/9 + C_\gamma/C_\beta k_\gamma/12) \quad (18)$$

and

$$D_\gamma^{eff} = k_\gamma(C_\beta/C_\gamma k_\beta/12 + k_\gamma/8), \quad (19)$$

where $C_\gamma/C_\beta \approx 0.99$.

References

1. M–A. Nicolet and S. S. Lau, in *VLSI Electronics: Microstructure Science*, N. G. Einspruch, treatise Ed., Vol. 6, *Materials and Process Characterization*, N. G. Einspruch and G. B. Larrabee, volume Eds. (Academic Press, New York, 1983), Ch. 6.
2. S. S. Lau, J. W. Mayer, and K. N. Tu, *J. Appl. Phys.* 49, 4005 (1978).
3. K. N. Tu, G. Ottaviani, R. D. Thompson, and J. W. Mayer, *J. Appl. Phys.* 53, 4406 (1982).
4. G. V. Kidson, *J. Nucl. Mater.* 3, 21 (1961).
5. U. Gösele and K. N. Tu, *J. Appl. Phys.* 53, 3252 (1982).
6. E. P. Donovan, F. Spaepen, D. Turnbull, J. M. Poate, and D. C. Jacobson: *Appl. Phys. Lett.* 42 698 (1983).
7. J. C. C. Fan and H. Anderson: *J. Appl. Phys.* 52 4003 (1981).
8. C.–D. Lien, M–A. Nicolet, and S. S. Lau (in preparation).
9. L. S. Hung, J. Gyulai, J. W. Mayer, S. S. Lau, and M–A. Nicolet, *J. Appl. Phys.* 54 5076 (1983).
10. C. S. Wu, S. S. Lau, T. F. Kuech, and B. X. Liu, *Thin Solid Films* 104 175 (1983).
11. C.–D. Lien, M–A. Nicolet, and S. S. Lau, *phys. stat. sol. (a)* 81, 123 (1984).
12. C.–D. Lien, M–A. Nicolet, and S. S. Lau, *Appl. Phys. A* (1984) (in press).
13. N. Cheung, S. S. Lau, M–A. Nicolet, and J. W. Mayer, in *Proceeding of Symposium on Thin Film Interfaces and Interactions*, J. E. E. Baglin and J. M. Poate, Eds., Vol. 80–2 (Electrochemical Society, Princeton, 1980), p. 494.

14. C.-D. Lien and M-A. Nicolet, in *Thin Film and Interfaces II*, edited by J. E. E. Baglin, D. R. Campbell, and W. K. Chu (Elsevier Science Pub. Co., New York, 1984), Mat. Res. Soc. Symp. Proc. Vol. 25, p. 131.

Figure Captions

- Figure 1 2 MeV RBS spectra of (a) Co/Si^c and (b) Co/Si^e samples annealed at 440 °C for 25 min (open circles) and 80 min (full circles).
- Figure 2 Thicknesses of (a) Co₂Si (X₁) and (b) CoSi (X₂) against \sqrt{t} . The open and full symbols show the data for the silicide grown on Si^e and Si^c, respectively. The annealing temperature (°C) is used as a parameter for the data.
- Figure 3 Arrhenius plots of effective diffusion constants of Co₂Si and CoSi. The open and full symbols show the data for silicide grown on Si^e and Si^c, respectively. The circles and triangles represent the data of Co₂Si and CoSi, respectively. The effective diffusion constant data calculated from the experimental data in refs. 3 ('×' for Co₂Si and '+' for CoSi) and 2 (dashed lines) are also shown here.
- Figure 4 Schematic plots of (a) the A_pB_{1-p} / A_qB_{1-q} / A_rB_{1-r} (with $p > q > r$) sample and (b) the Co/Co₂Si/CoSi/Si sample.

Fig.1

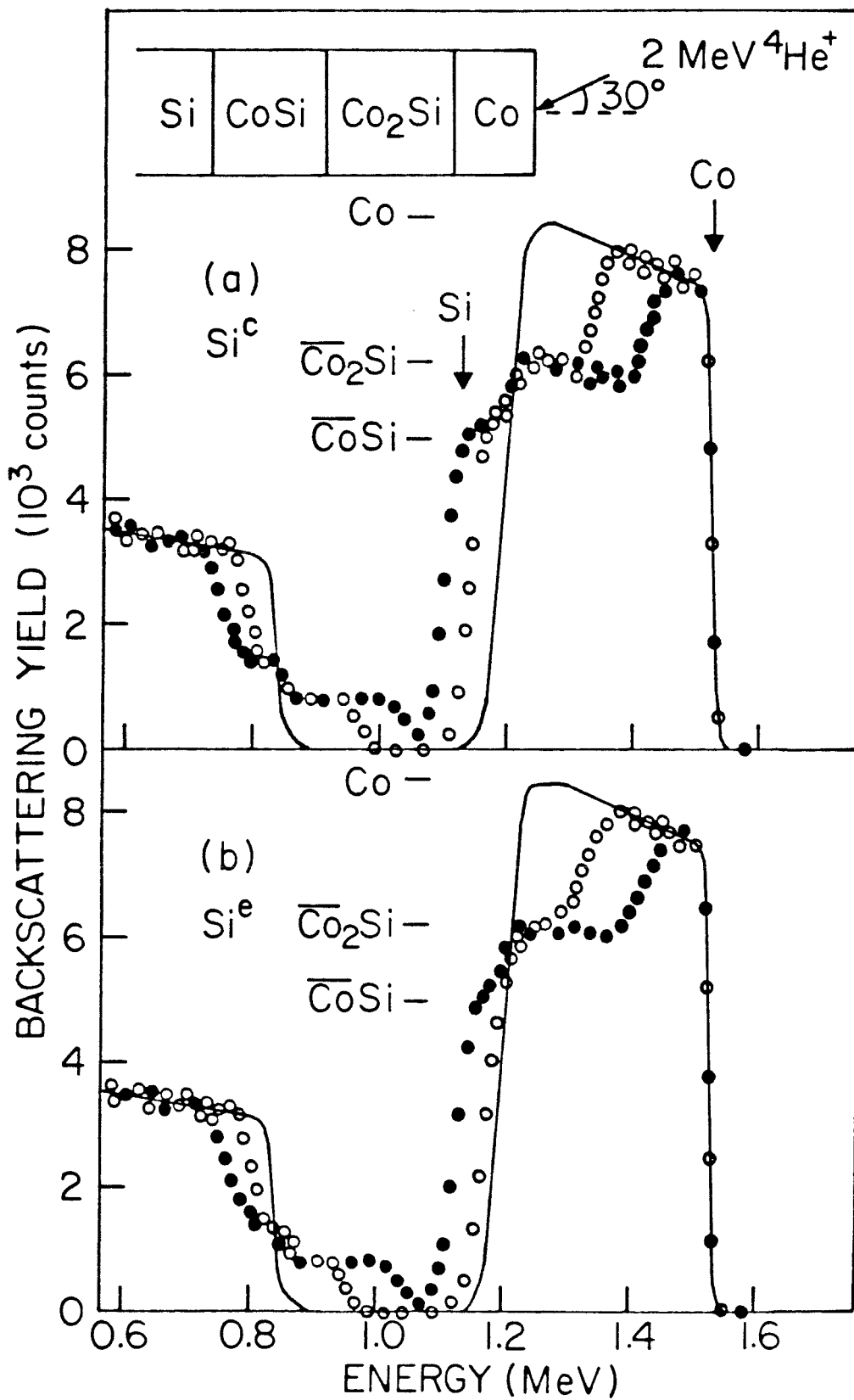


Fig.2

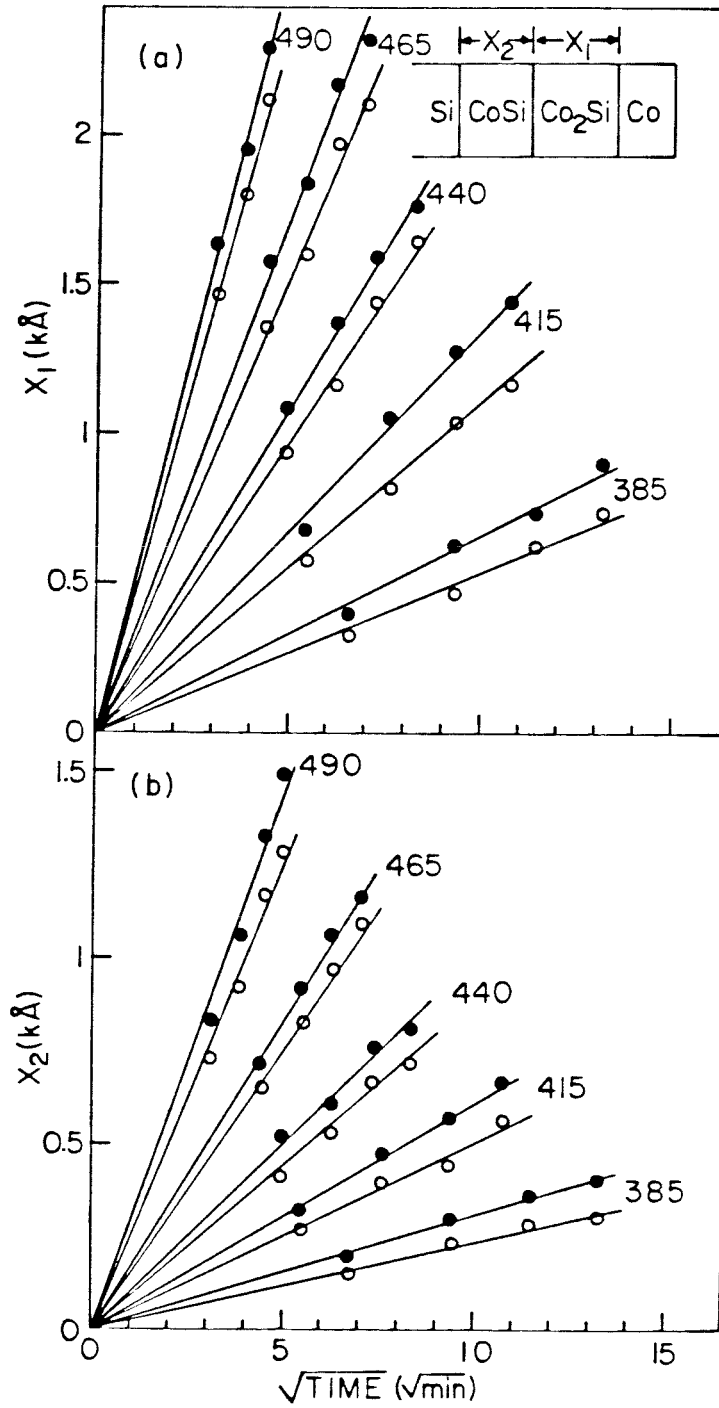


Fig.3

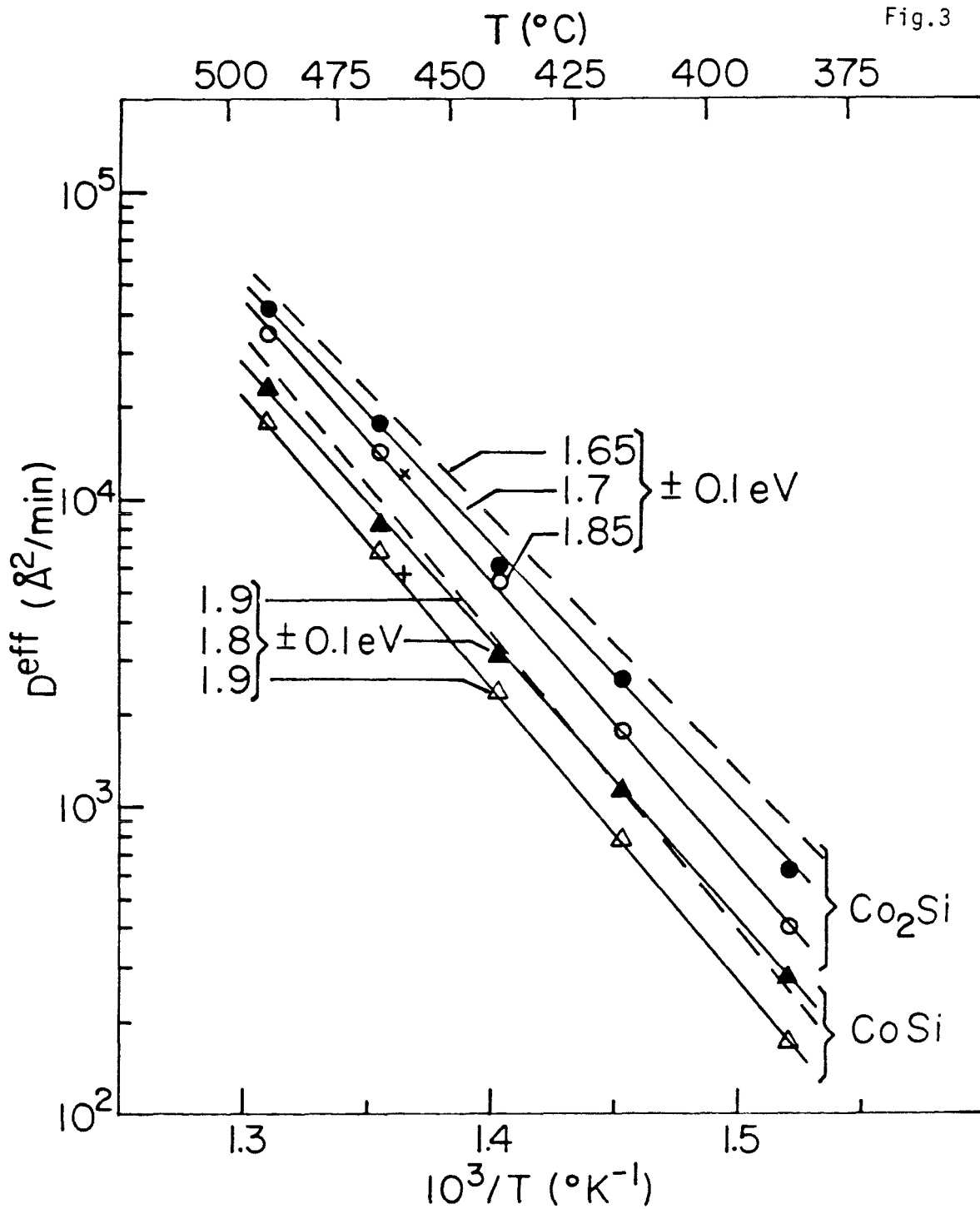


Fig.4

(a) $A_p B_{1-p} / A_q B_{1-q} / A_r B_{1-r}$

$J_A^p \Rightarrow$	$J_A^q \Rightarrow$	$J_A^r \Rightarrow$
$A_p B_{1-p}$	$A_q B_{1-q}$	$A_r B_{1-r}$
$\Leftarrow J_B^p$	$\Leftarrow J_B^q$	$\Leftarrow J_B^r$

(b) $Co/Co_2Si/CoSi/Si$

Co_1Si_0	$J_{Co}^\beta \Rightarrow$	$J_{Co}^\gamma \Rightarrow$	Co_0Si_1
	$Co_{2/3}Si_{1/3}$	$Co_{1/2}Si_{1/2}$	
	$\Leftarrow J_{Si}^\beta$	$\Leftarrow J_{Si}^\gamma$	
$\alpha=1$	$\beta=2/3$	$\gamma=1/2$	$\delta=0$

Appendix D -
Effects of Ion Irradiation
on
Thermally Formed Silicides
in the Presence of Interfacial Oxide

C.-D. Lien and M.-A. Nicolet
California Institute of Technology
Pasadena, CA 91125, U.S.A.

and

Peter Williams
Arizona State University
Tempe, Arizona 85287, U.S.A.

Abstract

Near-noble metal (Ni, Pt, and Pd) films were evaporated on Si substrates, the surfaces of which were slightly oxidized in an oxygen plasma. The samples were irradiated with Si^+ of different doses to break up the interfacial oxide. The samples were then annealed in vacuum at 400°C .

For the low-dose implanted samples, the silicides formed after thermal annealing are laterally nonuniform. The interfacial oxygen profiles were found to be quite broad and located in the silicide. For the high-dose implanted samples, the silicides are laterally uniform. The interfacial oxygen profiles were found to be narrow and were located at the sample surface for the cases of Ni and Pt, and at the Si/silicide interface for the case of Pd. A model was

proposed to explain the experimental results.

Introduction

Metal silicide films are widely used for Schottky barriers and ohmic contacts in Si devices [1]. As the trend toward VLSI technology reduces lateral and depth dimensions of devices, the uniformity of silicide contact becomes a very important consideration and difficult part of the technology. However, if the metal/silicon interface is not properly cleaned, the silicide formed from thermal annealing can be very laterally nonuniform [2-8]. One way to improve the lateral uniformity of thermally grown silicides is to use ion irradiation to break up the interfacial oxide before silicide formation [5-8]. The Si oxide (formed from H_2O_2) used in Refs. 5 and 6, however, is weak; and the silicides (e.g., Ni_2Si and Pt_2Si) used to demonstrate the effect of ion irradiation are not those (e.g., $PtSi$) used for device contacts. The location of interfacial oxide after silicide formation also was not reported in the above papers.

In this paper, we used oxygen ($^{18}O + ^{16}O$) plasma grown Si oxide as an interfacial impurity to interfere in the formation of $NiSi$, $PtSi$, and Pd_2Si . Different doses of the Si beam were implanted through the metal/Si interface before thermal annealing. Rutherford backscattering spectrometry (RBS) was used to monitor the formation of the silicides and their uniformity. $^{18}O(p,\alpha)^{15}N$ nuclear reaction (NRA) and secondary ion mass spectrometry (SIMS) were used to study the profiles of oxygen. A simple model was proposed to explain the lateral uniformity of silicides and the locations of the interfacial oxide after silicide formation.

Experimental procedures

Commercially prepared p-type Si (100) wafers of 1.5-2.5 Ω cm resis-

tivity were cleaned ultrasonically with TCE, acetone, and methanol, sequentially. Wafers were oxidized in an ^{16}O plasma for 30 min, etched in a 6% HF solution for 5 min, and then oxidized in an ^{18}O plasma (due to outgassing of wall, there is also ^{16}O in the plasma) for 10 min. The total ^{18}O on the Si surface amounts to $15 \pm 5 \text{ \AA}$ of SiO_2 as measured by $^{18}\text{O}(\text{P},\alpha)^{15}\text{N}$ NRA, and the ratio between ^{16}O and ^{18}O ($^{16}\text{O}/^{18}\text{O}$) is about 2.3 ± 0.5 as measured by SIMS.

Immediately after preparation, the wafers were loaded into an oil-free e-beam evaporator. A Ni film of $\approx 1000 \text{ \AA}$ or a Pt film of $\approx 700 \text{ \AA}$ or a Pd film of $\approx 1250 \text{ \AA}$ was deposited on the top of the wafers at a rate of $\approx 25 \text{ \AA/s}$ with the vacuum held below 4×10^{-7} Torr during evaporation. Samples were then implanted at room temperature with 260 keV Si^+ of doses ranging from 0.5 to $10 \times 10^{15} \text{ Si/cm}^2$. The calculated Si projected ranges (R_p) in Ni, Pt, and Pd are about 1160 \AA , 770 \AA , and 1100 \AA , respectively; and the corresponding range stragglings (ΔR_p) are 490 \AA , 560 \AA , and 600 \AA , respectively [9]. No visible silicide was formed in each sample after Si irradiation.

Implanted and unimplanted samples were then annealed in vacuum at 400°C for 1 hr. with the background pressure kept at $\approx 5 \times 10^{-7}$ Torr. The silicides formed and their uniformity were studied by MeV $^4\text{He}^+$ RBS. The amount and the location of ^{18}O were measured by the isotope-specific reaction $^{18}\text{O}(\text{p},\alpha)^{15}\text{N}$ NRA induced by 1.5 MeV H_2^+ [10, 11]. The locations of ^{16}O and ^{18}O were studied by SIMS.

Results

For a fixed metal, there is a general behavior for the metal Si reaction:

- (1) There is no visible metal–Si reaction after 400°C annealing for the unimplanted sample.
- (2) As the Si dose increases and over some value (say, D_1), the silicide starts

to form; however, it is laterally nonuniform.

- (3) When the Si dose further increases and exceeds another value (say, D_2), the silicide formed becomes laterally uniform.

The definition of these two numbers D_1 and D_2 is very vague, but a rough estimation of these numbers will give us some idea about the effect of the interfacial oxide in the metal-Si reaction. Table 1 gives the rough upper bounds of these two numbers for Ni, Pt, and Pd reacting with Si. From this table, we suggest that, among these metals, Pd is the most insensitive to the interfacial oxide. This result is consistent with the reported data [3, 4].

Si/Pd case

Figure 1 shows that the RBS spectra (solid line) of Si/Pd samples irradiated by (a) 0, (b) 0.5 , and (c) 1.5×10^{15} Si/cm² and then annealed at 400°C for 1 h. The RBS spectrum and the ¹⁸O profile of the as-prepared sample are the same as those of the unimplanted and annealed sample as shown in Fig. 1. As shown in Fig. 1, we observe that there is no visible reaction in the unimplanted sample after annealing (Fig. 1 (a)). If the sample was irradiated by 0.5×10^{15} Si/cm², all the Pd forms a silicide after annealing, but the silicide is laterally nonuniform (Fig. 1 (b)). For the 1.5×10^{15} Si/cm² implanted sample, not only is the Pd totally consumed, but the silicide formed is also laterally uniform (Fig. 1 (c)).

¹⁸O signals (circles, as measured from ¹⁸O(p,α)¹⁵N NRA) of the three samples mentioned above are also shown in the corresponding figure. The horizontal scale of ¹⁸O signal is adjusted so that the ¹⁸O and the metal (i.e., Pd) have the same physical position in the sample when their signals have the same horizontal position in the figure. In the unimplanted sample, the oxygen stays at the Si/Pd interface (Fig. 1 (a)). For the case of the sample implanted by 0.5×10^{15} Si/cm², the oxygen profile is located in the silicide and is very broad (Fig. 1 (b)). When implanted with 1.5×10^{15} Si/cm², the oxygen is located

at the Si/Pd₂Si interface and its profile is very narrow (Fig. 1 (c)). In each sample mentioned above, the total amount of ¹⁸O is the same as that of the as-prepared sample; i.e., there is no gain neither loss of ¹⁸O during annealing.

SIMS results (Fig. 2 (a)) show that both ¹⁶O and ¹⁸O are present at the Si/Pd interface of the as-prepared sample, and ¹⁶O/¹⁸O is about 2.5. Figure 2 (b) shows the SIMS spectrum of the sample implanted with 1.5×10^{15} Si/cm² and then annealed, which confirms the results for the ¹⁸O locations as measured by the ¹⁸O(p,α)¹⁵N NRA. It also shows that there are (i) a high surface peak of ¹⁶O, (ii) an ¹⁶O in-diffusion profile, and (iii) the amount of interfacial ¹⁶O increases (¹⁶O/¹⁸O is about 7). These prove that there is a lot of ¹⁶O diffusing from the ambient into the sample during annealing.

Si/Ni and Si/Pt cases

The RBS and NRA results are very similar in the cases of Si/Ni and Si/Pt, except for different D_1 and D_2 . Due to the similarity between these two cases, we will show the results for the Si/Pt case only. Figure 3 shows the RBS spectra of Si/Pt samples irradiated by (i) 0 (solid line), (ii) 2.5×10^{15} Si/cm² (dotted lines), and (iii) 5×10^{15} Si/cm² (dashed lines) and then annealed at 400°C for 1 hr.. The RBS spectrum and the ¹⁸O profile of the as-prepared sample are the same as those of the unimplanted and annealed sample as shown in Fig. 3. From this figure, we observe that the unimplanted sample has no Pt-Si reaction, that the 2.5×10^{15} Si/cm² implanted sample forms a laterally nonuniform silicide, and that the 5×10^{15} Si/cm² implanted sample forms a laterally uniform silicide.

The ¹⁸O signal of the above-mentioned samples are shown in Fig. 3. The horizontal axis of the ¹⁸O signal is adjusted as is discussed in the Si/Pd case. In the unimplanted sample, the oxygen stays at the Si/Pt interface (open circles). For the case of the sample implanted by 2.5×10^{15} Si/cm², the oxygen profile is located in the silicide and is very broad (triangles). When implanted with 5×10^{15} Si/cm², the oxygen is located at the silicide surface and its profile is very narrow (full circles). SIMS spectra (Fig. 4) show the same results

for the ^{18}O locations as measured by the $^{18}\text{O}(p,\alpha)^{15}\text{N}$ NRA. The amounts of the surface ^{16}O and in-diffusion ^{16}O in the Si/Pt case are much less than those in the Si/Pd case.

Discussion

Immobile impurities present at the Si/M interface can be characterized as thin, thick, or nonuniform interfacial barriers and are defined as follows (see Fig. 5) [12]:

- (I) Thin barrier: The interfacial impurity is not able to stop the uniform silicide formation and is therefore pushed to the silicide/moving species layer interface (see Fig. 5 (a)).
- (II) Thick barrier: The impurity stops the silicide formation completely (see Fig. 5 (b)).
- (III) Nonuniform barrier: The barrier is thin in some places and thick in others. From the above definition, the silicide forms only at the thin part of the barrier, initially. Once the silicide reaches the sample surface, the remaining metal will be consumed by the lateral growth of silicide [15] (see Fig. 5 (c)).

Using this definition, we can explain the experimental results as follows:

- (1) Before the Si dose reaches D_1 , the interfacial barrier is thick, and therefore there is no silicide reaction (see Fig. 5 (b)).
- (2) When the Si doses are in between the D_1 and D_2 , some part of the barrier becomes thin and the other part remains thick; therefore, the silicide formed is laterally nonuniform and the ^{18}O signal is broad and located in the silicide (see Fig. 5 (c)).

- (3) When the Si doses are higher than D_2 , the barrier becomes thin everywhere and the silicide formed is laterally uniform (see Fig. 5 (a)).

From the above discussion, we suggest that the location of oxygen in the high-dose implanted sample (thin interfacial barrier) can be used as an inert marker for silicide formation, if there is no interfacial drag. In the cases of Ni and Pt silicides in which metal is the dominant moving species [1], we thus predict that the ^{18}O is located at the sample surface after high-dose implantation and thermal annealing. The experimental results confirmed this prediction (e.g., see Fig. 5 (c)). Since the oxygen is located at the Si/ Pd_2Si interface as shown in the Fig. 1 (c), we thus suggest that Si is the dominant moving species in this case, if there is no interfacial drag. This result is, in fact, confirmed by the experimental results in Refs. 13 and 14.

Conclusion

Silicon irradiation was used to improve the near-noble metal silicide reaction when there is an interfacial oxide. For the low-dose implanted samples, the silicides formed are laterally nonuniform. The interfacial oxygen profiles were found to be quite broad and were located in the silicide formed. For the high-dose implanted samples, the silicides are laterally uniform. The interfacial oxygen profiles were found to be narrow and were located at the sample surface for the cases of Ni and Pt, and at the Si/silicide interface for the case of Pd. A model was proposed to explain the lateral uniformity of the silicide and the location of interfacial oxide.

Acknowledgment

References

1. M-A. Nicolet and S. S. Lau, in N. G. Einspruch (treatise Ed.) *VLSI Electronics: Microstructure Science*, Vol. 6, N. G. Einspruch and G. B. Larrabee (volume Eds.) *Materials and Process Characterization*, Academic Press, New York, 1983, Ch. 6.
2. H. Föll and P. S. Ho, *J. Appl. Phys.*, 52 (1981) 5510.
3. D. M. Scott, S. S. Lau, R. L. Pfeffer, R. A. Lux, J. Mikkelson, L. Wieluński, and M-A. Nicolet, in R. Ludeke and K. Rose (Eds.), *Proc. of MRS Symp. on Interfaces and Contacts*, Vol. 18, North-Holland, New York, 1983, p. 227.
4. S. S. Lau and W. F. van der Weg, in J. M. Poate, K. N. Tu, and J. W. Mayer (eds.), *Thin Films-Interdiffusion and Reactions*, Wiley, New York, 1978, p. 450.
5. L. S. Wieluński, C.-D. Lien, B. X. Liu, and M-A. Nicolet, *J. Vac. Sci. Technol.*, 20 (1982) 182.
6. L. S. Wieluński, C.-D. Lien, B. X. Liu, and M-A. Nicolet, in S. T. Picraux and W. J. Choyke, *Proc. of MRS Symp. on Metastable Materials of Formation by Ion Implantation*, Vol. 7, North-Holland, New York, 1982, p. 139.
7. B. Y. Tsaur and C. H. Anderson, *Appl. Phys. Lett.*, 41 (1982) 877.
8. E. Nagasawa, H. Okabayashi, and M. Morimoto, *Jap. J. Appl. Phys.*, 22 (1983) L57.
9. J. P. Biersack, *Nucl. Instrum. Methods*, 182/183 (1981) 199.
10. C.-D. Lien, L. S. Wieluński, and M-A. Nicolet, *Nucl. Instrum. Methods*, 213 (1983) 463.
11. J. W. Mayer and E. Rimini, *Ion Beam Handbook for Material Analysis*,

Academic Press, New York, 1977.

12. C.-D. Lien and M-A. Nicolet, *J. Vac. Sci. Technol.* (submitted).
13. D. M. Scott and M-A. Nicolet, *Nucl. Instrum. Methods*, 209/210 (1983) 297.
14. K. T. Ho, C.-D. Lien, U. Shreter, and M-A. Nicolet, *J. Appl. Phys.* (in press).
15. L. R. Zheng, L. S. Hung, and J. W. Mayer, in R. Ludeke and K. Rose (Eds.), *Proc. of MRS Symp. on Interfaces and Contacts*, Vol. 18, North-Holland, New York, 1983, p. 207.

	Pd	Ni	Pt
D_1 (10^{15} Si/cm ²)	0.5	1.5	2.5
D_2 (10^{15} Si/cm ²)	1.5	2.5	5

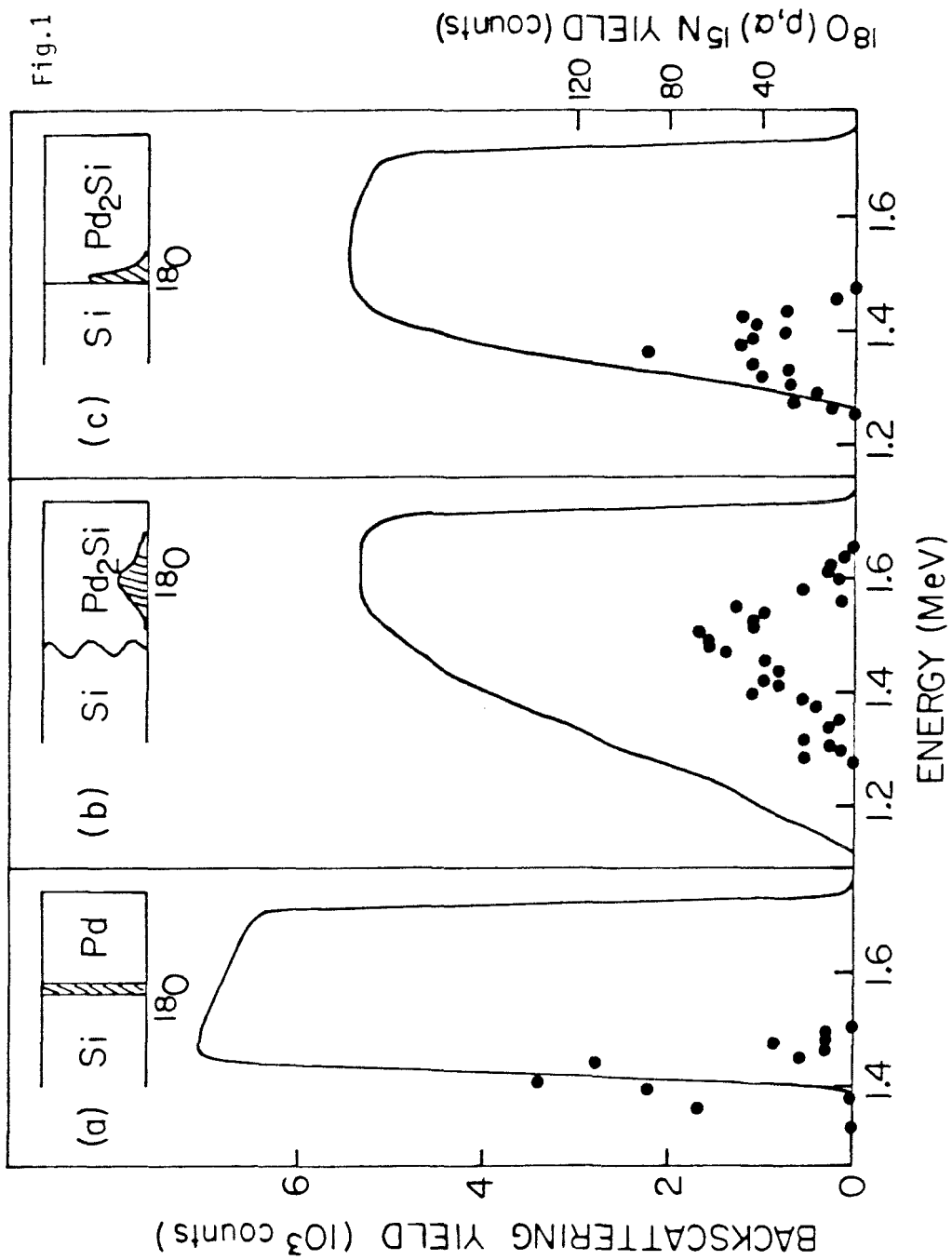
Table 1

The upper bounds of D_1 (dose of Si needed to form the silicide) and D_2 (dose of Si needed to form uniform silicide) for Pd, Ni, and Pt reacts with slightly oxidized Si. The oxygen located at the Si surface amounts to about 50 Å of SiO₂

Figure Captions

- Figure 1** 2 MeV $^4\text{He}^+$ RBS spectra (solid lines) of Si/Pd samples (Pd signal only) that were irradiated by (a) 0, (b) 0.5, and (c) 1.5×10^{15} Si/cm² and then annealed at 400°C for 1 hr.. During RBS measurements, the samples were tilted 60° away from the incident beam direction. $^{18}\text{O}(p,\alpha)^{15}\text{N}$ NRA ^{18}O signals (circles) of the samples mentioned above are also shown in the corresponding figure. The horizontal scale of ^{18}O signal is adjusted so that the ^{18}O and Pd have the same physical position in the sample when their signals have the same horizontal position in the figure.
- Figure 2** SIMS spectra of (a) the as-prepared Si/Pd sample and (b) the Si/Pd sample implanted with 1.5×10^{15} Si/cm² and then annealed.
- Figure 3** 2 MeV $^4\text{He}^+$ RBS spectra (Pt signal only) of Si/Pt samples that were irradiated by (i) 0 (solid line), (ii) 2.5 (dotted lines), and (iii) 5 (dashed lines) $\times 10^{15}$ Si/cm² and then annealed at 400°C for 1 h. During RBS measurements, the samples were tilted 70° away from the incident beam direction. $^{18}\text{O}(p,\alpha)^{15}\text{N}$ NRA ^{18}O signals ((i) open circles, (ii) triangles, and (iii) full circles) of the samples mentioned above are also shown in the figure. The horizontal scale of ^{18}O signal is adjusted so that the ^{18}O and Pt have the same physical position in the sample when their signals have the same horizontal position in the figure.
- Figure 4** SIMS spectra of (a) the as-prepared Si/Pt sample and (b) the Si/Pt sample implanted with 5×10^{15} Si/cm² and then annealed.
- Figure 5** A model is proposed to explain the redistribution of the im-

mobile interfacial impurity during silicide formation: (a) Thin barrier: the silicide is formed uniformly and the impurity is pushed to the silicide/moving species interface. (b) Thick barrier: no silicide formation. (c) Nonuniform barrier: the metal on the thin barrier is consumed during initial silicide formation and the metal on the thick barrier is consumed by lateral silicide growth. In all cases, the metal (M) is assumed to be the moving species and Si to be the stationary species. Corresponding cases exist when Si is the moving species.



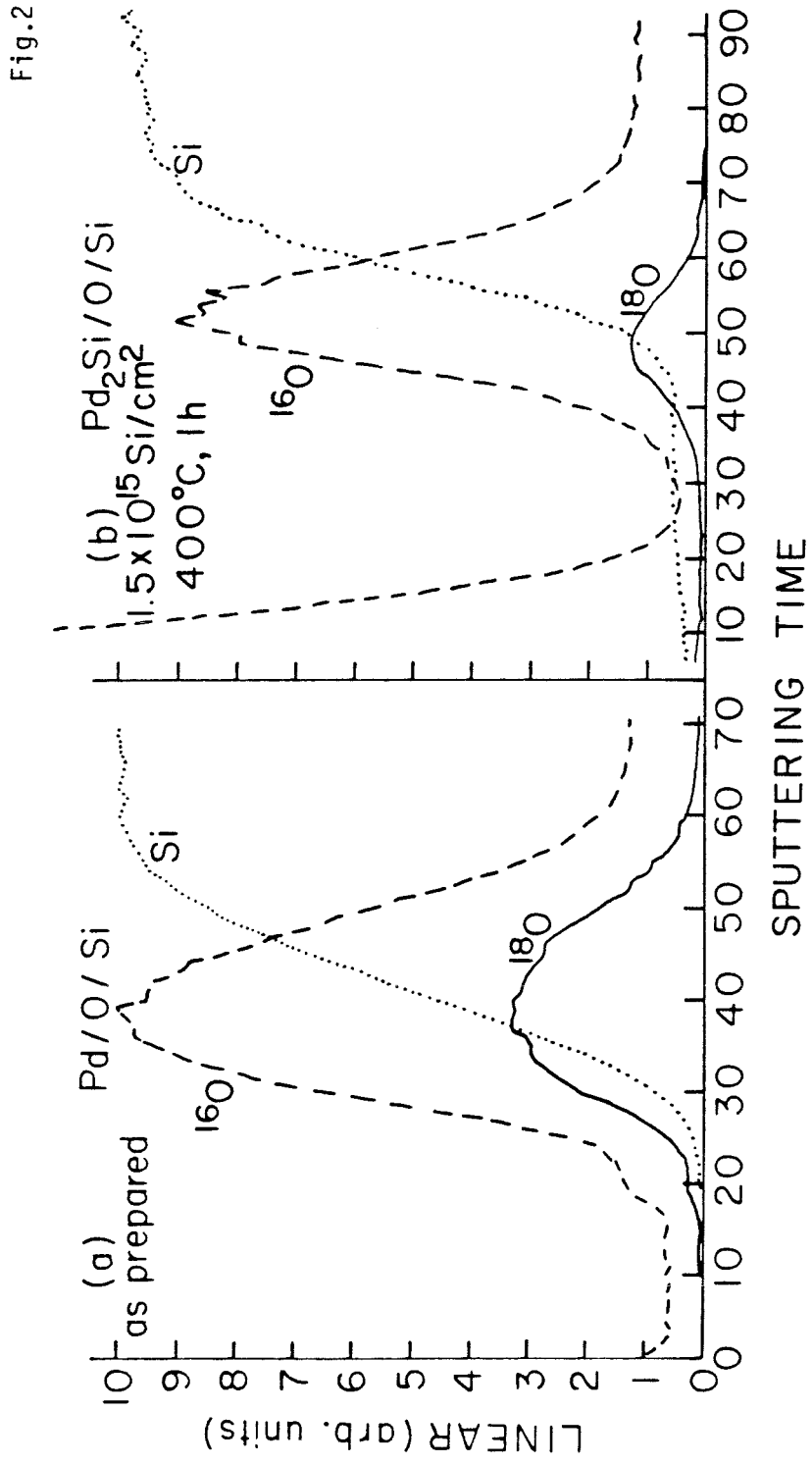


Fig.3

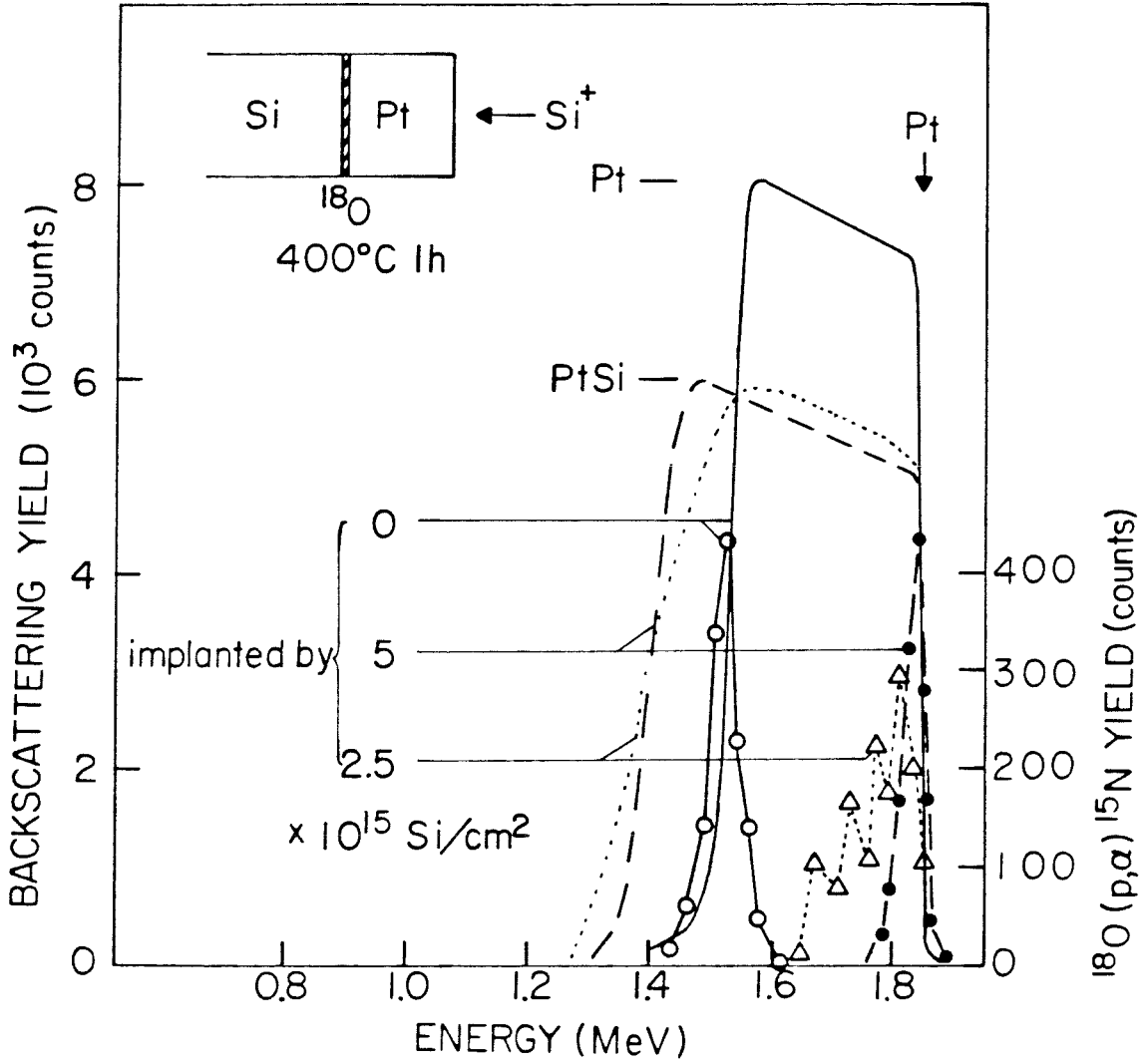


Fig.4

